A NEW CPT-BASED P-Y FORMULATION FOR PILES IN SAND

by

Emirhan Sancak

B.S., Civil Engineering, Halmstad University, 2012

M.S., Civil Engineering, Boğaziçi University, 2014

Submitted to the Institute for Graduate Studies in
Science and Engineering in partial fulfillment of
the requirements for the degree of
Doctor of Philosophy

Graduate Program in Civil Engineerring

Boğaziçi University

2024

ACKNOWLEDGEMENTS

I would like to express my sincere gratitude to my supervisor, Prof. Özer Çinicioğlu, who gave me a hand once and has never given up on me throughout this long journey. He not only taught me how to think and research, but also how to come through life's challenges. I will never forget the day he reminded me that there is the contentment come with the rigor. I admire him for the rest of my life.

I would like to thank the rest of my thesis committee for their constructive feedbacks that enriched this study during progress meetings.

I would like to express my gratitude Assist. Prof. Ahmet Talha Gezgin for his unwavering support. He had always time to make insightful discussions on this study. Beyond all, his fellowship is a valuable gift for me.

I cannot thank my colleagues enough, Mert Güner and Uğur Can Erginağ, for their support and patience.

I also appreciate the support from my friends: Assist. Prof. Sedat Semih Çağlayan, Assist. Prof. Semih Gönen, Emre Çıkar, Umut Can Uzun, Ali Ozan Özçiçek, Yavuz Çakmakçı and my roommate Okan Yamanoğlu.

This journey has become meaningful and real with her presence, Eda Nur Özcan. During last two and a half year, she was always there with me when I felt lost. No matter how much I express my gratitude to her, it is not enough.

And my dear parents, Fadime and İsmail Sancak. I do not know if there is a word in any language on earth that can describe my gratitude to you. I am very blessed to be your son. This dissertation is dedicated to you.

ABSTRACT

A NEW CPT-BASED P-Y FORMULATION FOR PILES IN SAND

The behavior of soils surrounding piles induced by lateral loading remains a significant research topic addressed under the soil-pile interaction problem. As laterally loaded piles have been crucial in onshore constructions for many decades, their use and enhancement have recently become essential in nearshore and offshore structures. This dissertation is dedicated to proposing new p-y formulations for piles in the sand through direct cone tip resistance (q_c) measurements from cone penetration test (CPT), considering loading modes, for finite element (FE) modeling purposes. To achieve this objective, a parametric study has been planned, involving a series of 3D finite element analyses on a single pile model placed within soil models representing a natural sand (Sile sand). The analysis program encompasses two loading modes: the "acting force at the pile head" and the "translation of whole pile body". Knowing that the deformation mechanism of CPT is analogous to spherical cavity expansion (SCE) theory, q_c profiles of the soil models used in the parametric study are determined through 2D axisymmetric FE model analyses in Plaxis 2D employing SCE in sand samples representing each 1-m-thick layer with varying stress conditions and densities. Results have been processed by Genetic Algorithm (GA) code to derive p-y formulations for different cases. Finally, three separate field tests on piles loaded at the pile head and three FE models, which are representative of anchor piles where another type of loading mode is concerned, are modeled in a structural FE analysis program using different p-y formulations, including the ones derived by this study. It is observed that the models created using the proposed formulations exhibit good agreement with the relevant source data.

ÖZET

KUMLARDA KONİ PENETRASYON TESTİNE GÖRE YENİ BİR P-Y FORMÜLASYONU

Kazıkları çevreleyen zeminlerin yanal yüklemeden kaynaklanan davranışı, zemin-kazık etkileşim problemi altında ele alınan önemli bir araştırma konusu olmaya devam etmektedir. Yanal olarak yüklenen kazıklar onlarca yıldır kıyıdaki inşaatlarda çok önemli olduğu gibi, son yıllarda kıyıya yakın ve açık deniz yapılarında bunların kullanımı ve geliştirilmesi zorunlu hale geldi. Bu tez, sonlu elemanlar (FE) modelleme amaçları için yükleme modlarını göz önünde bulundurarak koni penetrasyon testinden (CPT) doğrudan koni uç direnci (q_c) ölçümleri yoluyla kumdaki kazıklar için yeni p-y formülasyonları önermeye adanmıştır. Bu amaçla, gerçek bir kumu (Şile kumu) temsil eden zemin modellerine yerleştirilen tekil bir kazık model üzerinde bir dizi 3 boyutlu sonlu elemanlar analizini içeren parametrik bir çalışma tasarlanmıştır. Analiz programı iki tür yükleme modunu kapsar; bunlar "kazık başındaki kuvvet" ve "tüm kazık gövdesinin ötelenmesi"dir. CPT mekanizmasının küresel kavite genleşme (SCE) teorisine benzer olduğu bilinerek, parametrik çalışmada kullanılan zemin modellerinin q_c profilleri, her 1m kalınlığındaki katmanı temsil eden kum numunelerinde SCE kullanılarak Plaxis 2D'de oluşturulan 2D eksenel simetrik FE model analizleri yoluyla belirlenir. değişen stres koşulları ve yoğunluklarla. Sonuçlar, farklı durumlar için p-y formülasyonlarını türetmek üzere Genetik Algoritma (GA) koduyla işlendi. Son olarak, kazık başından yüklenen kazıklar üzerinde üç ayrı saha testi ve bundan farklı bir yükleme modunun söz konusu olduğu ankraj kazıklarını temsil eden üç FE modeli, bu formülle türetilenler de dahil olmak üzere farklı p-y formülasyonları kullanılarak yapısal bir FE analiz programında modellenmiştir. Önerilen formülasyonlar kullanılarak oluşturulan modellerin ilgili kaynak verilerle iyi bir uyum sergilediği görülmektedir.

TABLE OF CONTENTS

LIST OF FIGURES

LIST OF TABLES

LIST OF SYMBOLS

A	Adjustment factor
B	Width of the pile
C	Cohesion
C_c	Coefficient of gradation
C_u	Uniformity coefficient
D	Pile diameter
D_{50}	Median particle size
e	Void ratio
e_c	Void ratio at the critical state
e_d	Void ratio at the maximum densification
e_{max}	Maximum void ratio
e_{min}	Minimum void ratio
E_{50}^{ref}	Secant stiffness in standard drained triaxial test
E_{oed}^{ref}	Tangent stiffness for primary oedometer loading
E_p	Modulus of elasticity Young's modulus of the pile
E_{ur}^{ref}	Unloading/reloading stiffness
f_s	Sleeve friction
f_θ	Yield rotation factor
F_y	Yield displacement factor
G	Shear modulus
G_s	Specific gravity
H_u	Ultimate horizontal load
I	Elastic influence factor for rotation induced by moment
I'_D	Pressure-dependent density
$I_{\theta H}$	Elastic influence factor for rotation induced by horizontal load
$I_{\theta m}$	Elastic influence factor for rotation induced by moment
I_c	Critical length
I_P	Second moment of inertia for pile

I_{yH}	Elastic influence factor due to horizontal load
I_{yM}	Elastic influence factor due to moment
$I_{\theta H}$	Elastic influence factor for rotation
k	Subgrade modulus
k_g	Shape factor
K_0^{NC}	K_0 value for normal consolidation
K_{cz}	Cohesive passive earth pressure component
K_{qz}	Fricional passive earth pressure component
K_o	Lateral earth pressure coefficient
L	Length of the pile
m	Power for the stress-level dependency of stiffness
M_u	Ultimate moment
n_h	Constant of horizontal subgrade reaction
p	Soil resistance per unit length of the pile
P	Axial load
p_a	Atmospheric pressure
p'_o	Mean effective stress
p_{lim}	Limit pressure
p_u	Ultimate soil pressure
P_{cd}	Ultimate resistance of the sand well below the ground
P_{ct}	Ultimate resistance of the sand near the ground
P_{oz}	Effective overburden pressure
P_{ref}	Reference stress for stiffnesses
q	Vertical pressure
q_c	Cone tip resistance
r	Empirical line-fitting parameter
R_f	Failure ratio
u	Pore pressure
u_1	Pore pressure measured on the cone
u_2	Pore pressure at the shoulder of the cone
u_3	Pore pressure behind the sleeve

v_{ur}	Poisson's ratio for unloading-reloading
w	Vertical deflection
y	Lateral displacement
z	Depth
z_r	Depth of rotation point
Z	Depth
γ	Bulk unit weight
γ'	Submerged unit weight
η	Shape factor
ν	Poisson's ratio
σ'_h	Effective horizontal stress
σ_N	Effective normal stress
σ'_v	Vertical effective stress
τ_1	Horizontal shear stress
τ_2	Vertical shear stress
ϕ'	Effective friction angle
ϕ'_{cv}	Critical state friction angle
ϕ'_m	Mobilized friction angle
φ	Friction angle
ψ	Dilation angle
ψ_m	Mobilized dilation angle

LIST OF ACRONYMS/ABBREVIATIONS

2D	Two Dimensional
3D	Three Dimensional
CE	Cavity Expansion
CPT	Cone Penetration Test
FE	Finite Element
HS	Hardening-Soil
MC	Mohr-Coulomb
SCE	Spherical Cavity Expansion

1. INTRODUCTION

Piles are frequently employed structural elements tasked with resisting lateral loads originating from diverse factors, depending on the nature of the supporting structure. They facilitate the transfer of loads subject to various internal and external parameters, into the underlying soil or rock through different modes of interaction. Therefore, the design of piles subjected to lateral loads has remained a crucial area of focus for several decades.

The finite element method has become the most reliable and commonly used tool for static and dynamic analysis of structures and modeling piles under lateral loads. It is strongly suggested by Eurocode 7 (2004) and many other regional design codes worldwide. Many commercial software programs focus on geotechnical and structural analysis separately. Although significant developments have been made in both geotechnical and structural analysis programs based on FEM, neither of them is sufficient on its own to model complex civil engineering designs. There is still a need for the combined use of these programs. The Winkler method, also known as the p-y method, involves discrete and uncoupled non-linear springs. It is beneficial and essential for modeling of soil-pile interaction problems, as it allows the definition of soil response to lateral displacements of piles in structural analysis programs based on FEM.

Numerous well-structured research studies have proposed equations for defining nonlinear p-y springs through various approaches, including field tests (Igoe *et al.*, 2011; Li *et al.*, 2014; Matlock, 1970; Reese *et al.*, 1974), centrifuge tests (Choo and Kim, 2016; Dyson and Randolph, 2001; Mezazigh and Levacher, 1998; Qi *et al.*, 2016) and numerical methods (Suryasentana and Lehane, 2014, 2016). Many equations available in literature for sands typically rely on the friction angle (ϕ') as the sole input parameter, necessitating meticulous efforts involving both laboratory and field test results.

Therefore, research emphasizing the establishment of p-y springs through direct measurements of cone penetration testing (CPT) has gained significance. Several studies have demonstrated that cone tip resistance (q_c) extracted from CPT serves as a convenient parameter for soil response to lateral displacements (Houlsby and Hitchman, 1988; Salgado and Randolph, 2001; Schnaid and Houlsby, 1991).

The derivation of p-y formulations concerning q_c, through a parametric study, involves bringing together numerically modeled soils with varying parameters and predicting q_c profiles corresponding to those soils in each configuration. Given that CPT is analogous to the spherical cavity expansion (SCE) theory proposed by (Bishop *et al.*, 1945), which describes a pressure-deformation relationship with an expanding cavity, (Xu and Lehane, 2008) implemented a technique involving a two-dimensional axisymmetric FE analysis in Plaxis 2D to simulate SCE. They provided q_c values for sand with different initial conditions, numerically modeled using an elasto-plastic constitutive model.

This dissertation proposes a new CPT-based p-y formulation to model springs, defining soil reaction around a single pile due to lateral displacements and are generated in structural analysis-oriented FE software. Natural sand from the northern coast of Istanbul was analyzed to create the numerical model using the Hardening Soil constitutive model. The q_c profile for this soil model was numerically extracted with a verified SCE FE model in Plaxis 2D, considering anisotropic initial stress conditions.

Subsequently, a parametric study covering a single pile model with varying diameters within different configurations of Sile sand was conducted in the 3D version of the same analysis program, considering two types of loading modes: acting force at the pile head and translation of the whole pile body. Results were collated, anticipating depth factor and analyzed using the Genetic Algorithm (GA) code in MatLab.

Finally, the derived equations were employed in models created in a structural analysis program, SAP 2000 and validated through three distinct field tests and three

FE models of anchor pile in Plaxis 3D. Results showed that the loading mode had a significant impact on the soil reaction due to lateral displacements and the derived equations exhibited good agreement with corresponding cases.

1.1. Aims and Objectives

This dissertation seeks to propose a novel CPT-based p-y formulation for piles in sand, specifically designed for modeling in structural analysis-oriented finite element (FE) software. Additionally, it introduces and implements an approach for predicting cone tip resistance (q_c). The rationale behind selecting this research topic is briefly discussed below.

While there are established equations based on various laboratory and field tests to define nonlinear stiffness for p-y springs, using laboratory tests for this purpose presents evident challenges, such as sample disturbance and limited representation of in-situ conditions. Constructing these springs through direct and continuous measurements via CPT is more reasonable, considering the drawbacks associated with laboratory tests and discrete measurements from other field tests (SPT, PMT, etc.). Recent rigorous numerical and experimental studies proposing CPT-based formulations for p-y spring modeling in calcareous and siliceous sands have demonstrated good agreement with field tests, particularly when the same loading mode (acting force at the pile head) is employed in deriving p-y equations. However, this loading case does not cover the full spectrum of lateral loading scenarios encountered in geotechnical engineering practice.

To unveil a new CPT-based p-y formulation for piles in sand, a designated parametric study was conducted, considering various loading modes and anisotropic stress conditions in sand. Additionally, a natural sand named Sile, characterized by its engineering properties and q_c profile obtained through a series of laboratory tests and SCE analysis, was modeled. Another distinctive aspect of is the empirical transition equation, utilizing the pressure-dependent density index, I'_D, which was verified to be more

robust in predicting the q_c profile of sand from SCE analyses' results. This equation was implemented to generate different configurations of Sile sand by varying density and K_0.

1.2. Dissertation Structure

This dissertation, structured into seven chapters, investigates CPT-based p-y formulation through a comprehensive numerical analysis framework. It is rigorously organized to address specific objectives, including prediction of cone tip resistance, determination of p-y equations for piles in sand and validation through field test data and 3D numerical models. The dissertation unfolds

Chapter 1 presents an introduction that clarifies the purpose of this study, the observed gap in the subject and how this methodological effort achieves the objectives of this study. It also mentions previous research concerning the issues encompassed by this study.

Chapter 2 presents a literature survey covering previous researches on laterally loaded piles, the Winkler spring method, the so-called p-y method, cavity expansion theory and CPT-based approaches. Greater emphasis is placed on soils classified as sand following the extent of the study.

Chapter 3 presents an investigation of numerical prediction methods of cone tip resistance, q_c and a set of FE analyses that model spherical cavity expansion in widely used sands, Ticino and Toyoura and sand examined by this study, Sile. By the verified FE models, q_c profiles will be used in the parametric study in the subsequent chapter.

Chapter 4 presents a derivation of CPT-based p-y formulations by an extensive parametric study. Results from 3D FE analyses are processed using the Genetic Algorithm code (GA) to establish the equations considering different loading modes and depths and examine the effects of relevant parameters.

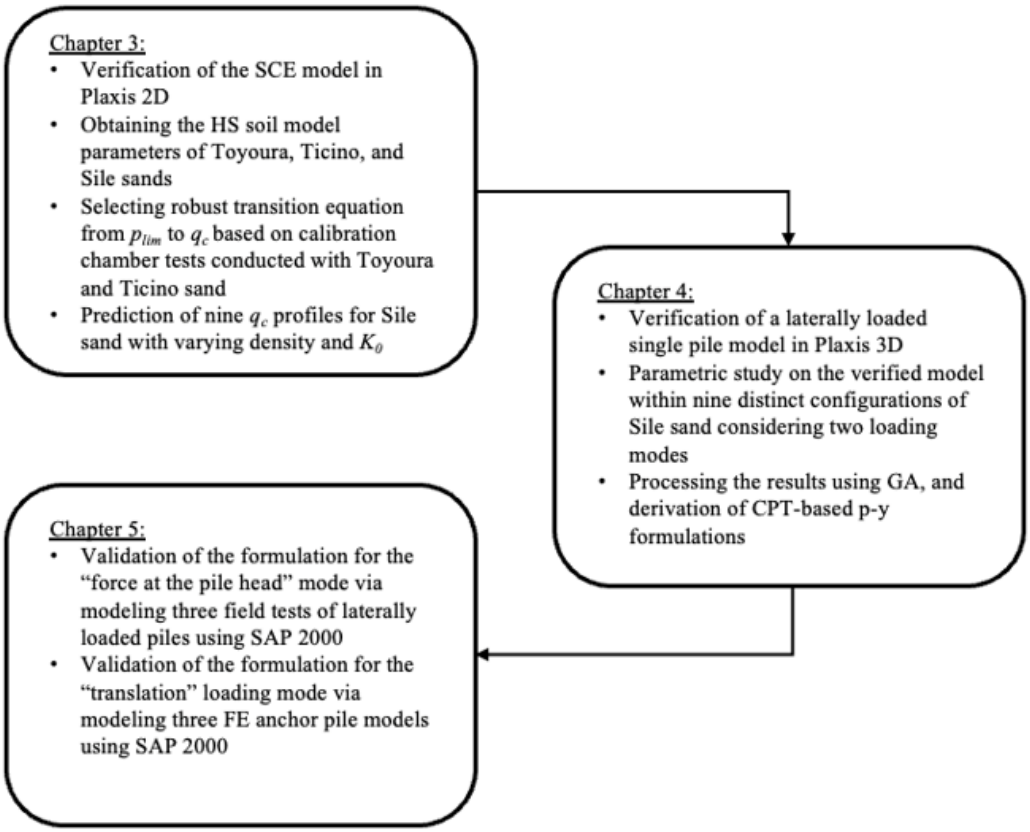

Figure 1.1. Flowchart of the dissertation structure.

Chapter 5 presents validation attempts for derived equations through field test data of lateral load testing on single piles provided in the literature and 3D numerical models of anchor piles. The derived equations, together with the equation suggested by API and a CPT-based equation proposed by Wang *et al.* (2022), are implemented on a structural modeling FE software SAP 2000.

Chapter 6 summarizes the findings throughout the dissertation. Following that, Chapter 7 presents a conclusion for the dissertation.

2. LITERATURE REVIEW

2.1. Cone Penetration Test

The cone penetration test, CPT, which has recently become one of the most widely used in-situ tests in geotechnical engineering, was first used in the 1950s. It was invented at the soil mechanics laboratory of Delft for use in determining soil bearing capacity. Its early design had mechanical devices measuring total resistance while pushing a cone into the ground. In the following decades, the equipment has been developed. A friction sleeve was adopted; thus, determination of cohesive strength was enabled. Electronic measurements and electric cones were acquired. Using electrical sensitive load cells led the equipment to collect continuous and substantially reliable data in a soil stratum.

Today, standard CPT equipment with essential components, as illustrated in Figure 2.1 can measure three main forces separately. One of them is cone tip resistance, q_c, as a product of the total force acting on the cone divided by the surface area of the cone. The other one is the sleeve friction, f_s, which is the result of the total force acting on the sleeve divided by the surface area of the sleeve. The third significant magnitude measured via CPT is the pore pressure, u.

As seen in Figure 2.1, the pore pressure is measured in three different locations on the penetrometer. Depending on the type of penetrometers, pore pressure transducers in these locations are all employed, or one or two are employed. In common practice, pore pressures measured on the cone are named u_1, at the shoulder of the cone, u_2 and behind the sleeve, u_3 (Lunne *et al.*, 2002).

Besides electric (CPT) and piezocone (CPTU) cone penetrometers that measure cone tip resistance, sleeve friction and pore pressure, there is another type of penetrometer called seismic cone penetrometer (SCPT/SCPTU). This type of CPT

provides shear wave velocity and P-wave velocity by sensors on a rod attached behind the cone penetrometer. Hence, as White (2022) mentioned, many advances have been made in CPT equipment regarding delivery, deployment, sensing, motion and the size of the equipment.

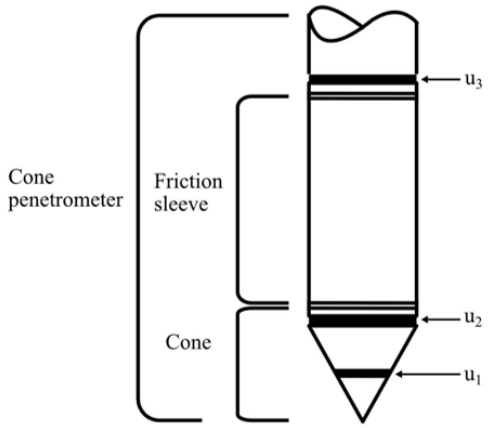

Figure 2.1. Main components of a cone penetrometer.

The test is run off by delivering the equipment mounted on various craft, such as a vessel, a truck, or a drone with recent technology. The penetrometer is pushed into the ground at a specified rate (1.5-2.5 cm/s), as depicted in Figure 2.2. A typical cone has a surface area of 10 cm^2 and a diameter of 35.7mm (White, 2022). As the cone advances down through the ground by means of a hydraulic ram, data from sensors, transducers and load cells are collected at 2-cm intervals.

There are three significant purposes for using the CPT for site investigation (Lunne *et al.*, 2002):

(i) to determine soil profile,
(ii) to obtain geotechnical engineering parameters and,
(iii) to lead direct geotechnical design.

Even though the CPT is sufficient for these purposes in the land with uniform geology and verified stratum, some other laboratory and in situ tests are cautiously undertaken. It will clarify soil type and verify CPT data for emergent soils.

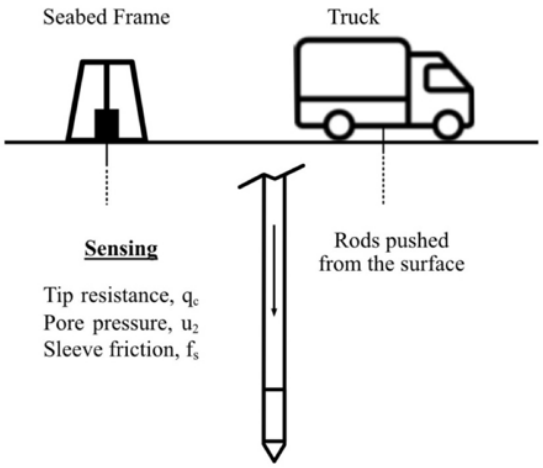

Figure 2.2. Onshore and offshore CPT systems.

CPT and its variety of types have been approved to be more advantageous over other in situ and related laboratory tests to provide continuous and reliable data and time and cost savings. Its great range of applicability, from soils having finer grains than gravel to clays and peat and being less disruptive have made the CPT more in demand for geotechnical investigation in recent years.

2.2. Cavity Expansion Theory

Cavity Expansion (CE) in soils is essentially a boundary value problem to be solved in terms of continuum mechanics and constitutive models (Yu, 2000). A variety of soil and rock models, including elastic, elastoplastic and viscoelastic to the cavity expansion technique was employed by many researchers in cohesive and cohesionless soils due to different drainage and stress conditions (Cao *et al.*, 2001; Carter *et al.*, 1986; Chen and Liu, 2019; Cudmani and Osinov, 2001; El Naggar and El Naggar, 2012; HS Yu, 2002; Huang *et al.*, 2021; Mo and Yu, 2017; Yu and Houlsby, 1991). The use of CE theory has provided realistic and accurate solutions in a wide range of areas of geotechnical engineering application. The cone penetration test is one in situ test analogous to the CE as Bishop *et al.* (1945) proposed.

An advancing cone through the ground leads a deformation similar to an expanding cavity of an initial finite or zero radius. According to the theory, as the cavity

expands, pressure occurring in the cavity increases. And at a certain level of displacement, the pressure occurring in the cavity reaches a limit. It is referred to as the limit pressure (p_{lim}). It is subsequently correlated with the cone tip resistance (q_c) through some relationships by (Cudmani and Osinov, 2001; Randolph *et al.*, 1994a; Rodrigo Salgado Rodrigues, 1993).

Rodrigo Salgado Rodrigues (1993) studied the relationship between q_c and p_{lim} by an approximate slip line analysis based on cylindrical cavity expansion. Salgado *et al.* (1997) applied this relationship to the software they developed, namely CONPOINT

$$q_c = 2f_v p_{lim} exp(2\Delta\lambda tan\phi_\tau)\frac{(1+c_\lambda)^{\eta+1} - C_\lambda(\eta+1) - 1}{C_\lambda^2\eta(\eta+1)}. \tag{2.1}$$

The parameters, $\Delta\lambda, \lambda, \phi_\tau$ and C_λ, were described in detail by Salgado and Prezzi (2007). Ladanyi and Foriero (1998), Randolph *et al.* (1994) and Yasufuku *et al.* (2001) has emphasized that the relationship between p_{lim} and q_c could be addressed by means of the spherical cavity expansion (SCE).

p_{lim} is obtained implementing an analytical closed-form solution or numerical method considering a soil constitutive model. The following relationship by Randolph *et al.* (1994) has been constructed based on the vertical equilibrium

$$q_c = p_{lim}(1 + tan\varphi tan\alpha), \tag{2.2}$$

where φ denotes friction angle; and α equals 60^o for a standard cone.

Cudmani and Osinov (2001) presents an approach to assess the condition of cohesionless soil based on cone penetration and pressuremeter test results. The solutions for cavity expansion problems are obtained using a hypoplastic constitutive model calibrated for the same soils involved in the calibration chamber tests.

The relationship between q_c from CPT and the p_{lim} calculated for a spherical cavity is established using a shape factor

$$q_c = p_{lim} \times k_q = p_{lim} \times (1.5 + \frac{5.8(I'_D)^2}{(I'_D)^2 + 0.11}), \tag{2.3}$$

where pressure-dependent density, $I'_D = (e_c - e)/e_c - e_d$ and e, e_c, e_d denote the void ratio, the void ratio at the critical state and the void ratio at the maximum densification, respectively. Cavity Expansion Theory offers a robust framework for interpretation of CPT data and estimation of soil resistance induced by lateral displacements of piles as it is confirmed that CPT cone tip resistance (q_c) is closely related to in-situ horizontal stress (σ'_h), φ and soil's stiffness characteristics (Houlsby and Hitchman, 1988; Salgado and Randolph, 2001). Hence, it is reasonable that the behavior of the sand in proximity to a laterally loaded pile is, to a great extent, associated with the CPT q_c value.

2.3. Single Piles under Lateral Loading

The analytical methods for assessing single piles under lateral loads are generally discussed in the topics of the simplified limit equilibrium approach, continuum approach and the widely accepted discrete load-transfer approach, which is commonly known as the p-y method and of concern of this dissertation.

2.3.1. Limit Equilibrium Approach

Ultimate lateral resistance can be simply determined by conventional static approach which is a part of limit equilibrium approach and mainly considering statics of pile. The ultimate soil pressure, p_u, is calculated due to acting horizontal load and moment for a free-head single pile with an assumption that it is rigid using equilibrium forces proposed by Poulos (1980)

$$H_u = \int_0^{z_r} p_u B dz - \int_{z_r}^{L} p_u B dz, \tag{2.4}$$

$$M_u = H_u e = -\int_0^{z_r} p_u B dz + \int_{z_r}^{L} p_u B dz, \tag{2.5}$$

where H_u and M_u denote the ultimate horizontal load and moment, respectively; z_r represent the depth of rotation point; Z is any depth along the pile; B is the width of pile; L is the length of the pile.

Broms (1964) proposed a method for laterally loaded free-head and restricted driven piles in uniform cohesionless soils. For this purpose, ultimate soil resistance was investigated for rigid and long piles under conditions either plastic hinge occurred or not. Broms (1964) makes following assumptions for cohesionless soils:

- The active earth-pressure that acts from the back of the pile in the load direction is neglected.
- The passive earth-pressure, acting against the pile, equals three times the Rankine passive pressure.
- The ultimate soil resistance is not affected by the shape of the pile.
- Movement of the pile mobilizes the full lateral soil resistance.

Broms (1964) defined the distribution of the soil pressure and subsequently the bending moments occurred along the pile placed in cohesionless soils in both cases of short pile and long pile, as shown in Figure 2.3.

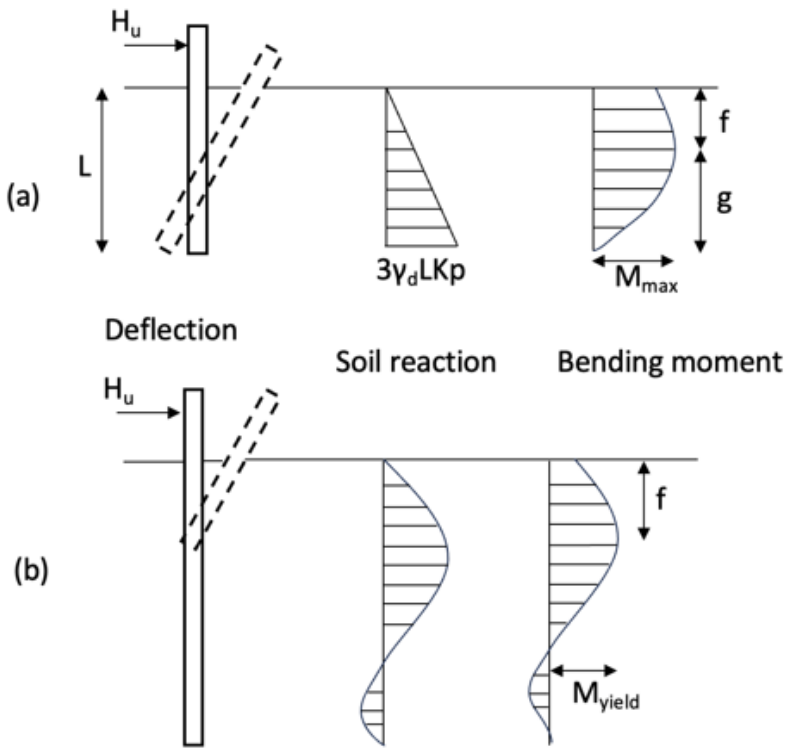

Figure 2.3. Free-head pile in cohesionless soils: (a) Short pile, (b) Long Pile (redrawn after Broms, 1964).

One of the methods covered in the limit equilibrium approach is the Brinch-Hansen method to determine the ultimate lateral soil resistance of short (rigid) piles. It can be applied to piles in layered soils, unlike the Broms method. According to this method, unit passive resistance at a depth z is calculated

$$P_z = p_{oz} K_{qz} + C K_{cz}, \tag{2.6}$$

where p_{oz} represents effective overburden pressure; C is the cohesion; K_{qz} and K_{cz} denote frictional and cohesive passive earth pressure component, respectively. The common point of all methods under limit equilibrium approach is that they all consider failure conditions of soils in which the pile is placed.

2.3.2. Elastic Continuum Approach

Elastic continuum approach is another method to assess the laterally loaded piles using either elasticity theory alone or both elasticity and plasticity theories. It covers three-dimensional analyses and two-dimensional analyses. Three-dimensional analyses provide the most realistic means of evaluating pile-soil interaction and they can be categorized into differential method analyses and integral equation (boundary element) method.

Poulos and Davis (1980) modeled a slender vertical strip with a width equivalent to the pile diameter (B), a length (L) and a constant flexibility ($E_p\ I_p$). They assumed that the emerging shear stress between the soil and the sides of the pile was zero for the simplification. The soil was modeled as a homogeneous, isotropic, semi-infinite elastic material with a Young's modulus of E_s and a Poisson's ratio of ν. The pile was discretized into n+1 elements, with each element subjected to a uniform horizontal stress p. They assumed that p is constant across the width of the pile.

Poulos and Davis (1980) asserted that the horizontal displacement of both the soil and the pile are identical, in the case that the purely elastic behavior governs in the soil. They conducted a comprehensive analysis employing the differential equation for bending of a slender beam, to find

$$E_p I_p \frac{d^4 y}{dz^4} = -pB, \tag{2.7}$$

where p denotes pressure, y stands for deflection, B for pile diameter; E_p and I_p are the pile modulus of elasticity and moment of inertia, respectively.

Solutions in finite difference forms for a free-head single pile subjected to a lateral load of H are presented by Poulos and Davis (1980) by incorporating boundary conditions and resulting matrix equations into Equation 2.7, to write

$$y = \frac{\frac{H}{E_s L}(I_{yH} + \frac{e}{L} I_{yM})}{F_y}, \tag{2.8}$$

$$\theta = \frac{\frac{H}{E_s L^2}(I_{\theta H} + \frac{e}{L} I_{\theta M})}{F_\theta}, \tag{2.9}$$

where denotes load eccentricity, I_{yH} and I_{yM} are elastic influence factor for displacement caused by horizontal load and moment; $I_{\theta H}$ and $I_{\theta M}$ are elastic influence factor for rotation induced by horizontal load and moment; F_y and F_θ are yield displacement and yield rotation factors. Poulos and Davis (1980) provides charts for I_{yH}, I_{yM}, $I_{\theta H}$ and $I_{\theta M}$ values. According to the varying conditions that involve the pile tip and top, solutions have been presented with design charts which are described in Poulos and Davis (1980).

2.3.3. Discrete Load-Transfer Approach (p-y Method)

For many types of structures such as tall buildings, bridges, near-shore and offshore structures, piles subjected to lateral loads are crucial elements to be considered during the design. The limit equilibrium and elastic continuum approaches consider that the soil around the pile deforms in an elastic range due to lateral loads acting on the piles.

The p-y method can facilitate modeling the soil behavior where the deformations exceed elastic range along the depth of the pile under lateral loads. Therefore, it has become an essential method for soil-pile interaction problems where soil lateral resistance and pile deflection are addressed to be interdependent.

Load-deformation curves, referred to as p-y curves, are created along the depth of a pile to define soil behavior due to pile deflections. Pile's shape and stiffness have no influence on the p-y curves, which represent a discrete vertical soil unit under lateral deformation. A finite difference model, in which the pile is modeled as a beam and the soil as a p-y curve, are commonly used in practice of pile design.

An isolated single pile behaves in a manner that it leads to a deformation and reaction in the soil, then the reaction in the soil has an impact on the deformation of the pile when it is subjected to a lateral loading. Therefore, both the soil properties and the pile properties play significant roles soil-pile interaction problems.

Winkler, (1867) was first to present the concept of subgrade reaction in soil mechanics. He idealized the soil foundation, namely Winkler foundation, as uncoupled springs arranged side by side and each holds a linear vertical pressure, q, per unit area against a vertical deflection, w, to write

$$k = \frac{qb}{w}, \tag{2.10}$$

where k denotes subgrade modulus of the beam. The general solution was given as

$$w = (C_1 cos\lambda x + C_2 sin\lambda x)e^{\lambda x} + (C_3 cos\lambda x + C_4 sin\lambda x)e^{\lambda x}, \tag{2.11}$$

where C_1, C_2, C_3 and C_4 are constants; λ is a parameter related to the properties of the beam and the soil combined. λ defines such an interaction between soil and beam that if the stiffness of the beam is a way greater than that of soil, any load applied on the beam deform the soil in a comparatively wide range; and if not so, it only influences the soil nearby the beam (Scott, 1981). In this context, the subgrade reaction theory is considerably dependent on relative stiffness, referred to as λ parameter and far from representing real soil behavior. Yet it constitutes the basis of soil-pile interaction.

In case of laterally loaded pile, the relative stiffness designates whether the pile is short (rigid) or long (flexible). These definitions assume a fairly intuitive perception of pile behavior; a very short and relatively rigid pile is expected to be rigidly anchored when loaded laterally, while a very long pile in the same situation is expected to exhibit a different behavior due to the increased embedment and anchoring that may occur in

this situation. There are many interconnected factors that affect the behavior of laterally loaded piles. Among these factors, pile stiffness plays a key role in determining the bending of the pile and determines whether the pile behaves like a structure that causes rotational mechanism failure, such as a short pile, or one that causes bending failure, such as a long pile. Reese (1986) studied the dependence of lateral response on pile length and observed that short piles can exhibit significant deflection at ground level when the pile tip moves, but as the depth of penetration increases, the soil resistance at the pile tip also increases and the deflection at ground level reaches a limiting value until a threshold value is reached. This length of penetration that leads to a limit ground level deflection is referred as "critical length", l_c. Therefore, a flexible pile is defined as a pile whose length is equal to or greater than its critical length. In terms of subgrade reaction theory, critical lengths have been determined, especially in cases where the horizontal subgrade modulus is constant with depth

$$l_c = \frac{\lambda}{4}, \tag{2.12}$$

$$\lambda = \sqrt[4]{\frac{k_h}{4E_pI_p}}, \tag{2.13}$$

where k_h stands for subgrade modulus for pile; E_p is Young's modulus of pile; and I_p represents second moment of inertia for pile. For a condition that the subgrade modulus linearly increases with depth

$$l_c = 4T, \tag{2.14}$$

$$T = \sqrt[5]{\frac{E_pI_p}{n_h}}, \tag{2.15}$$

$$k_h = n_h z, \tag{2.16}$$

where n_h is the constant of horizontal subgrade reaction and z is the depth.

However, the concept of critical length is universally valid and recognizes that lateral response depends on a particular mobilized soil depth, which may or may not cover the full length of the pile. Selection of a convenient subgrade modulus presents a significant challenge in solving pile design problems under lateral loading. (Terzaghi, 1955) expressed his concerns on this issue, highlighting the fundamental limitations

of subgrade reaction theory and the difficulty in determining a convenient subgrade reaction modulus value. According to Terzaghi (1955), the theory is scarcely valid for cases where pile-soil contact pressures under lateral loading are approximately half of the ultimate bearing capacity of the soil.

Emphasizing the importance of soil type and pile dimensions, he idealized stiff (overconsolidated) clay and sand soil characteristics with constant and linearly increasing subgrade reaction models, respectively. Additionally, Terzaghi (1955) briefly introduced the effect of the elastic stiffness of the pile on the subgrade reaction modulus and focused on theoretical considerations on this subject.

It is recognized by subsequently conducted studies and Terzaghi himself that the subgrade reaction theory is insufficient at some theoretical and physical points. McClelland and Focht (1958) observed that the subgrade modulus does not have a natural feature as a soil property; contrarily, it is a mathematical parameter expressing the ratio of soil response to pile deflection. Therefore, this parameter depends on a variety of factors, including pile characteristics, soil properties and how pile and soil properties change due to lateral loading.

In response to these complex concerns, design methodologies for singles pile under lateral loading have evolved that fall into two broad categories: a) Approaches that retain the basic features of subgrade reaction theory, which relate soil reaction to pile deflection using discrete, nonlinear load-transfer mechanisms along the length of the pile; and b) Approaches that treat the soil as a continuum (Dodds and Martin, 2007). Winkler (1867) was the first to introduce the discrete load-transfer approach in solving the piles under lateral loading. However, he employed linear load-transfer functions to depict soil in the solution as discussed above. Studies on the discrete load-transfer approach, namely p-y method, have been conducted in years in attempt to produce nonlinear load-transfer functions to define soil. The Winkler method is briefly examined below before delving into nonlinear load-transfer functions in cohesionless soils proposed lately.

According to the Winkler method, the soil is depicted by linear subgrade reaction modulus where the pressure is denoted as p and the deflection is y, to write

$$p = k_h y, \tag{2.17}$$

or rearranged

$$P = K.y, \tag{2.18}$$

where B is pile diameter; and units of k_h and K are force/L^3 and force/L^2.

$$K = k_h.B, \tag{2.19}$$

The pile definition is given as a differential beam equation by (Poulos and Davis, 1980) in terms of the discrete load-transfer approach, in the subsequent manner

$$E_p I_p \frac{d^4y}{dx^4} + p.B = 0, \tag{2.20}$$

$$E_p I_p \frac{d^4y}{dx^4} + k_h.By = 0, \tag{2.21}$$

where influence of axial load is not taken into account.

The axial load has little effect compared to other parameters in most cases. Nevertheless, Hetenyi (1946) utilized the axial load to derive differential beam equation, as below

$$\frac{dM}{dx} + P_x \frac{dy}{dx} - V_\upsilon = 0, \tag{2.22}$$

then considering equations from the strength of materials, the obtained equation was differentiated with respect to x, it gives

$$\frac{d^2M}{dx^2} + P_x \frac{d^2y}{dx^2} - \frac{dV_\upsilon}{dx} = 0, \tag{2.23}$$

considering equations from the strength of materials, as below

$$\frac{d^2M}{dx^2} = E_p I_p \frac{d^4y}{dx^4}, \tag{2.24}$$

$$\frac{dV_\upsilon}{dx} = p, \tag{2.25}$$

$$p = E_{py} y, \tag{2.26}$$

then the Equation (2.23) was rearranged

$$E_p I_p \frac{d^4y}{dx^4} + Px \frac{d^2y}{dx^2} - p = 0, \tag{2.27}$$

where P is the axial load that acts on the pile; y is the lateral deflection of pile at the depth x; p is the soil resistance per unit length of pile; and E_p, I_p stands for the flexural stiffness of the pile.

Assuming the soil as elastic springs with a modulus E_s, and the free-head pile as an elastic beam, (Reese and Matlock, 1956) proposed a solution for cohesionless and normally consolidated soils to obtain deflection, slope, bending moment, shear force, and soil reaction occurred in soil-pile interaction problem in case of lateral loadings

$$y = y_A + y_B = \frac{A_y H T^3}{EI} + \frac{B_y M_t T^2}{EI}, \tag{2.28}$$

$$S = S_A + S_B = \frac{A_s H T^2}{EI} + \frac{B_s M_t T}{EI}, \tag{2.29}$$

$$M = M_A + M_B = A_m H T + B_m M_t, \tag{2.30}$$

$$V = V_A V_B = A_v H + \frac{B_v M_t}{T}, \tag{2.31}$$

$$P = P_A + P_B = \frac{A_p H}{T} + \frac{B_p M_t}{T^2}, \tag{2.32}$$

where A and B constants that could be obtained by the charts provided by them.

One of the p-y methods included herein, which employs nonlinear load-transfer functions to model the soil behavior around a laterally loaded pile, was proposed by Reese *et al.* (1974). They developed a semi-empirical method to estimate p-y curves using a field test data which was a lateral loading test (both static and cyclic) of a single pile installed in a soil profile of sand and silty sand. The equation they suggested is a function of pile diameter and the properties of the sand. The test was conducted in Mustang Island, Texas. The water level was kept higher than the ground level in order to replicate an offshore case, specifically to simulate the presence of free water around the pile. Bending moments along the pile occurred due to lateral loadings were measured; additionally, the friction angle by means of laboratory tests. They provided the equations below

$$\begin{aligned} P_{ct} &= \gamma.H.[\frac{K_0.H.tan\phi.sin\beta}{tan(\beta-\phi)cos\phi\alpha} + \frac{tan\beta}{tan(\beta-\alpha)} \\ &+ K_0.H.tan\beta(tana.sin\beta - tan\alpha)K_a.B], \end{aligned} \tag{2.33}$$

$$P_cd = K_a.B.\gamma.H(tan^8\beta - 1) + K_a.B.\gamma.H.tan\phi.tan^4\beta, \tag{2.34}$$

where P_{ct} and P_{cd} represent ultimate resistance of the sand near and well below the ground surface, respectively. They provided a detailed step-by-step procedure for constructing a $p - y$ curve in sand in their published paper.

$$P = \eta AP_u tanh\left[(\frac{KZ}{\eta AP_u}y)\right], \tag{2.35}$$

$$A = 0.9 for\ cyclic\ loading, \tag{2.36}$$

$$A = 3 - 0.8\frac{z}{D}\ for\ static\ loading, \tag{2.37}$$

where P_u represents the unmodified ultimate soil resistance, A is the empirical adjustment factor and η is the shape factor. η is taken as 1.0 for circular piles, 1.5 for uniformly tapered piles.

Murchison and O'Neill (1983) expressed reservation on their research that some errors existed due to the small database. Nevertheless, the method they proposed performed better than the other methods they compared with.

API also suggests Equation (2.35) to establish p-y curves for sand by providing soil ultimate resistance, which is the value that gives the lowest result from the following equations

$$P_u = \gamma'.Z(C_1Z + C_2B), \tag{2.38}$$

$$P_u = B.\gamma'.Z.C_3, \tag{2.39}$$

where P_u represents the ultimate soil resistance; $'$ is the submerged unit weight; and B is the pile diameter. C_1, C_2, and C_3 represent coefficients determined by following equations based on ϕ'

$$C_1 = \frac{(tan\beta)^2 tan\alpha}{tan(\beta - \varphi')} + \left[K_0\frac{tan\phi'\beta}{cos\alpha tan(\beta - \phi')}tan\beta(tan\phi' sin\beta - tan\alpha)\right] \tag{2.40}$$

$$C_2 = \frac{tan\beta}{tan\alpha tan(\beta - \phi')} - K_\alpha, \tag{2.41}$$

$$C_3 = K_a[(tan\beta)^8 - 1] + K_0 tan\phi'(tan\beta)^4 \tag{2.42}$$

where

$$\alpha = \frac{\phi'}{2}; \beta = 45 + \frac{\phi'}{2}; K_0 = 0.4; and K_\alpha = \frac{1 - sin\phi'}{1 + sin\phi'}. \tag{2.43}$$

Hu *et al.*, (2022) emphasized the impact of soil layering on lateral load capacity of monopiles, unlike previous studies. They performed 3D FE analyses using a two-surface-plasticity material model and developed a design method for monopiles embedded in sand profiles. Alver and Eseller-Bayat, (2023) proposed a dynamic p-y model for cohesionless soils considering the nonlinear soil behavior as a result of an extensive parametric study. The proposed p–y model that facilitates hysteretic nonlinear soil behavior is capable of estimating the pile response accurately under earthquake excitation.

Dyson and Randolph (2001) conducted a centrifuge study to generate a CPT-based p-y formulation for pile in calcareous sand. They also investigated some several conditions regarding method of installation, pile head restraint and rate of loading and provided modification factor for those conditions. They proposed an empirical formulation

$$\frac{p}{\gamma D^2} = 1.35 \left(\frac{q_c}{\gamma D}\right)^{0.72} \left(\frac{\gamma}{D}\right)^{0.58}, \tag{2.44}$$

where q_c is the cone tip resistance; is the bulk unit weight; and D is the pile diameter. They concluded that the proposed formulation provides excellent match with the same data from which they constructed the equation. They indicated that calcareous sands must be treated separately from terrigenous sands.

Suryasentana and Lehane (2014) numerically derived a p-y formulation based on CPT cone tip resistance. They pointed that employing the existing p-y methods for piles with larger dimensions, which have been established on the data from small-scale pile tests, remained as an issue. In order to clarify this point, they perform a series of 3D FE analysis simulating a laterally loaded single pile with a wide range of pile diameter in sand. They related results with q_c using the CE analogue and generated the equation

$$\frac{p}{\gamma z D} = 2.4 \left(\frac{q_c}{\gamma z}\right)^{0.67} \left(\frac{Z}{D}\right)^{0.75} \times \left\{1 - exp\left[-6.2 \left(\frac{Z}{D}\right)^{-1.2} \left(\frac{y}{D}\right)^{0.89}\right]\right\}. \tag{2.45}$$

They compared the predicted response, using Equation (2.45), with measured responses in three lateral loading pile tests and three separate loading levels. According to convergent results, they suggest more emphasis on developing CPT-based p-y formulation for future studies.

Ariannia (2015) formulized combined p-y solutions for clay, sand and intermediate soils types based on CPT data. The PySimple3 material model was utilized within OpenSees FE software by the proposed method. The elastic stiffness, the ultimate capacity, the yield force, and the backbone shape parameter are inputs to the material model which are determined separately by CPT-based correlations proposed in the literature.

Wang *et al.* (2022) investigated large diameter, short monopiles under lateral loading. They conducted numerical analysis calibrated with field tests in order to examine the influence of pile base on soil behavior. They also presented an empirical equation

$$\frac{P}{\sigma'_v} = \left(\frac{2.7q_c}{\sqrt{\sigma'_v p_a}}\right)^{0.7} tanh\left[5\left(\frac{y}{D}\right)^{0.55}\right], \tag{2.46}$$

where P is the net lateral pressure (p/D), σ'_v is the vertical effective stress and p_a is the atmospheric pressure. They concluded that the pile base resistance has no influence on lateral response of sand and pile length to diameter ratio do not affect $p-y$ curves.

3. PREDICTION OF CONE TIP RESISTANCE

In this part of the study, upon making a relationship between cone tip resistance and lateral soil resistance, numerical prediction methods of q_c that are applicable to cohesionless soils are investigated. The recent studies in this area revealed that implementing the spherical cavity expansion theory in a FE model created in PLAXIS 2D has resulted in accurate determination of cavity expansion limit pressure, p_{lim}, values. Verified SCE models with well-known Toyoura and Ticino sand in varying densities and stress states are analyzed and the obtained p_{lim} values are used in two different empirical equations to predict q_c values and then compared to calibration chamber test results.

The convenient index has a substantial meaning of being a foundation stone of the entire study. Apart from previous studies that construct empirical relationships between q_c and lateral soil resistance using predominantly friction angle of the soil, facilitating an index considering critical state void ratio forms the basis of the second part.

3.1. Methodology

3.1.1. Numerical Modelling of SCE

PLAXIS 2D is a commercial FE code capable of creating a spherical cavity expansion model and obtaining p_{lim} for soils using non-linear constitutive models. The finite element model that represented CPT by the term of spherical cavity expansion theory was constructed by following similar procedures to those effectively implemented in (Suryasentana and Lehane, 2014; Suzuki and Lehane, 2015; Tolooiyan and Gavin, 2011; Xu and Lehane, 2008)).

3.1.1.1. Soil Model. In the beginning, an elastic, perfectly plastic soil constitutive model, Mohr-Coulomb (MC), is employed to verify the FE model of the cavity expansion using the results of the analytical closed-form solution proposed by Yu and Houlsby (1991). It is a convenient soil constitutive model for the initial assessment of soil response. MC model consists of two parts: the linear elastic, which relies on Hooke's law and the perfectly plastic part regarding the MC failure criterion. That plastic part comprises the unrecoverable part of strains in deformed soil. A fixed yield function, f, is distinctive in whether plastic strains occur. A yield function formulated by stress and strain represents a surface in principal stress space when $f = 0$. Soils exhibit elastic response if the representative stress state points in the principal stress space fall within the yield surface. The input parameters required for the MC model are shown in Table 3.1.

Table 3.1. MC input parameters.

Study Reference	**Findings**
Parameter	**Notation**
Young's odulus	E
Shear modulus	G
Poisson's ratio	ν
Cohesion	c
Friction angle	ϕ
Dilation angle	ψ

After the verification of the cavity expansion model, as discussed in Chapter 3.2, is finalized using the MC model, the Hardening-Soil (HS) constitutive model is used to predict the q_c profiles of the Ticino and Toyoura sands. The formulation of the HS model is significantly more realistic than that of the MC model. It has multiple yield surfaces that are not fixed in the principal stress space compared to the MC model. The yield surface extends when the soil starts plastic straining (Schanz *et al.* 1999). It contains a cap by which volumetric hardening takes place. The failure parameters ϕ, ψ and c defined in the MC model are also used in the formulation of the HS model. Schanz *et al.* (1999) proposed the other HS model parameters as listed in Table 3.2.

$$E = 2E_{50}\left(1 - R_f\frac{q}{q_f}\right), \tag{3.1}$$

$$E_{50} = E_{50}^{ref}\left(\frac{\sigma_3'}{p^{ref}}\right)^m, \tag{3.2}$$

the HS model utilizes a hyperbolic relationship to determine Young's modulus, E, as given in Equation (3.1), where q is the deviator stress, q_f is the deviatoric stress at failure, σ_3' is the confining pressure and p^{ref} is the reference confining pressure. p^{ref} is the value that corresponds to 50% of q_f. Mohr-Coulomb failure criterion is included in the HS model

$$sin\phi_{cv} = \frac{sin\phi' - sin\psi}{1 - sin\phi' sin\psi}. \tag{3.3}$$

According to the MC failure criterion, the critical state friction angle, ϕ_{cv}', is formulated on friction angle, ϕ' and peak dilation angle, ψ, as given in Equation (3.3).

$$sin\psi_m = max\left(\frac{sin\phi_m' - sin\phi_{cv}}{1 - sin\phi_m' sin\phi_{cv}}, 0\right) for sin\phi_m'/sin\phi' \geqslant 0.75 \tag{3.4}$$

Mobilized dilation angle, ψ_m, is used to obtain the ratio of the plastic volumetric strain rate to the plastic shear strain rate as indicated in (3.4). For the negative values of ψ_m and low mobilized friction angle, ϕ_m', ψ_m is taken as zero. Likewise, the HS model sets ψ_m to zero, so that ϕ' equals zero in terms of total stress analysis.

Table 3.2. Basic HS model parameters.

Parameter Description	**Notation**
Secant stiffness in standard drained triaxial test	E_{50}^{ref}
Tangent stiffness for primary oedometer loading	E_{oed}^{ref}
Power for the stress-level dependency of stiffness	m
Unloading/ reloading stiffness	E_{ur}^{ref}
Poisson's ratio for unloading-reloading	υ_{ur}
Reference stress for stiffnesses	p_{ref}
K_0-value for normal consolidation	K_0^{NC}
Failure ratio,	R_f

3.1.1.2. Mesh Settings. Analyses were performed in terms of axisymmetric conditions. The model shown in Figure 3.1 consisted of triangular elements, each containing 15

nodes and 12 Gauss stress points. The height of the mesh domain was 21m and the radius was 10m. Horizontal and vertical displacements were restrained at the bottom, whereas horizontal displacements were fixed at the model's left and right boundaries. The left boundary is also the axis of the model. 1m-thick dummy layer was placed on the top of the 20 m-height weightless soil deposit, which provided convenience in adjusting the stress state around the cavity at the mid-depth of the soil layer. Instead of rearranging the location of the cavity by changing the geometry of the mesh, varying the unit weight of the dummy layer enables determining the required stress magnitudes at the cavity level.

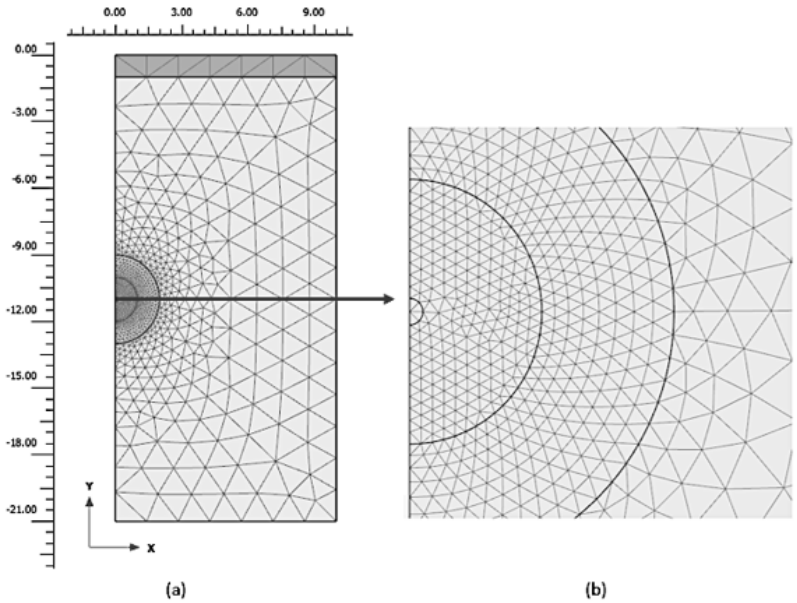

Figure 3.1. The mesh of the numerical model: (a) The entire model, (b) the mesh in/around the cavity.

Mesh was generated with a medium coarseness level for the model except for the vicinity of the cavity, which was made of two layers of half circles. It was stated by X_u (2007) that mesh coarseness did not affect the results as long as the mesh around the cavity was refined sufficiently. Accordingly, the coarseness factor was adjusted to 0.0625 around the cavity; hence, 1572 elements were generated in the mesh set-up. Nine nodes on the cavity border were selected to measure the radial displacement and ten stress points inside the cavity were selected for pressure measurement throughout the analysis, as shown in Figure 3.2.

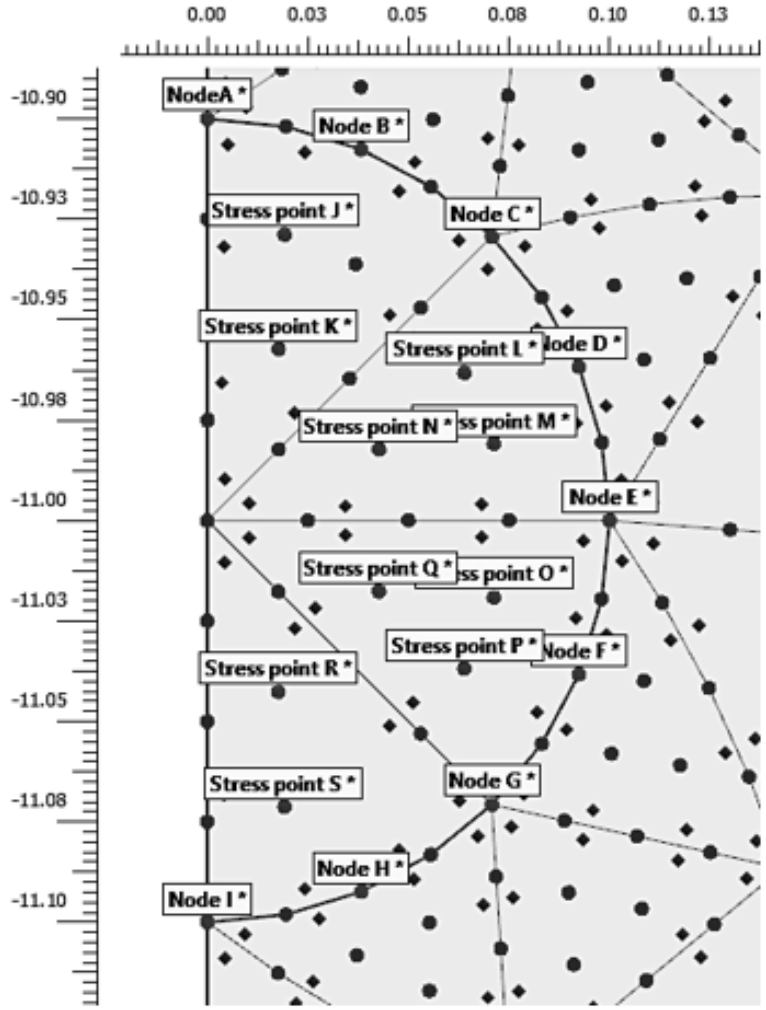

Figure 3.2. Selected stress points and nodes in the cavity to be expanded.

3.1.1.3. Analysis Procedure. SCE analysis in Plaxis2D with the defined axisymmetric mesh geometry was conducted by following these steps:

(i) A 10m x 21m axisymmetric mesh is created (details in "Mesh settings"). The cavity cluster material is defined as a Linear Elastic model with E of 2000 kPa and v of 0.2, whereas the soil around the cavity is defined as MC or HS.

(ii) Water and initial stress conditions are generated. The water level was set below the bottom of the model for all the analyses in this study. K_0 procedure is selected for the initial phase with varying K_0 values.

(iii) Nine nodes on the border and ten stress points inside the cavity are selected to measure pressure and displacement.

(iv) Two hundred fifty to three hundred fifty calculation phases in the staged construction are defined after generating initial stresses and equilibrium. A volumetric strain of 3% is defined equally in each direction to the cavity cluster for each calculation phase. The "Updated mesh" option is checked in the deformation control parameters. In numerical control parameters, "Max steps" is adjusted to 7000 to have sufficient steps to reach the limit and "arc-length control type" is turned to "Off" to avoid instability problems.

(v) After the analysis, radial displacements and maximum effective principal stresses are taken from 9 nodes and ten stress points using the curves manager in the Output program of Plaxis2D to an Excel spreadsheet. Values from stress points and nodes are averaged and then limit pressure, p_{lim}, is determined as the highest pressure value.

(vi) Finally, cone tip resistance, q_c, values are calculated from the obtained plim values using the equation given below proposed by Randolph *et al.* (1994) by Osinov and Cudmani (2001)

$$q_c = p_{lim} \times (1 + tan\phi'.tan60^o), \tag{3.5}$$

$$q_c = p_{lim} \times k_q = p_{lim} \times \left(1.5 + \frac{5.8(I'_D)^2}{(I')^2 + 0.11}\right), \tag{3.6}$$

where pressure-dependent density, $I'_D = (e_c - e)/(e_c - e_d)$ and e, e_c, e_d denote the void ratio, the void ratio at the critical state and the void ratio at the maximum densification, respectively.

3.1.2. Derivation of Hardening Soil Parameters

HS parameters of a total of three distinct types of sand, namely Ticino, Toyoura and Sile, were derived based on triaxial compression test results to be used in the numerical analyses throughout the entire study. The triaxial compression test results of Ticino, Toyoura and Sile sands were acquired from the studies of Porcino and Marcianò (2017), Fukushima and Tatsuoka (1984) and Arda and Cinicioglu (2021), respectively. A parameter optimization tool provided in Plaxis 2D, named SoilTest, was utilized to derive and optimize the parameters by defining the deviatoric stress (q)-axial strain

(ε_a) and volumetric strain (ε_v)-axial strain (ε_a) results. In Figure 3.3 and Figure 3.4, green and orange lines represent the numerical triaxial test results by the Soil Test tool conducted with preliminary and optimized HS parameters for the sand, respectively. Blue lines stand for the real laboratory test results for the related sand. The module mainly creates a finite element model of the triaxial test with specified stress, density and loading conditions with a preference for defining a range for each HS model parameter. Furthermore, it generates parameters with best-fit results concerning the real test results given as "input".

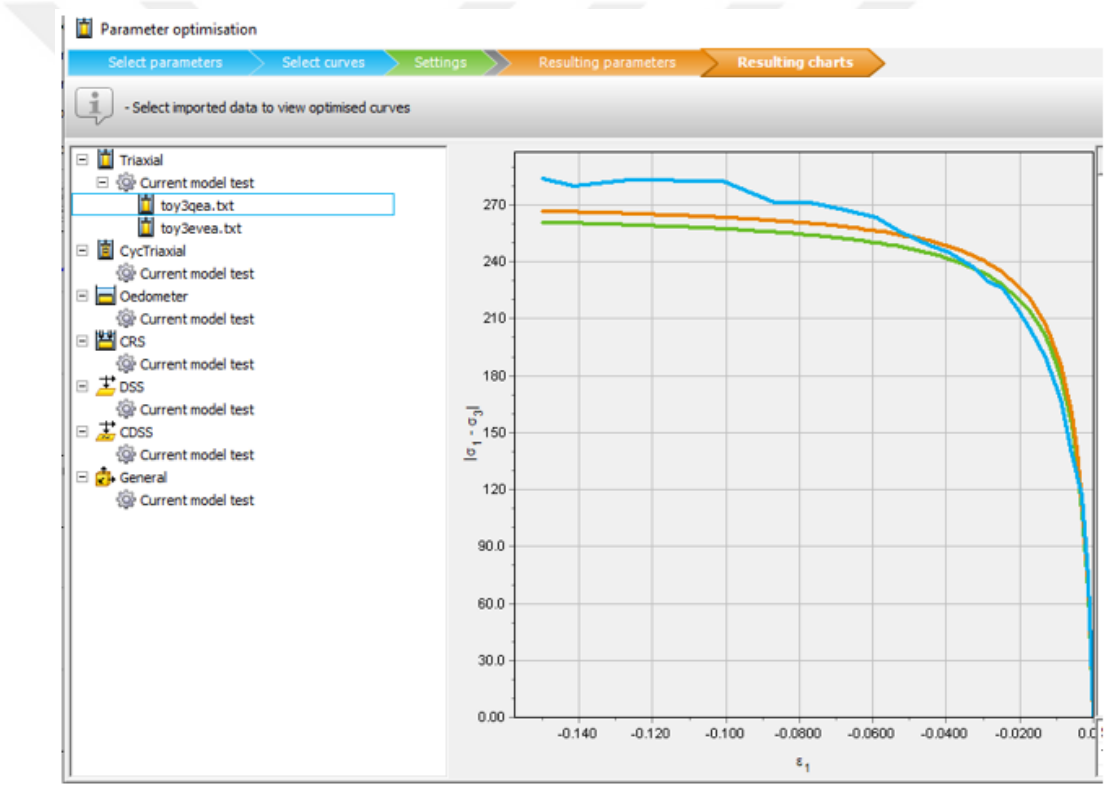

Figure 3.3. Defining deviatoric stress (q)-axial strain (ε_a) results in Soil Test.

HS parameters for Ticino and Toyoura sands were determined after an optimization process via SoilTest, as shown in Table 3.3. Alongside the SoilTest results, two FE models of the triaxial compression test, as shown in Figure 3.5, for each sand in Plaxis 2D, were created using the obtained parameters to ensure that coherent results with real laboratory tests have been acquired. The model was created in axisymmetric geometry, which confirmed the model to be a cylindrical triaxial test sample.

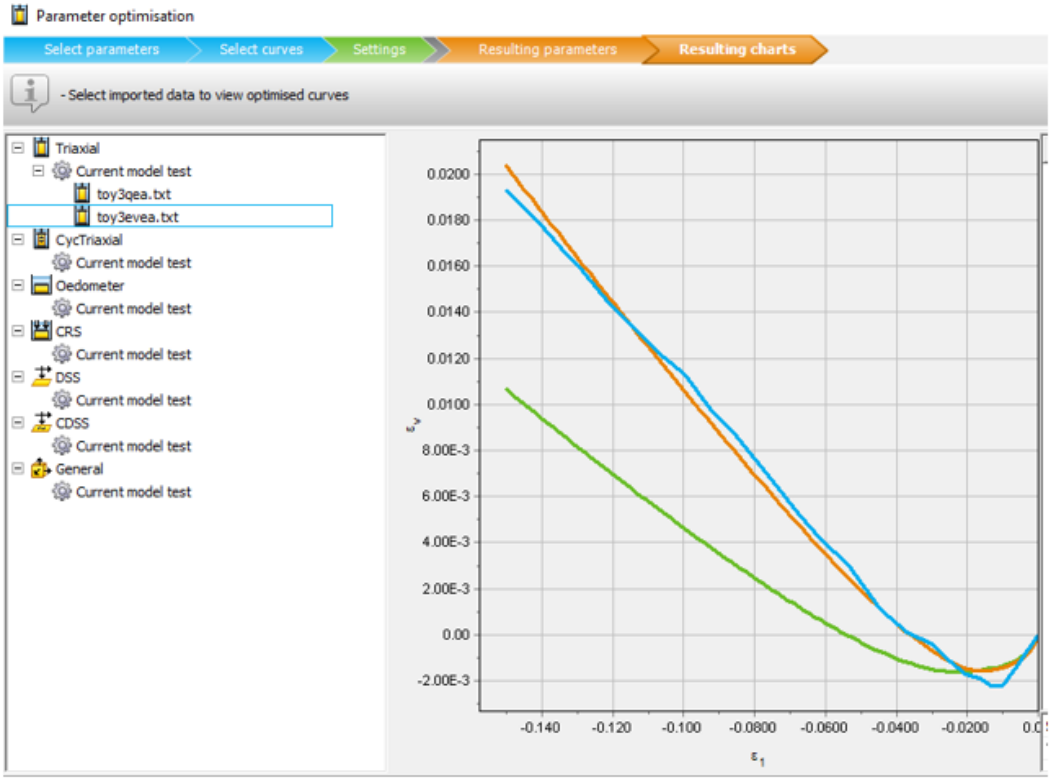

Figure 3.4. Defining the volumetric strain (ε_v)-axial strain (ε_a) results in SoilTest.

It was fixed horizontally at the left-hand side and vertically at the bottom. The uniformly distributed stress applied at the right-hand side stands for the cell pressure, σ_3 and the stress involved at the top for axial stress, σ_1, which equals σ_3 in the first analysis phase for isotropic consolidation. In the second phase, referred to as "shearing", σ_1 increases gradually until the sample fails, whereas σ_1 is kept constant.

Table 3.3. HS parameters for Ticino and Toyoura sands.

Sand	e_{min} -	e_{max} -	p'_{ref} kPa	$E_{50,ref}$ kPa	$E_{oed,ref}$ kPa	$E_{ur,ref}$ kPa	ϕ ^{o}	ψ ^{o}	c'_{ref} kPa	R_f -	υ_{ur}	m
Ticino	0.373	0.733	100	97000	25000	200000	42.40	6.60	0.00	0.90	0.20	0.50
Toyoura	0.605	0.977	100	32870	44340	101400	34.85	5.22	0.00	0.90	0.23	0.60

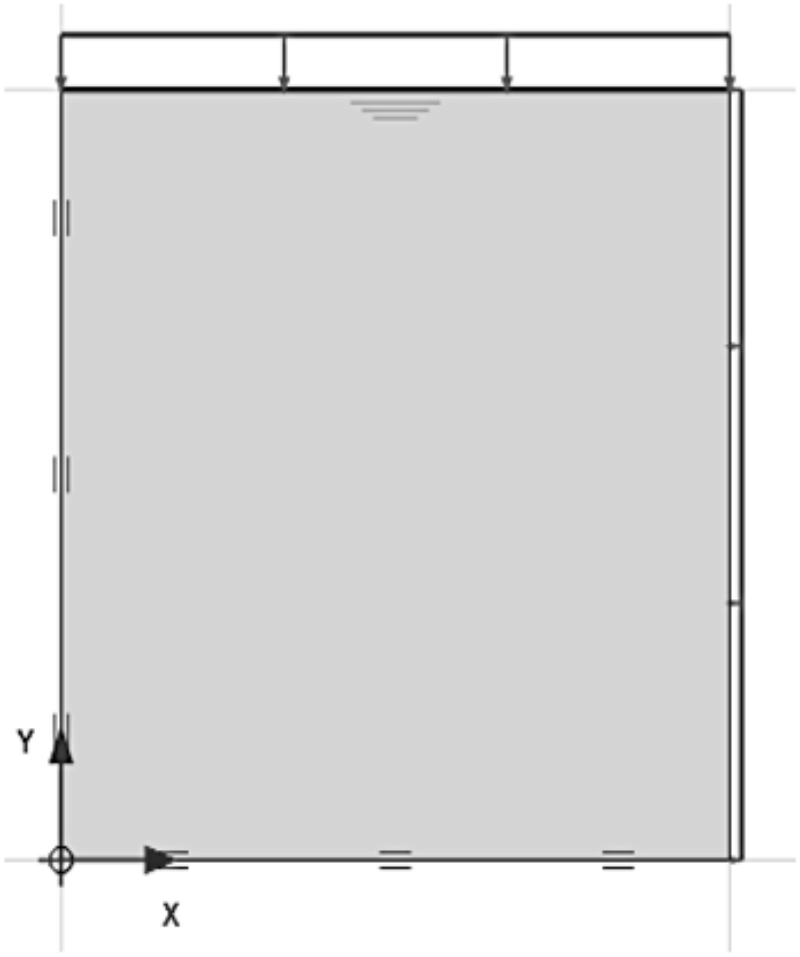

Figure 3.5. The numerical model of a triaxial compression test on Plaxis 2D.

The numerical and the real triaxial compression test results for Ticino sand are shown together in Figure 3.6. The samples with identical void ratios of 0.75 were prepared under three distinct consolidation pressures (110 kPa, 200 kPa and 300 kPa). Dashed lines show the real test results, whereas the continuous lines represent numerical test results. It is observed that the results exhibit a significant convergence between the numerical models and the real tests. Likewise, Figure 3.7 compares the results of the numerical and the real triaxial tests conducted with Toyoura sand. Tests were conducted under three consolidation pressures: 100, 200 and 400 kPa. Void ratio values were 0.4 for two samples and 0.38 for one that can be regarded as equal to the other. The results are significantly compatible for Toyoura sand as those for Ticino sand.

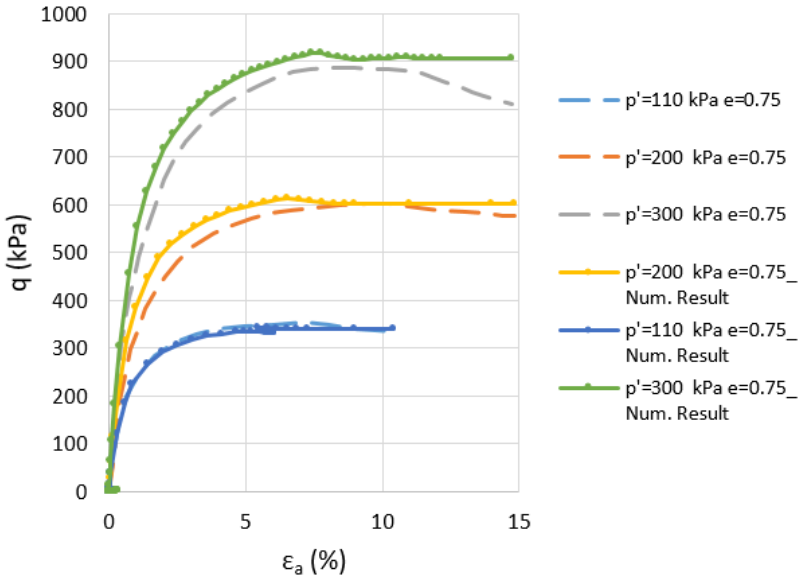

Figure 3.6. Comparison of the laboratory and the numerical triaxial test results for Ticino sand.

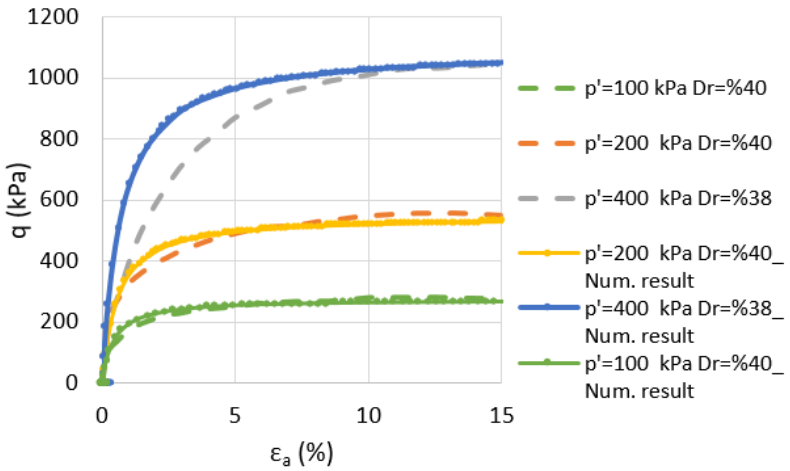

Figure 3.7. Comparison of the laboratory and the numerical triaxial test results for Toyoura sand.

3.2. Verification Analyses

The spherical cavity expansion FE model built in Plaxis 2D has been verified using a closed-form solution proposed by Yu and Houlsby (1991). p_{lim} values and pressure-expansion curves are obtained for cohesionless sands according to the Mohr-Coulomb material model by following the steps below:

(i) Mohr-Coulomb parameters for the sand $(E, \nu, c, \varphi, \psi)$ are specified with an in-situ mean effective stress (p_0). The parameter "m" is introduced to distinguish the cavity expansion whether it is spherical or cylindrical. It is taken as 2 so that the spherical analysis is concerned. It is taken as 1 in the case of cylindrical analysis. "a_0" denotes the initial cavity radius, whereas "a" is for the current radius.

(ii) The following terms are calculated with the specified parameters

$$G = \frac{E}{2(1+\upsilon)}, \tag{3.7}$$

$$M = \frac{E}{1-\upsilon^2(2-m)}, \tag{3.8}$$

$$Y = \frac{2ccos\phi}{1-\upsilon^2(2-m)}, \tag{3.9}$$

$$\alpha = \frac{1+sin\phi}{1-sin\phi'}, \tag{3.10}$$

$$\beta = \frac{1+sin\psi}{1-sin\psi'}, \tag{3.11}$$

$$\gamma = \frac{\alpha(\beta+m)}{m(\alpha-1)\beta'}, \tag{3.12}$$

$$\delta = \frac{Y+(\alpha-1)p_0}{2(m+\alpha)G}, \tag{3.13}$$

$$\eta = exp\left\{\frac{(\beta+m)(1-2\upsilon)[Y+(\alpha-1)_{p_0}][1(2-m)\upsilon]}{E(\alpha-1)\beta}\right\}, \tag{3.14}$$

$$\zeta = \frac{[1-\nu^2(2-m)](1+m)\delta}{(dx1+\nu)(\alpha-1)\beta} \; x\left[\alpha.\beta m(1-2\upsilon)+2\upsilon-\frac{m.\upsilon(\alpha+\beta)}{1-\upsilon(2-m)}\right]. \tag{3.15}$$

(iii) If the required pressure to initiate the plasticity

$$p_1 = 2mG\delta + p_{_0}, \tag{3.16}$$

greater than the current pressure, p, a current radius of the cavity is then calculated according to the small-strain elastic expression

$$\frac{(a-a_0)}{a_o} = \frac{(p-p_0)}{2mG}. \tag{3.17}$$

(iv) The cavity pressure ratio, R, is calculated with Equation (3.18)

if the case is $p_1 < p < p_{lim}$

$$R = \frac{(m+\alpha)[Y+(\alpha-1)p]}{\alpha(1+m)[Y+(\alpha-1)p_0]}. \tag{3.18}$$

(v) The following explicit expression then obtains the pressure-expansion relationship

$$\frac{a}{a_0} = \left\{ \frac{R^Y}{(dx1-\delta)^{(\beta+m)/\beta} - (\gamma/\eta)\Lambda_1(R,\zeta)} \right\}^{\beta/(\beta+m)}, \tag{3.19}$$

where

$$\Lambda_1(x,y) = \sum_{n=0}^{\infty} = A_n^1, \tag{3.20}$$

$$A_n^1 = \frac{y^n lnx}{n!} if n = \gamma, \tag{3.21}$$

$$A_n^1 = \frac{y^n}{n!(n-\gamma)}(x^{n-\gamma}-1) otherwise. \tag{3.22}$$

Iterative calculations are made on Equation (3.19) for $\frac{a}{a_0}$ to approach + to determine p_{lim}. MC parameters for three samples (MC1, MC2 and MC3) were specified in Table 3.4. These parameters were put in the closed-form solution described above and parameters for the closed-form solution were derived as listed in Table 3.5. Alongside these analytical solutions to obtain pressure-expansion curves and subsequently p_{lim} value, three spherical cavity expansion FE models were created with the same parameters. Analyses were performed as described in Chapter 3.1.1 and the results are illustrated in Figure 3.8 p_{lim} values obtained from both methods for three samples are listed in Table 3.6. The difference, at most 8.5%, is acceptable.

Table 3.4. Mohr-Coulomb parameters for three samples for verification.

Case	p_0 kPa	E MPa	υ -	c' -	ϕ' degrees	ψ degrees	m	a_0
MC1	120	100000	0.2	0.2	42	12	2	0.1
MC2	60	70000	0.2	0.2	40	0	2	0.1
MC3	120	70000	0.2	0.2	35	0	2	0.1

Table 3.5. The parameters derived by the closed-form solution.

Case	G	M	a	β	Y
MC1	41666.7	100000.0	504.468	152.497	0.89841
MC2	29166.7	70000.0	459.891	100.000	0.85780
MC3	29166.7	70000.0	369.017	100.000	0.76839
Case	γ	δ	η	ζ	p_1
MC1	144.150	0.00083	100.167	0.00224	258.05
MC2	191.679	0.00056	100.155	0.00155	125.71
MC3	205.759	0.00097	100.310	0.00309	233.74

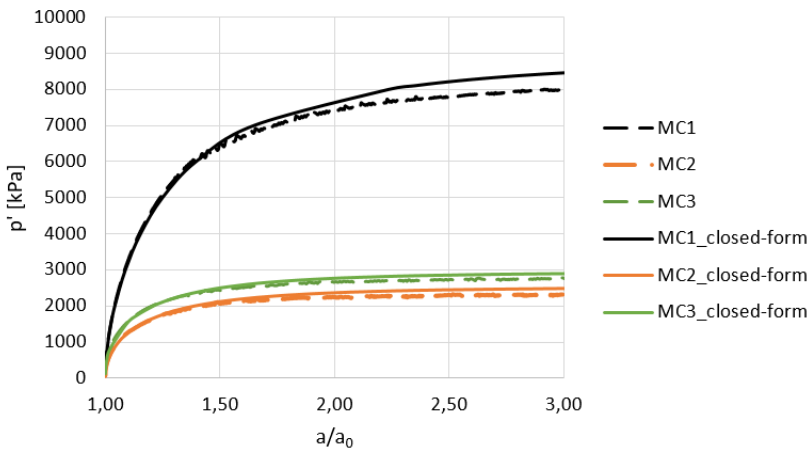

Figure 3.8. Comparisons of the results by the spherical cavity expansion FE analyses and the closed-form analytical solutions.

Table 3.6. The pressure limit values obtained by both FE analyses and the closed-form analytical solutions.

Case	p_{lim1} **(closed-form) kPa**	p_{lim2} **(Plaxis2D) kPa**	$(p_{lim2}$-$p_{lim1})$ $/p_{lim1}$ %
MC1	8910	8226	7.7
MC2	2529	2315	8.5
MC3	2943	2757	6.3

3.3. Results and Discussions

3.3.1. Comparison of Different Approaches

Fioravante and Giretti (2015) conducted calibration chamber tests with a large seismic geotechnical centrifuge, which had a potential of 600g, with Ticino and Toyoura sands in their comprehensive study. According to their experimental data, FE models were generated for spherical cavity expansion analyses for both sands with identical stress and density conditions. The initial void ratio for Ticino sand was 0.73; for Toyoura sand was 0.72 within the SCE analyses in Plaxis 2D. p_{lim} values were determined using the derived HS parameters for Ticino and Toyoura sands as described in Chapter 3.1. Figure 3.9 shows pressure-expansion curves obtained from the cavity expansion analyses made under three distinct stress states for Toyoura sand.

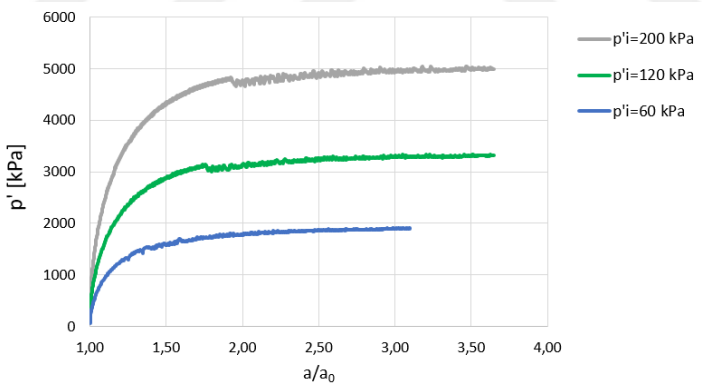

Figure 3.9. Three cavity expansion analysis results with varying initial mean effective stress for Toyoura sand.

$$q_c = p_{lim} \times (1 + tan\varphi'.tan60^o), \tag{3.23}$$

$$q_c = p_{lim} \times k_q = p_{lim} \times \left(1.5\frac{5.8(I'_D)^2}{(I'_D)^2 + 0.11}\right), \tag{3.24}$$

as the pressure-dependent density, $I'_D = (e_c - e)/(e_c - e_d), e_c$ must be calculated for each initial stress state of sands. Two empirical $e - p'$ relationships constructed based on a series of triaxial tests were utilized. For Toyoura sand, the critical state line was determined by Li and Dafalias (2000)

$$e_c = 0.934 - 0.019 \left(\frac{p'}{p_a} \right)^{0.7}, \tag{3.25}$$

where p_a denotes atmospheric pressure assumed to be 100 kPa. For Ticino sand, Fioravante and Giretti (2015) constructed a critical state line based on data from drained and undrained triaxial compression tests

$$e_c = 0.923 - 0.046 \left(\frac{p'}{p_a} \right)^{0.5}. \tag{3.26}$$

It is observed in Figure 3.10 and Figure 3.11 that the q_c values, determined numerically using Equation (3.6), exhibit more significant convergence with the calibration chamber results than those obtained from Equation (3.5) for both Ticino and Toyoura sands. According to these results, Equation (3.6) will be used in the following parts of the study.

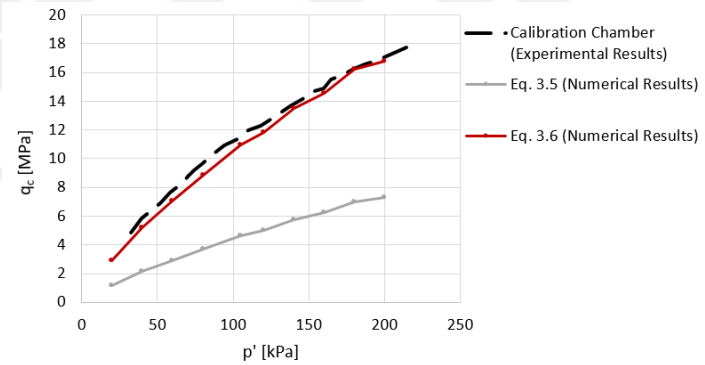

Figure 3.10. The results from calibration chamber tests and numerical analyses for Ticino sand.

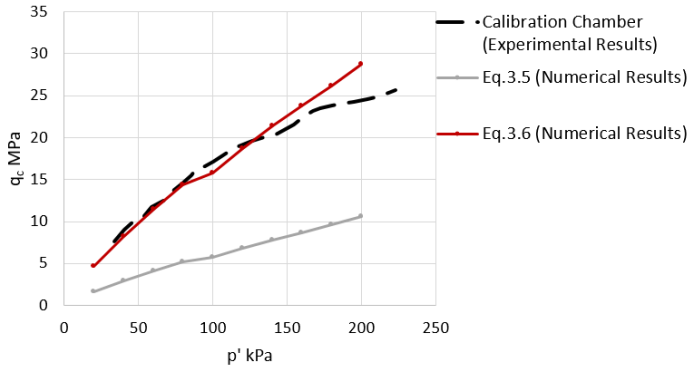

Figure 3.11. The results from calibration chamber tests and numerical analyses for Toyoura sand.

3.3.2. Prediction of Cone Tip Resistance Profile for Sile Sand

Arda (2019) and Arda and Cinicioglu (2021) studied Sile sand, a poorly graded quartz sand, with a comprehensive laboratory test program. It was collected from a district named Sile, located on the east Black Sea Coast of Istanbul, Türkiye. The physical properties are listed in Table 3.7.

Table 3.7. Physical properties of Şile sand.

Material	Median particle size D_{50}	Uniformity Coefficient C_u	Coefficient Of gradation C_c	Specific Gravity G_s	Maximum void ratio e_{max}	Minimum void ratio e_{min}	Critical State friction angle ϕ^o_{cs}
Sile sand	0.71	2.8	1.12	2.61	0.78	0.52	33.4

A series of triaxial compression tests were conducted on twelve samples of Sile sand by Arda (2019), as listed in Table 3.8. The samples were reconstituted with varying relative densities, D_r, in a range between 29 and 85 and they were consolidated under different pressures (50 kPa, 150 kPa, 250 kPa, 300 kPa). Within the scope of this study, variations in q_c with depth to be predicted for nine distinct numerical soil profiles out of Sile sand. These profiles were grouped into three categories based on relative density (loose, medium and dense), each characterized by three distinct lateral earth pressure coefficients at rest, denoted as K_0.

Table 3.8. The list of triaxial tests conducted with Sile sand.

Sample	e	D_r	Consolidation Pressure (kPa)
1	0.676	40	150
2	0.698	32	250
3	0.704	29	300
4	0.663	45	250
5	0.605	67	150
6	0.651	50	300
7	0.587	74	150
8	0.649	50	150
9	0.589	73	250
10	0.565	83	300
11	0.685	37	50
12	0.560	85	50

The HS parameters for numerical soil models of Sile sand with three different relative densities were obtained following the procedure described in Chapter 3.1.2. In addition to the parameters listed in Table 3.9, peak friction angle, ϕ_p and peak dilation angle, ψ_p, values were determined separately for each 1-m-thick layer along the depth of the soil profile with varying stress conditions. The following formula proposed by Cinicioglu and Abadkon (2015) was utilized to obtain peak dilation angle based on in-situ conditions

$$\phi_p = tan^{-1}\left[\alpha_\psi \left(\frac{p_i'}{p_\alpha}\right) + m_\psi I_D\right], \tag{3.27}$$

where a_ψ and m_ψ are referred to as material constants and calculated as -0.0352 and 0.38325 for Sile sand by Arda and Cinicioglu (2021). By using the following equation proposed by Bolton (1986), peak friction angle values corresponding to each layer of the soil model were determined

$$\varphi_p - \varphi_{cs} = r\psi_p, \tag{3.28}$$

where r represents an empirical line-fitting parameter and equals determined as 0.55 for Sile sand as a result of triaxial tests by Arda and Cinicioglu, (2021).

Table 3.9. The obtained HS parameters of Sile sand with three relative densities.

Sand	e_{min} -	e_{max} -	p'_{ref} kPa	$E_{50,ref}$ kPa	$E_{oed,ref}$ kPa	$E_{ur,ref}$ kPa	ϕ	ψ	c'_{ref} kPa	R_f -	v_{ur}	m
Loose Sile	0.52	0.78	100	45000	45000	135000	-	-	0.00	0.90	0.25	0.54
Medium Sile	0.52	0.78	100	69500	69500	208500	-	-	0.00	0.93	0.22	0.53
Dense Sile	0.52	0.78	100	79000	79000	237000	-	-	0.00	.94	0.25	0.54

One hundred eighty spherical cavity expansion analyses were conducted on Plaxis 2D to generate the 20-meter-long q_c profiles of nine numerical soil models of Sile sand. Equation (3.6) was utilized for the transition from p_{lim} to q_c as it was found to be a more robust relationship within this study.

The parameters for each layer of one profile out of nine, which is a medium-dense Sile sand with a lateral earth pressure coefficient at rest value, K_0, of 0.3, are shown

in Table 3.10. The q_c profile of the same soil is plotted in Figure 3.12. The other eight profiles that were obtained to be used in the parametric study are given in Appendix B.

Table 3.10. The parameters obtained for each layer of medium dense Sile sand numerical model with K_0= 0.3.

Layer No	Depth m	σ'_v kPa	p'_i kPa	ψ_p (Cinicioglu) degrees	$\phi - p$ degrees	e_d	e_c	e	I_D'	p_{lim} kPa	q_c kPa
1	0.5	7.7	4.1	10.4	39.1	0.520	0.740	0.654	0.391	580.00	2824.34
2	1.5	23.2	12.4	10.3	39.0	0.520	0.732	0.654	0.367	1139.00	5344.03
3	2.5	38.7	20.6	10.1	38.9	0.520	0.727	0.654	0.351	1690.00	7718.40
4	3.5	54.2	28.9	10.0	38.8	0.520	0.723	0.654	0.339	2241.00	9996.05
5	4.5	69.7	37.2	9.8	38.7	0.520	0.719	0.654	0.327	2619.00	11427.10
6	5.5	85.1	45.4	9.6	38.7	0.520	0.716	0.654	0.317	2997.00	12800.48
7	6.5	100.6	53.7	9.5	38.6	0.520	0.714	0.654	0.308	3356.00	14035.77
8	7.5	116.1	61.9	9.3	38.5	0.520	0.711	0.654	0.298	3715.00	15214.69
9	8.5	131.6	70.2	9.1	38.4	0.520	0.709	0.654	0.290	4008.50	16073.39
10	9.5	147.1	78.4	9.0	38.3	0.520	0.706	0.654	0.281	4302.00	16884.35
11	10.5	162.5	86.7	8.8	38.2	0.520	0.704	0.654	0.273	4546.50	17458.00
12	11.5	178.0	94.9	8.7	38.1	0.520	0.702	0.654	0.265	4791.00	17989.47
13	12.5	193.5	103.2	8.5	38.0	0.520	0.700	0.654	0.256	5084.00	18655.44
14	13.5	209.0	111.5	8.3	37.9	0.520	0.698	0.654	0.248	5377.00	19268.38
15	14.5	224.5	119.7	8.2	37.9	0.520	0.696	0.654	0.240	5582.50	19521.10
16	15.5	239.9	128.0	8.0	37.8	0.520	0.695	0.654	0.232	5788.00	19733.72
17	16.5	255.4	136.2	7.8	37.7	0.520	0.693	0.654	0.224	6002.00	19933.65
18	17.5	270.9	144.5	7.7	37.6	0.520	0.691	0.654	0.216	6216.00	20090.49
19	18.5	286.4	152.7	7.5	37.5	0.520	0.689	0.654	0.208	6394.50	20092.20
20	19.5	301.9	161.0	7.4	37.4	0.520	0.688	0.654	0.200	6573.00	20056.48

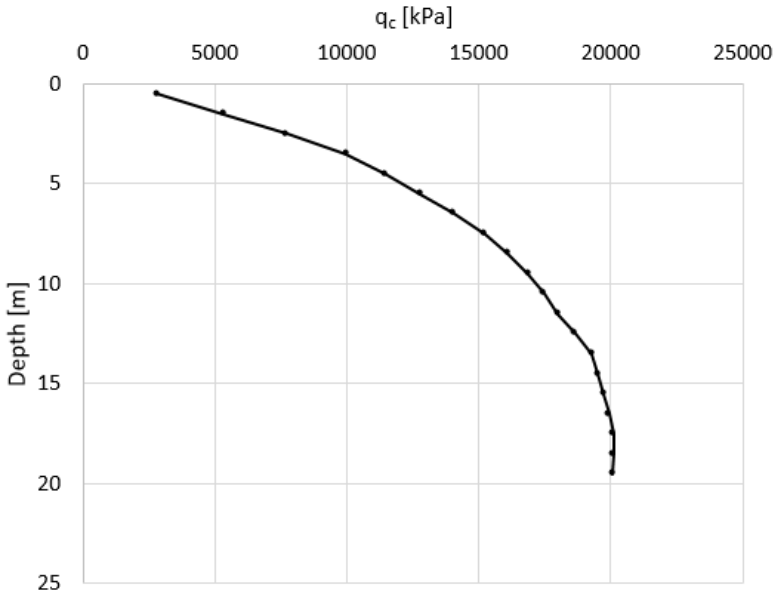

Figure 3.12. An obtained q_c profile out of nine numerical models of Sile sand: Medium dense with K_0=0.3.

4. CPT-BASED DETERMINATION OF P-Y CURVES FOR RIGID PILES IN SAND ACCORDING TO LOADING MODES

In this chapter, CPT-based empirical p-y equations for piles in sand are obtained considering different loading modes. Contrary to most of the experimental and numerical studies on laterally loaded single piles that were concentrated on the loading mode of acting a force at the pile head, a series of numerical analyses comprising both acting a force at the pile head and lateral translation of whole pile body were designed in a commercial FEM software Plaxis3D. A benchmark full-scale field test conducted in Mustang Island by Reese *et al.* (1974), a laterally loaded single pile test, was first modeled for verification. Following this, to generate the models for this study, Sile sand, which was already analyzed by the laboratory tests and for which HS parameters and q_c profiles were determined for three distinct densities and K_0 values, was used as the soil media within the numerical analyses for both loading modes. Free-head single piles used in the FE models have substantially high stiffness and can be referred to as long piles in p-y research terminology. Therefore, stress and deflection data are extracted along the entire length of the piles under conditions where no plastic hinge occurred.

Collected data are analyzed using Genetic Algorithm (GA) code in MatLab and used for optimization; hence, p-y equations are obtained for both loading modes; pile head loading and pile lateral translation. In this current section, ultimate soil resistance and effects of specific parameters are investigated alongside the determination of p-y equations.

4.1. Methodology

4.1.1. Numerical Model

The 3D FE model created in Plaxis 3D for the parametric study is shown in Figure 4.1. The model geometry is made of 25m depth, twenty-five times the pile diameter longer than the pile embedded length, 40m width (40 times the pile diameter) and 20m length considering boundary effects, as Zhang *et al.* (2016) suggested in their research.

A single circular volume pile with a constant embedded length of 20m is modeled by using one-half along the pile axis due to the symmetry condition of the whole model. The volume pile is a rigid linear elastic material with a considerably high Young's modulus of 2x108 kPa. The unit weight of the pile is taken as nearly zero so that the vertical reactions at the bottom of the pile are not of concern in this study. All properties of the pile are listed in Table 4.1.

Table 4.1. Pile properties.

Linear elastic model	**Notation**	**Pile**
Unit weight of the pile [kN/m^3]	γ	0.1
Drainage Type	-	Non-porous
Young's Modulus [kPa]	E_{ref}	2.00E+08
Poisson's ratio	ν	0.3

10-node tetrahedral elements discretize the FE model with a medium element distribution. The mesh refinement is employed by a ratio of 0.15 in a specified zone around the pile that spans 2 to 3 times the pile diameter away from the centerline of the pile. A negative interface structure is defined all around and along the half-pile model, considering a sand-pile interface is fully rough.

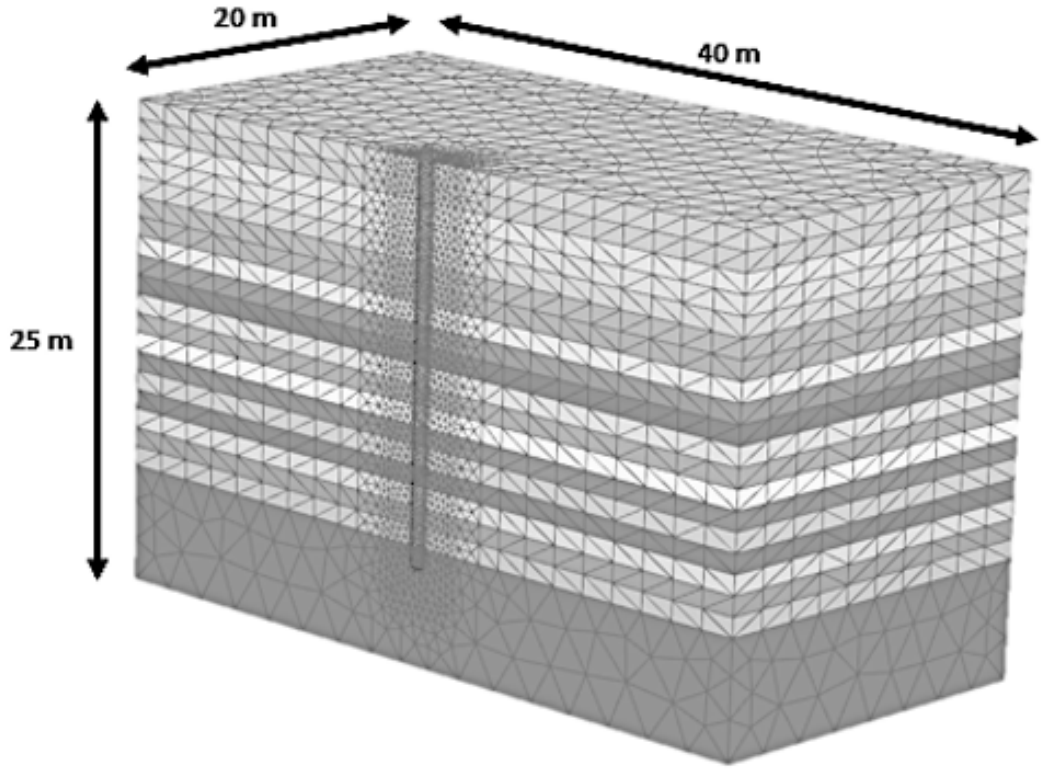

Figure 4.1. The model geometry in Plaxis 3D.

A 3D FE analysis program consisting of fifty-four analyses was carried out within the parametric study. As listed in Table 4.2, nine HS soil model profiles of Sile sand, previously established based on varying density and K_0 in the previous chapter, were used in 3D FE models with three distinct pile diameters (0.65m, 0.8m and 1.0m). Each of the nine soil model profiles of Sile sand comprises nineteen 1-m-thick soil layers and one 6-m thick bottom layer. Each layer's friction and dilatancy angles are adjusted individually due to the particular stress state and density condition using the formulas proposed by Cinicioglu and Abadkon (2015) and Bolton (1986) described in Chapter 3.3.2. Furthermore, all those FE models made of the specified pile-sand combinations were analyzed twice for two loading modes (translation of the whole pile body and acting force at the pile head). All analyses considered "Drained" and "Dry" conditions.

Table 4.2. The analysis program of the parametric study.

#	**Analysis ID**	**Loading Mode**	**Soil Density**	K_0	**Pile Diameter (m)**
1	Sile_py_K03D_P065	Translation	Dense	0.3	0.65
2	Sile_py_K05D_P065	Translation	Dense	0.5	0.65
3	Sile_py_K07D_P065	Translation	Dense	0.7	0.65
4	Sile_py_K03L_P065	Translation	Loose	0.3	0.65
5	Sile_py_K05L_P065	Translation	Loose	0.5	0.65
6	Sile_py_K07L_P065	Translation	Loose	0.7	0.65
7	Sile_py_K03M_P065	Translation	Medium	0.3	0.65
8	Sile_py_K05M_P065	Translation	Medium	0.5	0.65
9	Sile_py_K07M_P065	Translation	Medium	0.7	0.65
10	Sile_py_K03D_P080	Translation	Dense	0.3	0.8
11	Sile_py_K05D_P080	Translation	Dense	0.5	0.8
12	Sile_py_K07D_P080	Translation	Dense	0.7	0.8
13	Sile_py_K03L_P080	Translation	Loose	0.3	0.8
14	Sile_py_K05L_P080	Translation	Loose	0.5	0.8
15	Sile_py_K07L_P080	Translation	Loose	0.7	0.8
16	Sile_py_K03M_P080	Translation	Medium	0.3	0.8
17	Sile_py_K05M_P080	Translation	Medium	0.5	0.8
18	Sile_py_K07M_P080	Translation	Medium	0.7	0.8
19	Sile_py_K03D_P100	Translation	Dense	0.3	1
20	Sile_py_K05D_P100	Translation	Dense	0.5	1
21	Sile_py_K07D_P100	Translation	Dense	0.7	1
22	Sile_py_K03L_P100	Translation	Loose	0.3	1
23	Sile_py_K05L_P100	Translation	Loose	0.5	1
24	Sile_py_K07L_P100	Translation	Loose	0.7	1
25	Sile_py_K03M_P100	Translation	Medium	0.3	1
26	Sile_py_K05M_P100	Translation	Medium	0.5	1
27	Sile_py_K07M_P100	Translation	Medium	0.7	1

Table 4.2 The analysis program of the parametric study. (cont.)

#	**Analysis ID**	**Loading Mode**	**Soil Density**	K_0	**Pile Diameter (m)**
28	Sile_py_K03D_P065	Force at the pile head	Dense	0.3	0.65
29	Sile_py_K07L_P065	Force at the pile head	Loose	0.7	0.65
30	Sile_py_K07D_P065	Force at the pile head	Dense	0.7	0.65
31	Sile_py_K05D_P065	Force at the pile head	Dense	0.5	0.65
32	Sile_py_K05M_P065	Force at the pile head	Medium	0.5	0.65
33	Sile_py_K05L_P065	Force at the pile head	Loose	0.5	0.65
34	Sile_py_K07M_P065	Force at the pile head	Medium	0.7	0.65
35	Sile_py_K03M_P065	Force at the pile head	Medium	0.3	0.65
36	Sile_py_K03L_P065	Force at the pile head	Loose	0.3	0.65
37	Sile_py_K03D_P080	Force at the pile head	Dense	0.3	0.8
38	Sile_py_K03L_P080	Force at the pile head	Loose	0.3	0.8
39	Sile_py_K03M_P080	Force at the pile head	Medium	0.3	0.8
40	Sile_py_K05D_P080	Force at the pile head	Dense	0.5	0.8
41	Sile_py_K05M_P080	Force at the pile head	Medium	0.5	0.8

Table 4.2 The analysis program of the parametric study. (cont.)

#	**Analysis ID**	**Loading Mode**	**Soil Density**	K_0	**Pile Diameter (m)**
42	Sile_py_K05L_P080	Force at the pile head	Loose	0.5	0.8
43	Sile_py_K07L_P080	Force at the pile head	Loose	0.7	0.8
44	Sile_py_K07M_P080	Force at the pile head	Medium	0.7	0.8
45	Sile_py_K07D_P080	Force at the pile head	Dense	0.7	0.8
46	Sile_py_K03D_P100	Force at the pile head	Dense	0.3	1
47	Sile_py_K07L_P100	Force at the pile head	Loose	0.7	1
48	Sile_py_K07D_P100	Force at the pile head	Dense	0.7	1
49	Sile_py_K05D_P100	Force at the pile head	Dense	0.5	1
50	Sile_py_K05M_P100	Force at the pile head	Medium	0.5	1
51	Sile_py_K05L_P100	Force at the pile head	Loose	0.5	1
52	Sile_py_K07M_P100	Force at the pile head	Medium	0.7	1
53	Sile_py_K03M_P100	Force at the pile head	Medium	0.3	1
54	Sile_py_K03L_P100	Force at the pile head	Loose	0.3	1

The calculation phases of the FE analyses for both loading modes start with the "Initial Phase" where the calculation type is selected as "K_0 procedure". The initial stress state of the sand is generated here in this phase. In the second phase (Phase 1), all structures of the FE model, including pile and interface, are installed.

During the FE analyses with the loading mode of applying a force at the pile head (Figure 4.2 a), the acting of the force starts with "Phase 2" at a point 0.5m above the ground surface with a magnitude of 100 kN. Linear force increment is sustained in each consecutive phase until the model fails or till the end of "Phase 15", where the magnitude reaches 3900 kN.

For the analyses regarding the loading mode of translation (Figure 4.2 b), a prescribed lateral displacement is applied to the pile vertical surface in the positive X direction in the third phase (Phase 2). Here, the lateral displacement starts with a magnitude of 0.005m and a linear increment is applied in each phase until the end of Phase 14, where the lateral displacement reaches 0.22m.

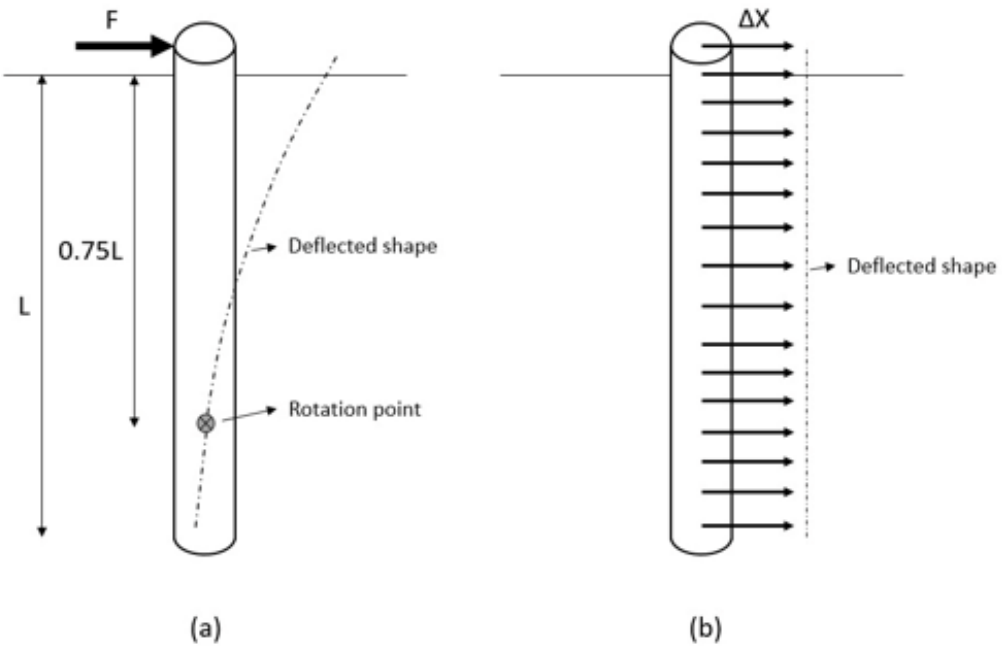

Figure 4.2. Loading modes of analyses: (a) acting a force at the pile head, (b) lateral translation of the whole pile body.

4.1.2. Deriving Soil Resistance (p) and Displacement (y) Values

The pile model is created with interface elements all around. The interface elements between the volume pile and the soil contain stress points and nodes. The 20m-long half-pile model generated in this study has 540 interface elements, with six stress points on each, as shown in Figure 4.3.

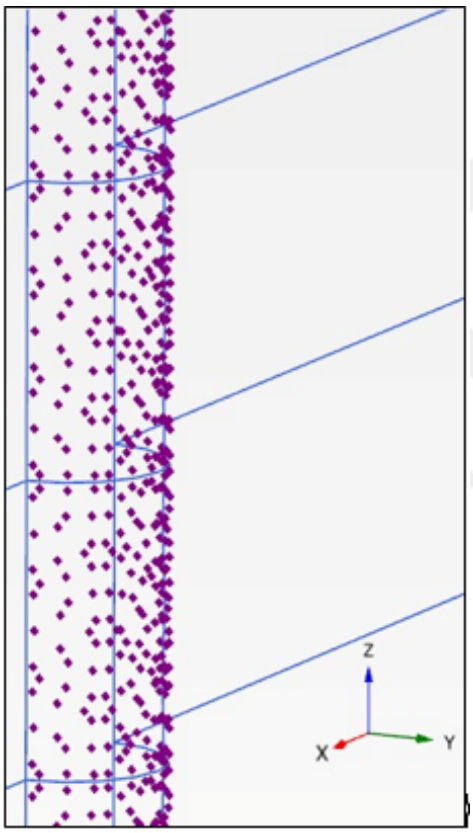

Figure 4.3. Stress points on interface elements on the pile model.

The stress points on the interface elements have three stress components due to horizontal loading or translation of the pile, as depicted in Figure 4.4. These are:

(i) The effective normal stress (σ_N)
(ii) The horizontal shear stress (τ_1)
(iii) The vertical shear stress (τ_2)

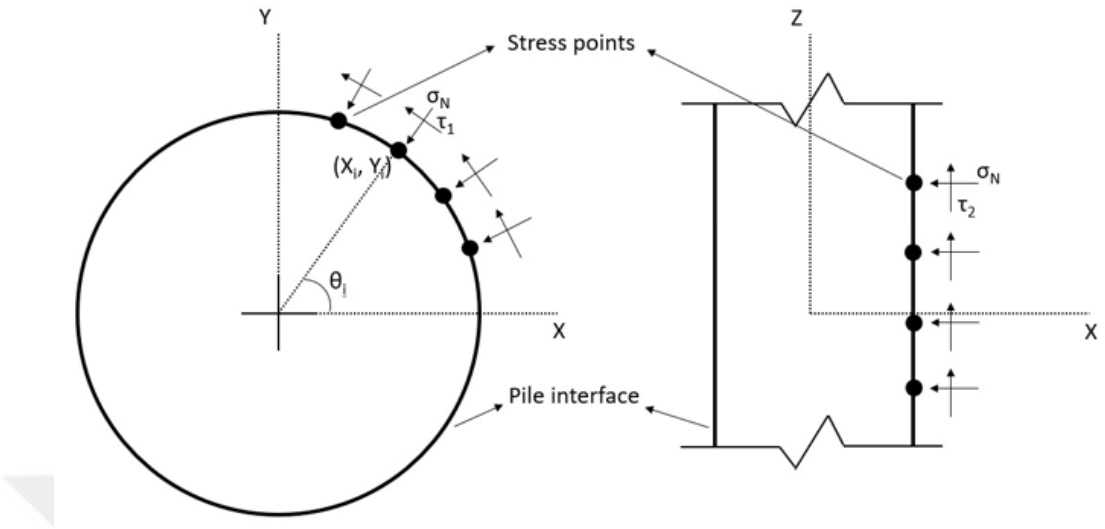

Figure 4.4. Stress components of stress points on the interface elements.

To obtain soil resistances (p) occurring due to loading or translation in a positive X direction, firstly, stress points on interface elements with positive X coordinates are selected and extracted into an Excel spreadsheet. They are grouped into 1-m-thick slices according to their Z coordinates. Later, σ_N, τ_1 and τ_2 developed in each stress point are subtracted for every calculation phase that applies an increment on the load

$$\sigma_{Nxi} = \sigma_{Ni} \times cos\theta_i \tag{4.1}$$

$$\tau_{1xi} = \tau_{1i} \times sin\theta_i \tag{4.2}$$

$$\tau_{2xi} = \tau_{2i} \times cot\beta \tag{4.3}$$

$$\theta_i = tan^{-1}\left(\frac{Y_i}{X_i}\right). \tag{4.4}$$

Using Equation (4.1), Equation (4.2), Equation (4.3) and Equation (4.4), horizontal components of σ_N, τ_1 and τ_2 are subtracted. "θ_i" represents the angle that σ_N and τ_1 on a stress point made with the horizontal axis and "i" denotes the stress point number. "β" represents the angle of the loading/translation that the pile is forced in case of anchor pile model analyses

$$p_{xi} = \sigma_{Nxi} + \tau_{1xi} + \tau_{2xi} \tag{4.5}$$

$$p = \frac{(\sum_{i=1}^{n} p_{xi})}{n} \tag{4.6}$$

$$P = p \times D \times H_s. \tag{4.7}$$

Lateral soil resistances, p_{xi}, for each stress point, are determined by Equation (4.5). However, τ_2 is not considered in the case of pure lateral loading/translation analyses. Then, the average of the lateral soil resistance values at each stress point obtained is calculated for the corresponding 1-m-thick pile slice by Equation (4.6). "n" herein denotes the number of the stress points within the interface of the pile slice. The calculated average lateral soil resistance, p, is then multiplied by the pile diameter, D and the height of the pile slice, H_s, the force magnitude of soil resistance for the corresponding slice is obtained by Equation (4.7).

For all three types of loading used in this study, which are applying a pure lateral load at the pile head, translation of the whole pile body and combined vertical and lateral displacement at a point that 6-m-depth of the pile, the lateral displacement, y, that a pile slice achieves is subtracted directly from the Plaxis 3D using the "Line cross-section" command. A value corresponds to the centerline and the mid-depth of the slice is recorded as "y" of the slice for the related calculation phase.

4.1.3. Determining the p-y Equations using Genetic Algorithm (GA)

3D FE results from both loading modes are first matched with the q_c profile that has already been constructed for Sile sand by SCE analysis

$$\frac{p}{\sigma'_D} = f\left(\frac{q_c}{\sigma'_v}, \frac{y}{D}, \frac{z}{D}, K_o\right), \tag{4.8}$$

$$\frac{p}{p'_0 D} = f\left(\frac{q_c}{p'_0}, \frac{y}{D}, \frac{z}{D}, K_0\right), \tag{4.9}$$

where p is the lateral soil resistance, σ_v is the vertical effective stress, D is the pile diameter, q_c is the cone tip resistance, y is lateral displacement, K_0 is the lateral earth pressure coefficient at rest, p'_0 is the mean effective stress and z is the depth.

All these parameters were measured in the same step of the analysis and examined using Genetic Algorithm code in MatLab environment, as it was employed by Gavin and Xue (2009) for reliability analysis of unsaturated soil slopes.

Along with the attempt to find a meaningful relationship between p and y, in addition to the previous studies by Dyson and Randolph (2001) and Suryasentana and Lehane (2014), K_0 was inserted into the formulations and σ'_v was replaced by p'_0 to generate a second form of formulation. Hence, the objective was to examine the potential impact of these variations on the formulations, considering the direct dependence of both q_c and the p-y problem itself on lateral earth pressure. The collated data in the Excel spreadsheet are defined into MatLab Genetic Algorithm code

$$\frac{p}{\sigma'_0 D} = \alpha_1 \left(\frac{q_c}{\sigma'_\nu}\right)^{b_1} \left(\frac{y}{D}\right)^{c_1} \left(\frac{Z}{D}\right)^{d_1} (K_0)^{e_1}, \tag{4.10}$$

$$\frac{p}{p'_0 D} = \alpha_2 \left(\frac{q_c}{p'_0}\right)^{b_2} \left(\frac{y}{D}\right)^{c_2} \left(\frac{Z}{D}\right)^{d_2} (K_0)^{e_2}, \tag{4.11}$$

where $a_1, a_2, b_1, b_2, c_1, c_2, d_1, d_2, e_1$ and, e_2 are unknown parameters. GA applies iterative calculations selecting best-fit unknown parameters among variables in the range of particular upper and lower boundaries that yield the closest result to zero for the difference between the calculated by the specified formulation and the measured $\frac{p}{\sigma'_\upsilon D}$ or $\frac{p}{p'_0 D}$. The unknown parameters are determined for each structure, given by Equation (4.11) and Equation (4.12), after the completion of these two analyses. Thus, the significance of each variable is available, besides the comparison of the calculated $\frac{p}{\sigma'_\upsilon D}$ or $\frac{p}{p'_0 D}$ with the optimized unknown parameters and the measured $\frac{p}{\sigma'_\upsilon D}$ or $\frac{p}{p'_0 D}$ values.

In the subsequent analyses, a hyperbolic tangent functional form is

$$\frac{p}{\sigma'_\upsilon D} = \alpha_3 \left(\frac{q_c}{\sigma'\upsilon}\right)^{b_3} tan\left(c_3 \left(\frac{y}{D}\right)\right), \tag{4.12}$$

where a_3, b_3, c_3, d_3 are the unknown parameters investigated by GA analyses considering the ultimate soil resistance behavior at soil levels near the ground surface. Results of both the raw functional form, Equation (4.11) and hyperbolic tangent functional form, Equation (4.13), concerning loading modes and depth, provide the final form of the CPT-based p-y equations suggested in this study.

4.2. Verification Analysis

A full-scale lateral loading test on a single pile was conducted on Mustang Island and well-reported in their studies by Reese *et al.* (1974). A FE model with an identical geometry and modeling basis to the one created for this study was generated, as shown in Figure 4.5 to verify the numerical model designed for the parametric study in Plaxis 3D.

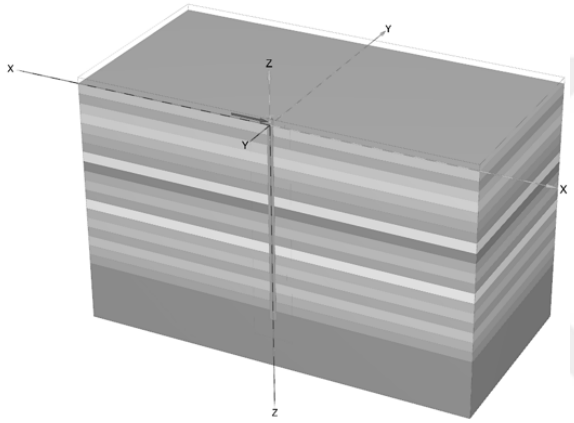

Figure 4.5. Mustang Island pile lateral loading test 3D model in Plaxis 3D.

The soil was modeled with the HS constitutive model, the parameters of which are listed in Table 4.3. In their numerical modeling, Dodds and Martin (2007) used an equivalent linear soil stiffness profile for the Mustang Island test. By following their approach, twenty-two soil layers with 1m thicknesses were created in the FE model. $E_{50,ref}$ values were calculated for each layer, referring to the midpoint level of each. The saturated unit weight, γ_{sat}, of the soil was specified as 20.4 kN/m^3 as given by Reese *et al.* (1974).

Table 4.3. Soil properties of Mustang Island sand used in the numerical model.

Sand	$E_{50,ref}$ kPa	$E_{oed,ref}$ kPa	$E_{ur,ref}$ kPa	ϕ ^{o}	ψ	c'_{ref} kPa	R_f -	vur	m
Mustang Island	25000z (z=depth in meters)	E50,ref	3E50,ref	39.0	0.0	0.0	0.90	0.33	0.50

A hollow steel pile with 0.61m width and 21m length was used in the field and with a 9.35mm wall thickness, it had a flexural stiffness of 163 MN.m^2. The pile in the numerical model in Plaxis 3D was modeled as a volume pile with a linear elastic material model. The other parameters are specified in Table 4.4.

Table 4.4. The pile parameters used in the numerical model for the Mustang Island test.

Material type	**Linear elastic model**
Drainage type	Non-porous
Unit weight of the pile [kN/m^3], γ	0.1
Young's Modulus [kPa], E_{ref}	2.40E+07
Poisson's ratio, υ	0.25
Length [m]	21
Diameter [m]	0.61

An incremental load of 22.2 kN was applied as its half in the numerical model since only half of the pile was modeled due to the symmetry condition. The location of the load at the pile head was 0.3m above the ground surface, as in the field test. The load was increased in each calculation phase up to 266.9 kN in "Phase 16" (loading was started in "Phase 2").

A load-deflection at the groundline curve was extracted, as shown in Figure 4.6 as a result of the described FE analysis. A comparison of bending moment distributions along the pile due to measurements from the field test and the FE analysis held in this study is shown in Figure 4.7. It is seen that results from the FE analysis closely match those obtained from the field test. Therefore, the FE modeling approach in Plaxis 3D constructed for the parametric study is confirmed to be valid.

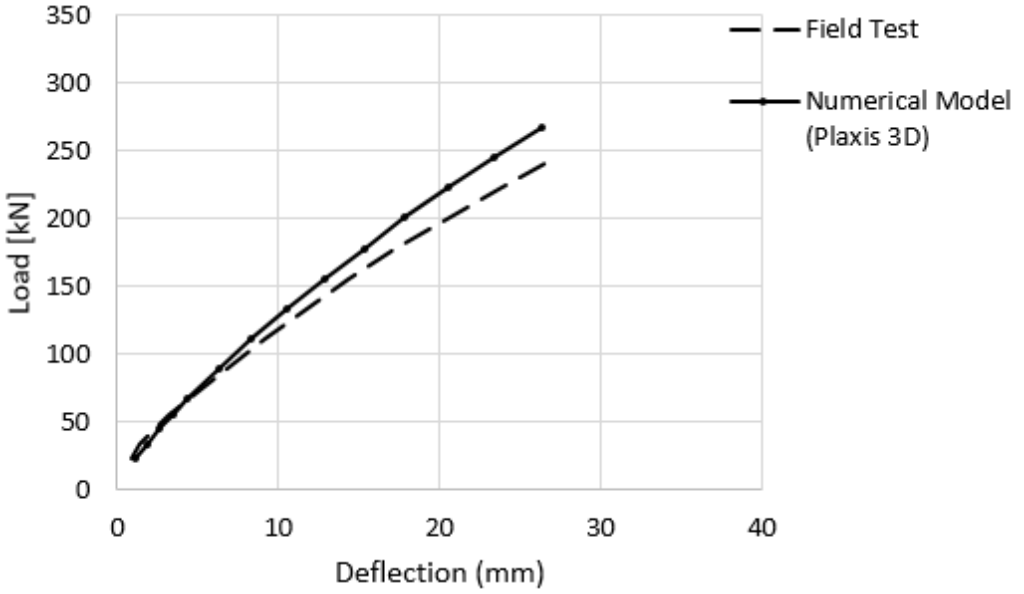

Figure 4.6. The Mustang Island test: Load-deflection at groundline results of the field test and the numerical model.

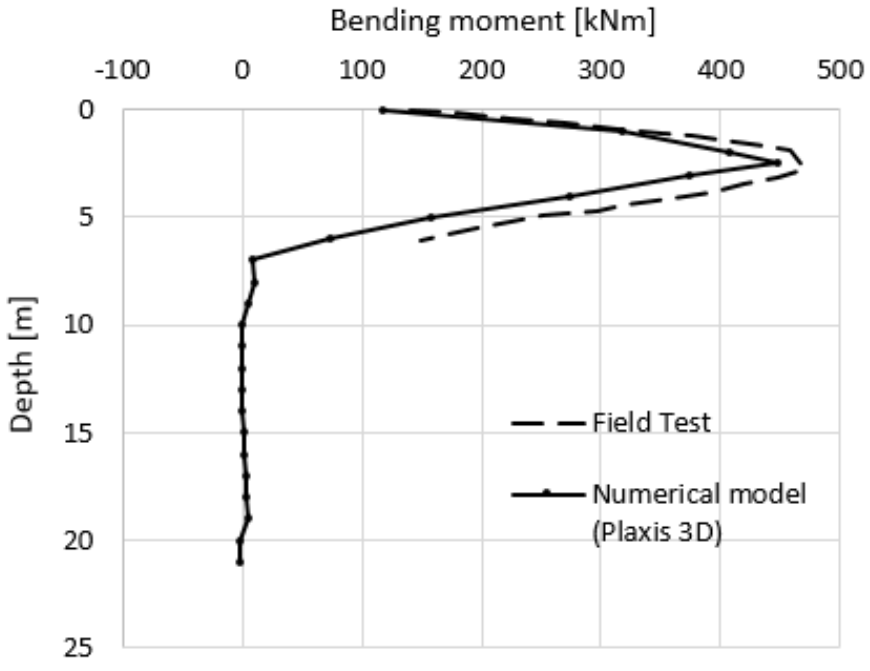

Figure 4.7. The Mustang Island test: Bending moment distribution along the pile measured from the field test and the numerical model.

4.3. Results and Discussions

4.3.1. Effects of Loading Modes on p-y Curves

Four FE analyses of two soil configurations conducted under terms of acting force at the pile head and lateral translation of the whole pile were examined to see the loading mode effect on soil resistance-deflection curves. Figure 4.8 shows the results of the FE model consisting of a 0.65m-diameter pile and dense Sile sand with K_0 of 0.3 for three depths. The observed ratio of soil resistance values from the "force at the pile head" and the "translation" modes for 0.1D deflection are 0.55, 0.56 and 0.67 for the depths of 0.5, 1.5 and 3.5m, respectively.

In Figure 4.9, the results of two FE analyses with the same soil configuration of loose Sile sand with K_0 of 0.7 are shown due to loading modes. The pile has a diameter of 1m. Figure 4.9a shows curves extracted at a depth of 0.5. The ratio of soil resistance values determined for 0.1D deflection is obtained as 0.62 at this level. The ratio, soil resistance in the "force at the pile head" mode to that in the "translation" mode is obtained as 0.69 and 0.71 at a 0.08D deflection at depths of 1.5m and 3.5, respectively, as seen in Figure 4.9b and Figure 4.9c.

The deviation observed in the parametric study between the extracted soil resistances from both loading modes corresponding to the identical lateral displacements substantiates the conclusions of Kirk *et al.* (2013). They investigated p-y curves through a series of FE analyses, modeling a 30 m-long monopile. Therefore, in establishing p-y equations, it is crucial to consider the causality resulting from the loading mode, which is the focus of this study.

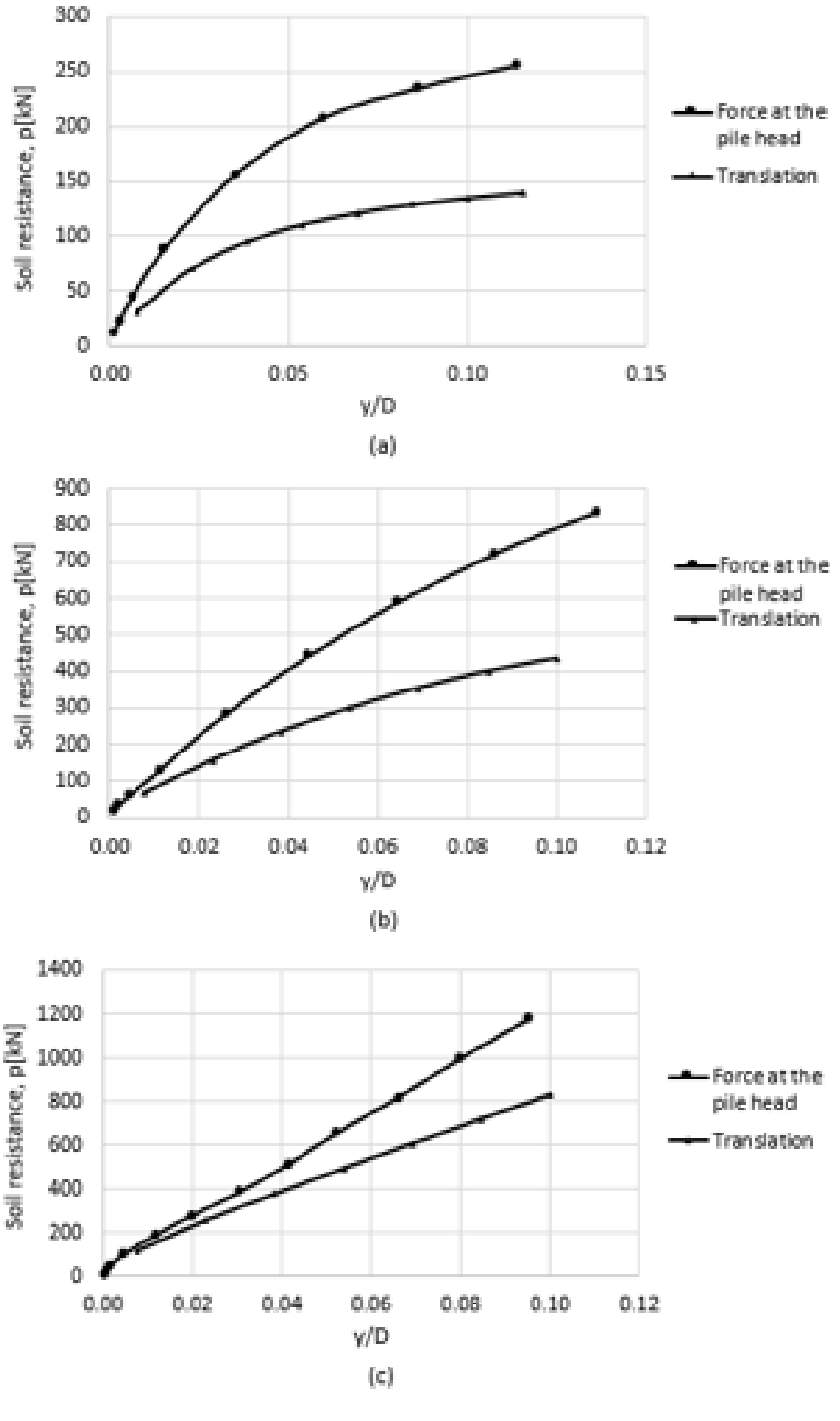

Figure 4.8. Comparison of. p-y/D curves by depth due to loading mode in dense Sile sand, K_0= 0.3, D= 0.65 m:(a) z= 0.5m, (b) z= 1.5m, (c) z= 3.5m.

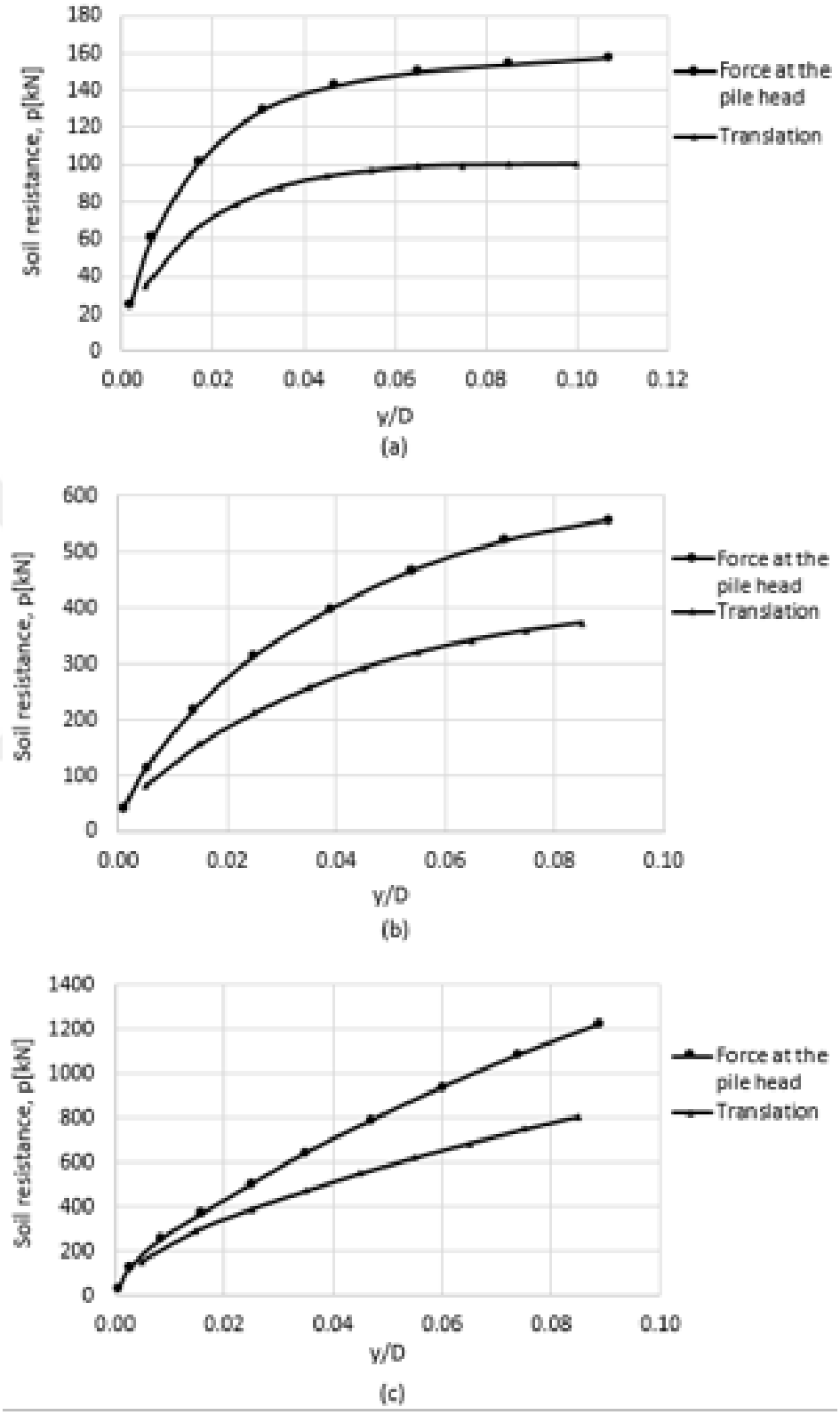

Figure 4.9. Comparison of. p-y/D curves by depth due to loading mode in loose Sile sand, K_0= 0.7, D= 1.00 m:(a) z= 0.5m, (b) z= 1.5m, (c) z= 3.5m.

4.3.2. Ultimate Soil Resistance

Preceding the derivation of CPT-based p-y formulations, the results of finite element model analyses conducted under the translation mode of loading were examined to identify the depth at which the soil around the pile reaches ultimate resistance. This investigation provided insights into the critical assessment of stress points selected for obtaining p-y equations. It emphasized the need to evaluate whether the soil near these stress points reached the ultimate level of resistance. Consequently, stress data collected along the entire pile interface were categorized into two distinct groups at a specific depth where no ultimate resistance was observed for the prescribed translation magnitude of the whole pile, set at 0.1D for all analyses. As a result, two distinct equations were derived, each yielding accurate results for the translation mode of loading.

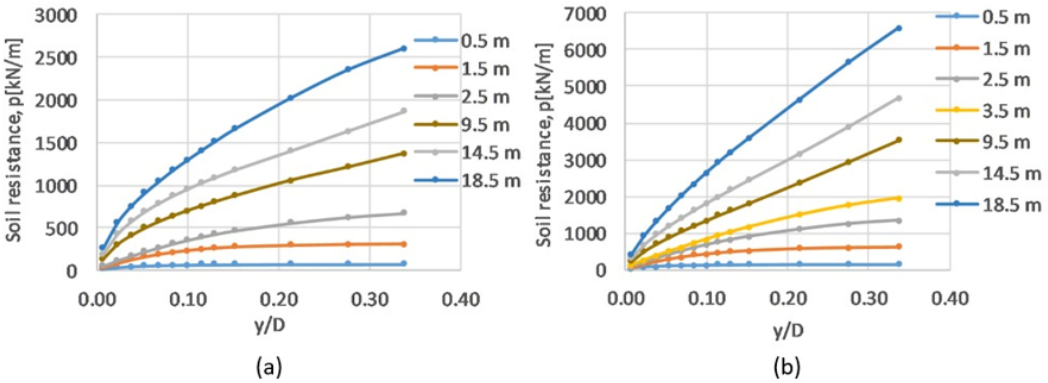

Figure 4.10. p-y/D curves by depth for parameters: (a) K_0= 0.3; D= 0.65 m; loose, (b) K_0= 0.3; D= 0.65 m; dense.

Results of two analyses using a pile with a similar diameter of 0.65m and sand with an identical K_0 value of 0.3, yet two different relative densities, are shown in Figure 4.10. The soil resistance in both analyses, conducted with loose and dense Sile sand, reaches an ultimate value at depths of 0.5m and 1.5m through successive translation loading of the entire pile body. The ultimate value at a depth of 2.5m, which is approximately four times the pile diameter, is barely detectable. It is observed that the soil resistance continues to increase with displacement for lower levels from 4D-depth.

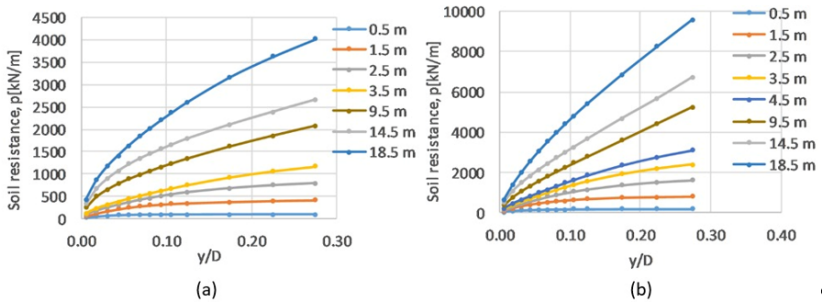

Figure 4.11. p-y/D curves by depth for parameters: (a) K_0= 0.5; D= 0.80 m; loose, (b) K_0= 0.5; D= 0.80 m; dense.

Figure 4.11 shows the results of two analyses for a pile diameter of 0.80m. Analyses were conducted in two different density configurations, i.e., loose and dense, of Sile sand with a constant K_0 value of 0.5. The ultimate soil resistance value is not observed in the displacement range of analyses at depths lower than 3.5m for both loose and dense Sile sand profiles.

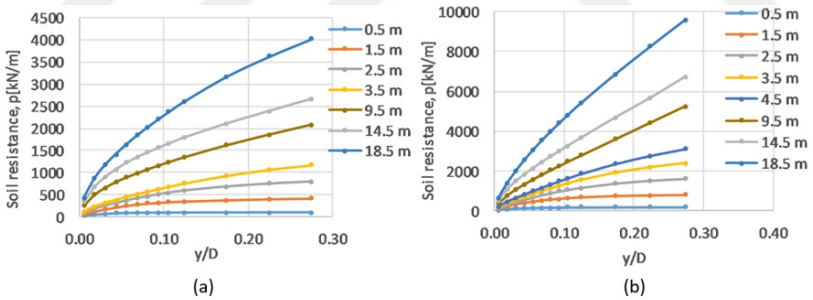

Figure 4.12. p-y/D curves by depth for parameters: (a) K_0= 0.7; D= 1.00 m; loose, (b) K_0= 0.7; D= 1.00 m; dense.

Numerical analyses for piles with 1.00 m-diameter, placed in loose and dense sand profiles with a constant K_0 of 0.7, result in similar p-y/D curves by depths, as shown in Figure 4.12. Hence, it is reasonable to assess soil resistance-deflection data in two groups, i.e., lower and higher depths than four times the diameter, according to these results among 27 analyses conducted in the "translation" mode of loading. Suryasentana and Lehane (2014) processed only the data collected from down to the 4D-depth in their research.

4.3.3. Effects of Parameters and Establishing the CPT-Based Equations

A power law format that was implemented for CPT-based equations constructed in the previous researches by Dyson and Randolph (2001) and Suryasentana and Lehane (2014) was first applied with variables

$$\frac{p}{\sigma'_v D} = f\left(\frac{q_c}{\sigma'_v}, \frac{y}{D}, \frac{z}{D}, K_0\right) \tag{4.13}$$

without any limitation or subdivision on a dataset. Results from the optimization process by Genetic Algorithm code have given a best-fit equation

$$\frac{p}{\sigma'_v D} = 9.2\left(\frac{q_c}{\sigma'_v}\right)^{0.35}\left(\frac{y}{D}\right)^{0.57}\left(\frac{Z}{D}\right)^{0.02}(K_0)^{0.017}, \tag{4.14}$$

where depth and lateral earth pressure coefficient components, $\frac{z}{D}$ and K_0 respectively, have no significant effects on p-y equations in general terms. In Figure 4.13, measured and calculated $\frac{p}{\sigma'_\nu D}$ values were compared and Equation (4.8) was found inappropriate with no limitation on specified variables. Data obtained from the analyses of the "translation" mode of loading were further used with variables shown in Equation (4.9) to investigate whether using mean effective stress, p'_0, at the vicinity of the related stress points instead of vertical effective stress, σ'_v, as used in Equation (4.7) is reasonable

$$\frac{p}{p'_0 D} = f\left(\frac{q_c}{p'_0}, \frac{y}{D}, \frac{z}{D}, K_0\right). \tag{4.15}$$

The optimization process using, p'_0, has given a resultant normalized soil resistance, $\frac{p}{p'_0 D}$, equation

$$\frac{p}{p'_0 D} = 11.1\left(\frac{q_c}{p'_0}\right)^{0.36}\left(\frac{y}{D}\right)^{0.55}\left(\frac{Z}{D}\right)^{0.0008}(K_0)^{0.002}, \tag{4.16}$$

where depth, $\frac{z}{D}$ and lateral earth pressure coefficient at rest, K_0, have negligible effect. After that, measured and calculated $\frac{p}{p'_0 D}$ values, computed using Equation (4.10), were compared in Figure 4.14 . It is observed that the data shown in Figure 4.14 , with a coefficient of determination value, R^2, of 0.8441, are more scattered than those in Figure 4.13. Therefore, further optimization efforts were undertaken, incorporating $'_v$.

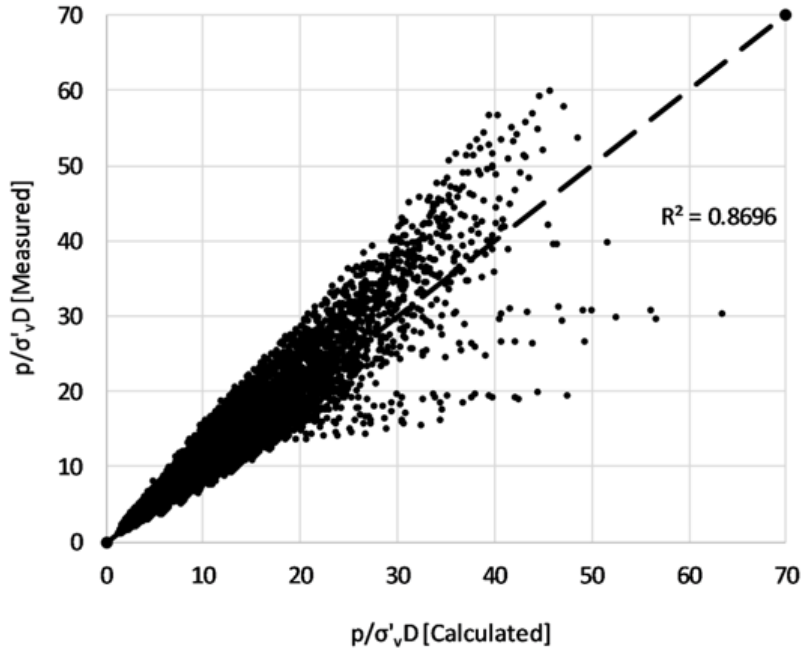

Figure 4.13. Comparison of measured and calculated normalized soil resistance values for Equation (4.8).

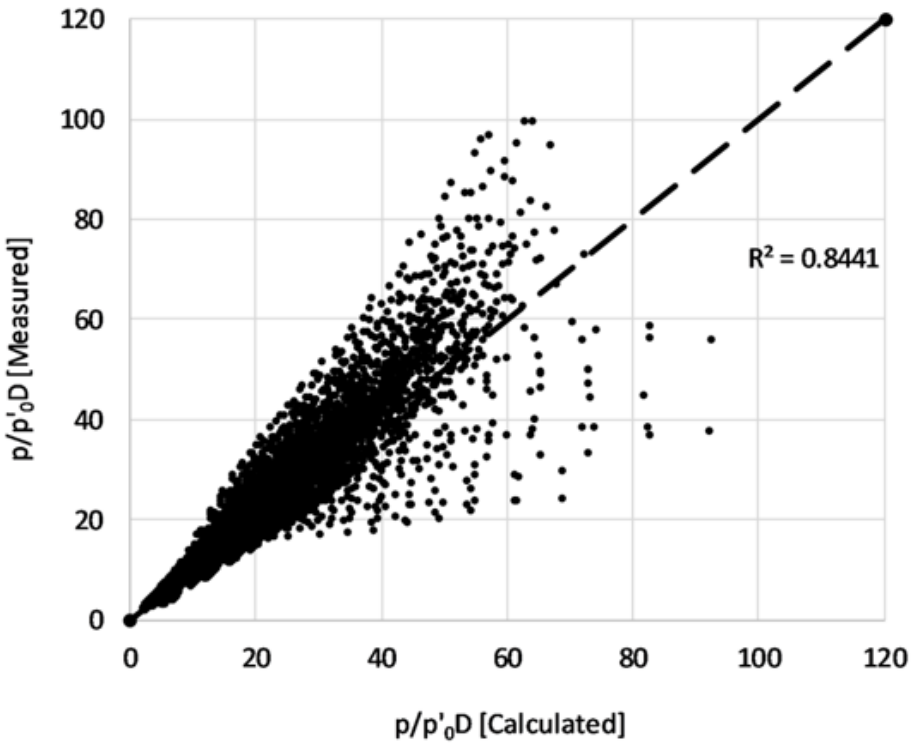

Figure 4.14. Comparison of measured and calculated normalized soil resistance values for Equation (4.10).

The optimization process was then applied to the collated data with $\frac{y}{D}$ values less than 0.1 for both loading modes aligned with previous researches (Dyson and Randolph, 2001; Suryasentana and Lehane, 2014). Firstly, an analysis based on the data from shallow depths (less than four diameters) of translation mode of loading, in which the variables K_0 and $\frac{z}{D}$ were excluded, provided a raw functional form of the p-y equation

$$\frac{p}{\sigma'_v D} = 17.5 \left(\frac{q_c}{\sigma'_v}\right)^{0.27} \left(\frac{y}{D}\right)^{0.58}. \tag{4.17}$$

However, this raw functional form fails to satisfy the soil behavior for varying ultimate resistance. In this regard, the hyperbolic tangent functional form of the equation was derived for each relevant case. For the translation mode of loading and shallow depths case, the p-y equation was determined

$$\frac{p}{\sigma'_v D} = 5.8 \left(\frac{q_c}{\sigma'_v}\right)^{0.29} tan\left(4.2 \left(\frac{y}{D}\right)^{0.66}\right). \tag{4.18}$$

The accuracy of both raw and hyperbolic tangent functional forms of equations is observed in Figure 4.15. The use of hyperbolic tangent functional form is justified, as it has a larger coefficient of determination value, R^2, of 0.874 compared to that of the raw functional form.

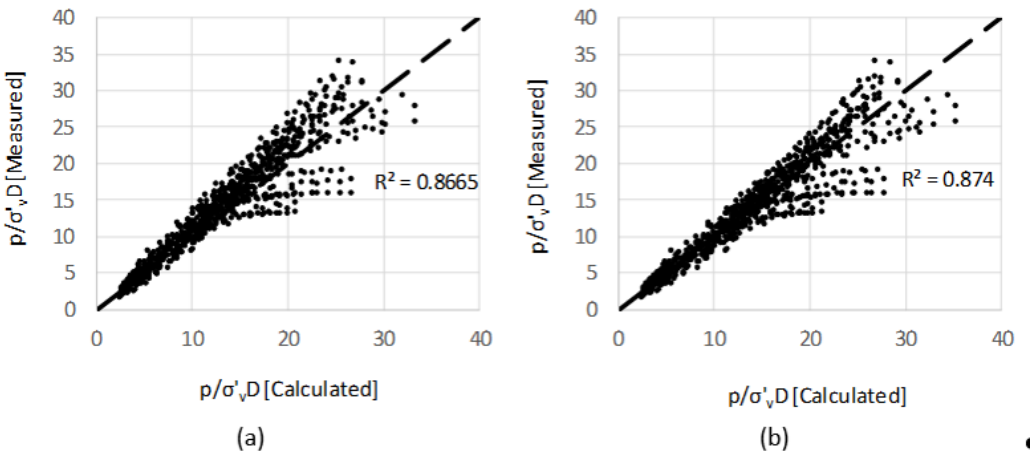

Figure 4.15. Accuracy of the obtained equations for shallow depths due to translation mode of loading: (a) raw functional form, (b) hyperbolic tangent functional form.

To obtain soil resistance-deflection curves for depths beyond four diameters, the data from corresponding stress points were also optimized using Genetic Algorithm. Subsequently, raw and hyperbolic tangent functional forms of the equation for the translation mode of loading were determined

$$\frac{p}{\sigma'_v D} = 26.1 \left(\frac{q_c}{\sigma'_v}\right)^{0.26} \left(\frac{y}{D}\right)^{0.62} \tag{4.19}$$

$$\frac{p}{\sigma'_v D} = 7 \left(\frac{q_c}{\sigma'_v}\right)^{0.29} tan\left(4.2 \left(\frac{y}{D}\right)^{0.66}\right). \tag{4.20}$$

The accuracy of Equation (4.13) and Equation (4.14) is observed in Figure 4.16a and Figure 4.16b, respectively. The hyperbolic tangent functional form has a slightly more R^2 value on a basis of linear correlation between measured and calculated values of $\frac{p}{\sigma'_v D}$.

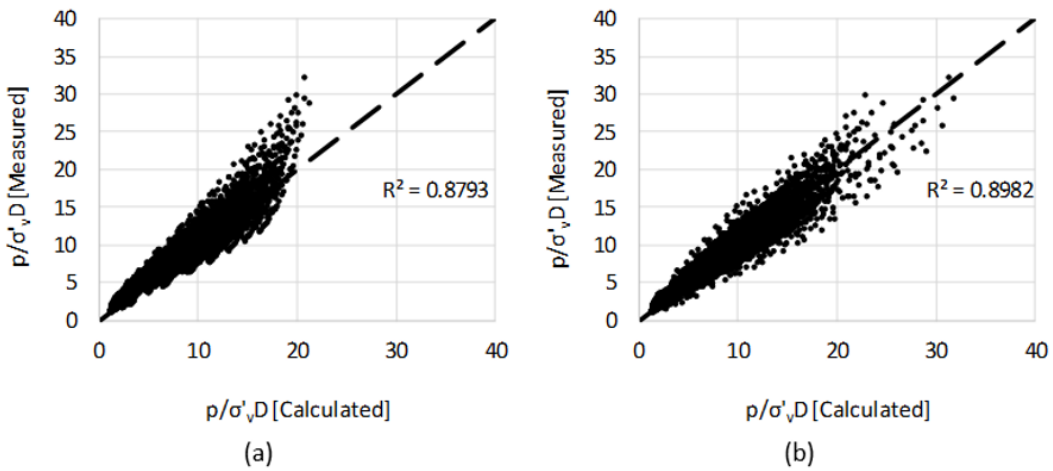

Figure 4.16. Accuracy of the obtained equations for deeper levels of depths due to translation mode of loading: (a) raw functional form, (b) hyperbolic tangent functional form.

Finally, two forms of the p-y equation were established for the loading mode of acting force at the pile head using the data from twenty-seven relevant numerical analyses

$$\frac{p}{\sigma'_v D} = 15 \left(\frac{q_c}{\sigma'_v}\right)^{0.42} \left(\frac{y}{D}\right)^{0.66}, \tag{4.21}$$

$$\frac{p}{\sigma'_v D} = 5.2\left(\frac{q_c}{\sigma'_v}\right)^{0.39} tanh\left(4.2\left(\frac{y}{D}\right)^{0.73}\right). \quad (4.22)$$

The equations exhibit significantly high R^2 values, indicating a strong linear correlation with no intercept, as depicted in Figure 4.17a and Figure 4.17b. The hyperbolic tangent functional form, which yielded an R^2 of 0.9411, was chosen to calculate the loading mode of acting force at the pile head.

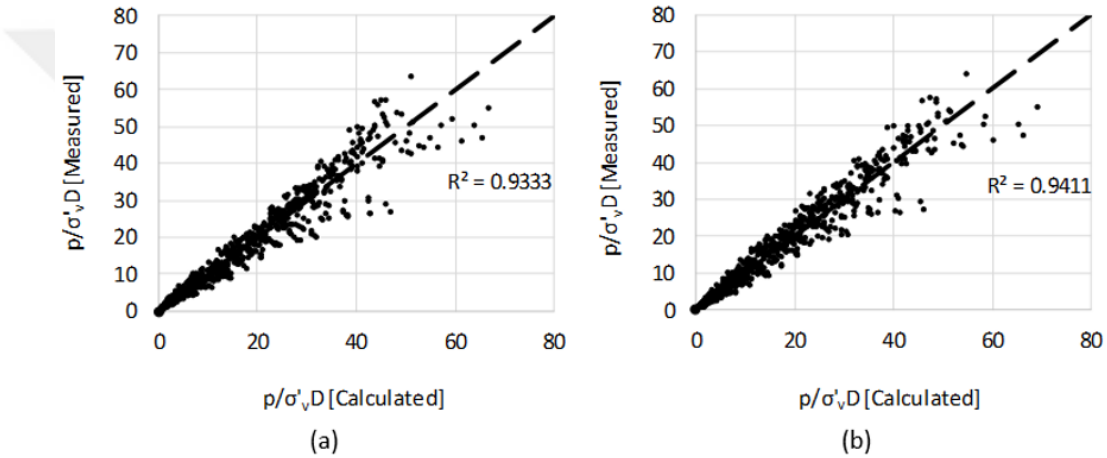

Figure 4.17. Accuracy of the obtained equations due to the acting force at the pile head mode: (a) raw functional form, (b) hyperbolic tangent functional form.

To sum up, preceding the validation chapter, three nonlinear CPT-based p-y (Equation (4.12), Equation (4.13), Equation (4.14) and Equation (4.16)) have been developed for two distinct loading modes. The $\frac{p}{\sigma'_v D}$ values, both measured and calculated using the derived equations, demonstrate a notable alignment within each grouped dataset.

5. VALIDATION OF THE DERIVED P-Y FORMULATIONS

In this chapter, three field tests involving laterally loaded piles are modeled using SAP 2000, a widely-used commercial structural FE analysis program. The simulations the CPT-based p-y equations derived in this study, the equation proposed by Wang *et al.* (2022) and the API method. Detailed information on site conditions, test setup and data from the literature is considered for these field tests. The validity of the obtained equation for the "force at the pile head" mode is confirmed and the performance of the other equations is thoroughly examined.

Additionally, three FE models representing anchor pile structures, where the 'translation' loading mode governs, are generated and analyzed first in Plaxis 3D and subsequently in SAP 2000. The lateral soil resistances due to deflections obtained from the FE analysis in Plaxis 3D are compared with those from the analyses in SAP 2000, providing validation for the derived CPT-based equation under the "translation" loading mode.

5.1. Description of Field Test Data

5.1.1. Shenton Park Test Site, Australia

5.1.1.1. Soil Condition. A series of lateral static pile load tests were carried out by Wang *et al.* (2022) to investigate the lateral response of rigid piles in the sand at the Shenton Park test site owned by the University of Western Australia. This test site has been extensively utilized in various experimental studies, leading to a comprehensive understanding of the soil conditions (Anusic *et al.*, 2019; Lehane *et al.*, 2004; Li and Lehane, 2010; Lim and Lehane, 2014). The soil profile consists of siliceous sand at depths ranging from 0 to 5m and limestone below a depth of 5m. The properties of the sand are shown in Table 5.1. The bulk unit weight and relative density of the

sand, as determined and reported by (H. Wang *et al.*, 2022), are 16.4 kN/m^3 and 64%, respectively. The groundwater table is reported to be below the sand layer.

Table 5.1. Properties of Shenton Park sand.

Material	**Median particle size** D_{50}	**Uniformity Coefficient Cu**	**Maximum void ratio** e_{max}	**Minimum void ratio** e_{min}	**Peak friction angle** ϕ_{peak} (^{o})
Shenton Park sand	0.47	2.2	0.81	0.45	38

The two CPT results provided have been averaged to obtain the profile shown in Figure 5.1. The average q_c approaches 5100 kPa at a depth of 1.5m.

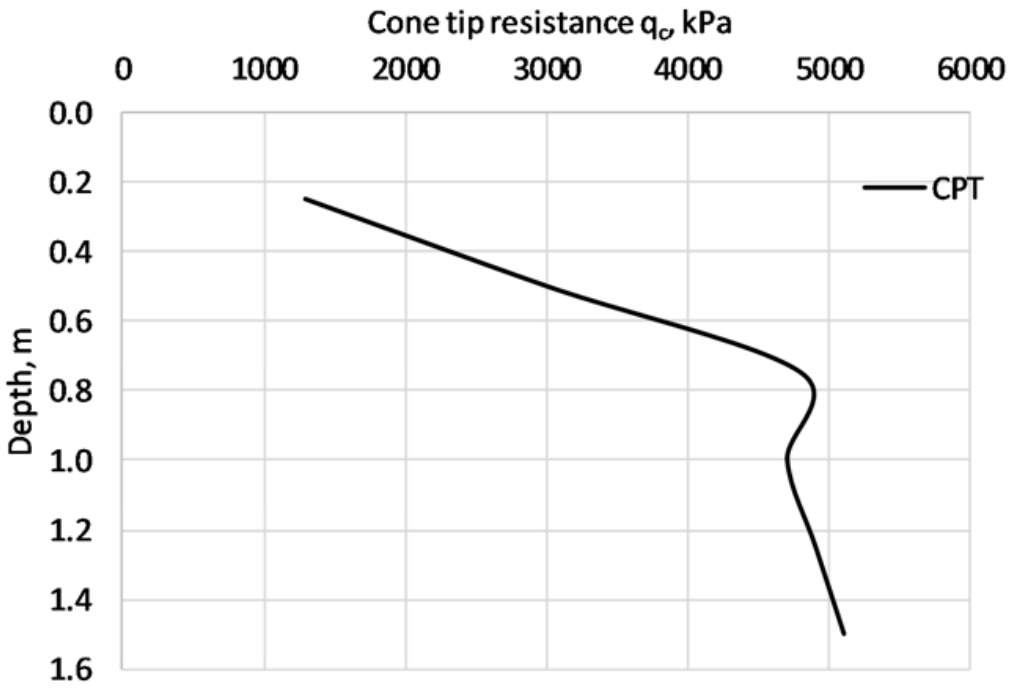

Figure 5.1. CPT q_c profile for the Shenton Park field test as an average of two CPT measurements.

5.1.1.2. Pile Properties and Load Test Description. The field test used in this validation study was conducted on a pipe with a diameter of 0.273m, an embedded length of 1.5m and a wall thickness of 6.35 mm. Strain gauges were attached along the pile

to acquire bending strains during the test. The pile was driven to the ground using an air hammer. A lateral load by means of a hydraulic jack was applied to the pile head at an elevation of 0.34m. A load cell and a linear variable differential transformer (LVDT) measured the resulting displacements and corresponding stresses.

5.1.2. Blessington Test Site, Ireland

5.1.2.1. Soil Condition. The field test was performed by (Li *et al.*, 2014) at the University College Dublin sand test bed in Blessington, Ireland. The soil profile comprises an over-consolidated sand with a bulk unit weight of 20 kN/m^3 and a relative density of approximately 100%. The median particle size, D_{50}, is 0.1mm (Gavin and O'Kelly, 2007). Peak friction angle, v_{peak}, for the sand, was measured within triaxial tests as 54^o to 42^o for the samples representing a depth of 1m to 5m. The groundwater table was reported to be 2.3m below the surface (Li *et al.*, 2014). According to the CPT measurements, q_c develops from 12000 kPa to 20000 kPa, as observed in Figure 5.2.

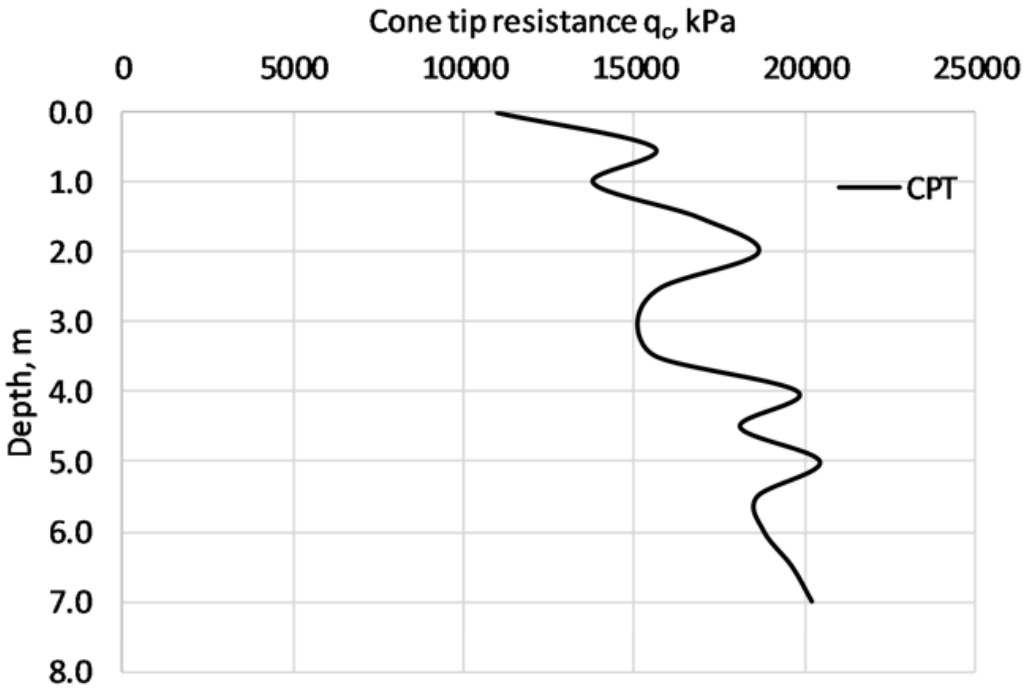

Figure 5.2. CPT q_c profile for the Blessington field test according to CPT measurements.

5.1.2.2. Pile Properties and Load Test Description. A driven open-ended pile with a diameter of 0.34m, an embedded length of 7m and a wall thickness of 14mm was used for the static lateral load test. During the test, an incremental lateral load by means of a 5 t Junntan hydraulic hammer was applied to the pile head at an elevation of 1.32m. Resulting displacements and rotations due to the applied load were measured by a load cell, an LVDT and an inclinometer.

5.1.3. Dunkirk Sand Deposit Test Site, France

5.1.3.1. Soil Condition. The test site is located at Dunkirk, in northern France. As part of the PISA study, several researches have examined this site thoroughly (McAdam *et al.*, 2020; Taborda *et al.*, 2020; Zdravković *et al.*, 2020). The sand constituting the test site is a dense marine Pleistocene deposit, known as Flandrian sand. It has a relative density of 75%. The bulk unit weight is estimated to be 17.1 kN/m^3 and 19.9 kN/m^3 above and below the groundwater table, respectively. The properties Zdravković *et al.* (2020) provide are summarized in Table 5.2. The groundwater table was observed at a depth of 5.4m during the test period.

Table 5.2. Properties of Dunkirk sand.

Material	**Median particle size** D_{50}	**Uniformity Coefficient Cu**	**Maximum void ratio** e_{max}	**Minimum void ratio** e_{min}	**Peak friction angle** ϕ_{peak} (^{o})
Dunkirk sand	0.28	0.72	0.91	0.54	32

Furthermore, the q_c profile in the vicinity of the test pile is extracted, as shown in Figure 5.3 due to the CPT measurements (Taborda *et al.*, 2020). The magnitude was recorded as around 10000 kPa near the surface, peaking at 41000 kPa at a depth of 4m.

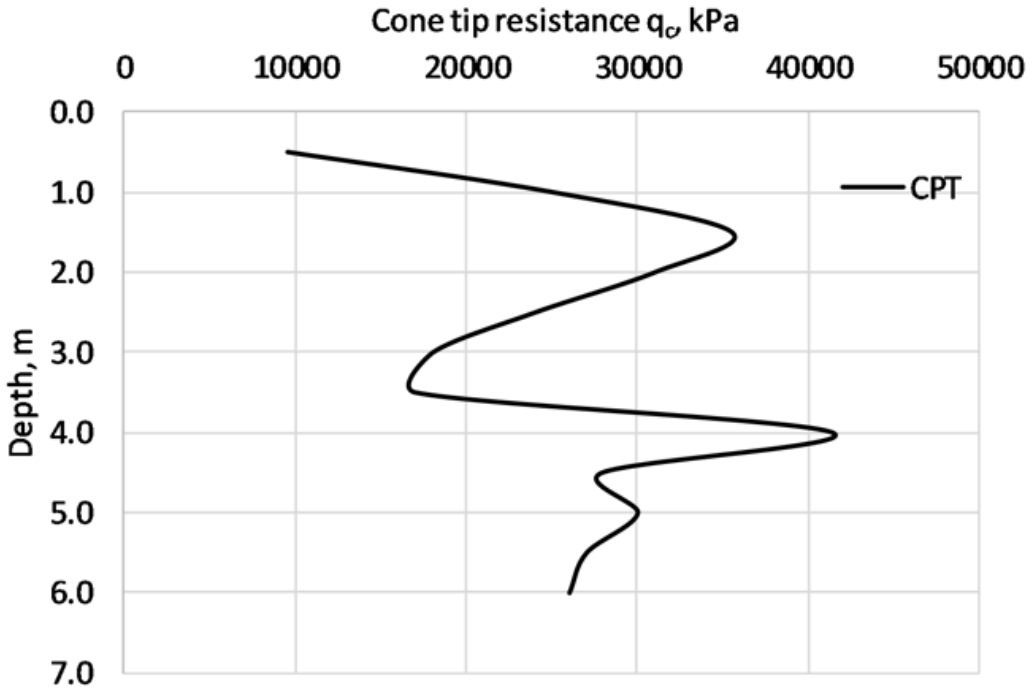

Figure 5.3. CPT q_c profile for the Dunkirk field test according to CPT measurements.

5.1.3.2. Pile Properties and Load Test Description. The pile used for the static lateral load test had a diameter of 0.762m, an embedded length of 6.02m and a wall thickness of 25 mm. During the test, an incremental lateral load by means of a hydraulic hammer was applied to the pile head at an elevation of 10.06m. Resulting displacements and rotations due to the applied load were measured by a load cell, an LVDT and an inclinometer in a range up to a displacement of 0.1 times the diameter and a rotation of 2^0.

5.2. Methodology

5.2.1. Numerical Modeling of Field Tests using SAP 2000

A single pile FE model that represents field tests investigated by this study is generated as a frame element in SAP 2000 as shown in Figure 5.4. The pile properties, such as shape, material (i.e., steel, concrete), the outside diameter and wall thickness, are defined according to the information provided by the related research. A static

joint force acting at the pile's free-head at height as described by the corresponding field test is selected as a "Nonlinear Static" where none of the geometric nonlinearity parameters is anticipated.

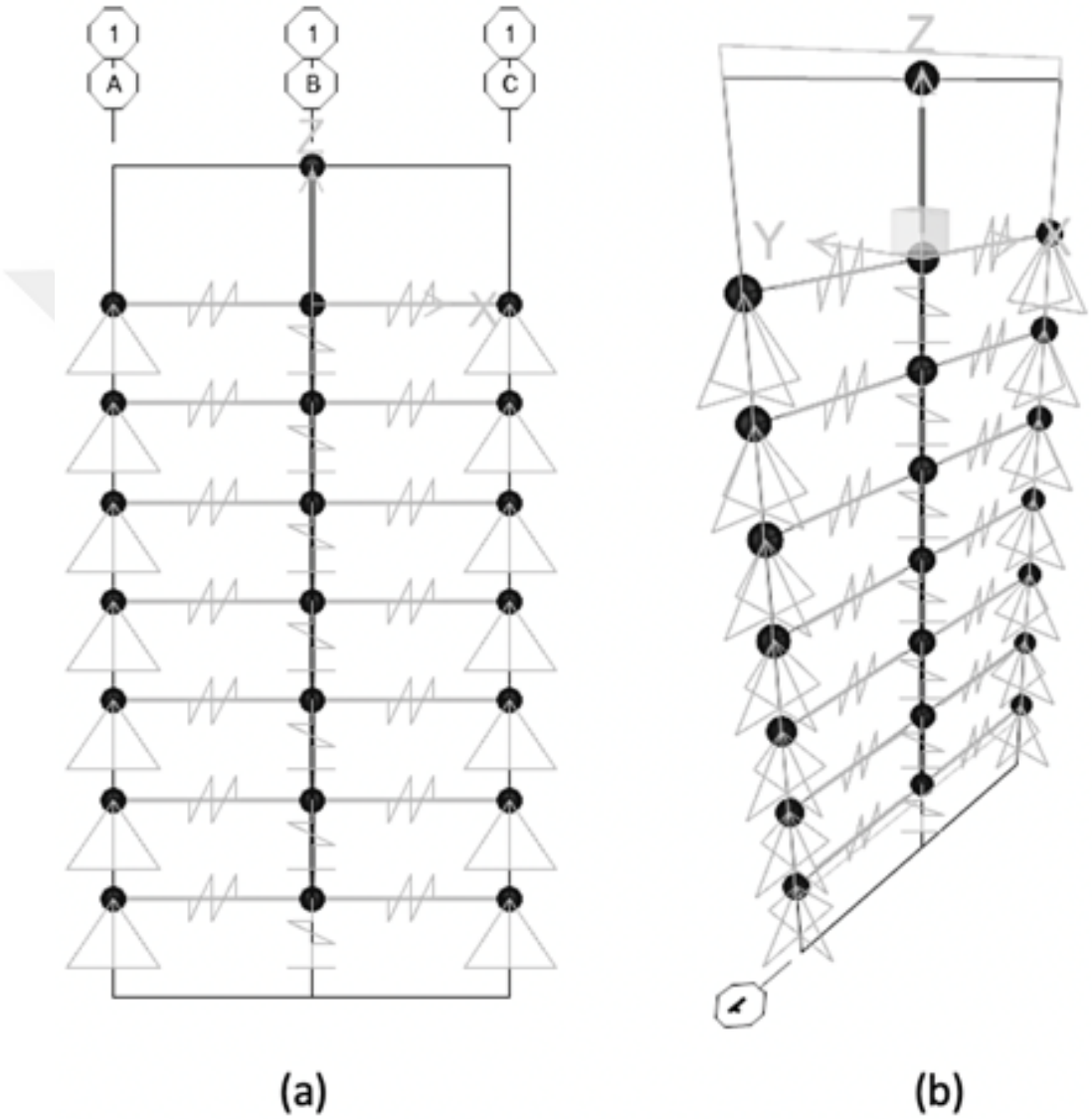

Figure 5.4. A single pile FE model in SAP 2000:(a) X-Z plane (b) 3-D view.

The part of the pile embedded in the ground is divided by joints, which are placed at intervals of at least 0.25m and at most 1m, supported by link/support elements from both sides of the pile. This type of structural element enables the implementation of the p-y curves extracted by the particular equation along the embedded length of the pile in SAP 2000. Figure 5.5 illustrates that one end of a link/support element joins

with the pile while the other has translational restraints against all directions. All link/support elements are defined as "Multilinear Elastic" with no mass/weight.

Figure 5.5. A link/support element in the FE model in SAP 2000.

Using an Excel spreadsheet, we obtain

$$\frac{p}{\sigma'_v D} = 5.8\left(\frac{q_c}{\sigma'_v}\right)^{0.29} tanh\left(4.2\left(\frac{y}{D}\right)^{0.66}\right), \tag{5.1}$$

$$\frac{p}{\sigma'_v D} = 7\left(\frac{q_c}{\sigma'_v}\right)^{0.29} tanh\left(2.4\left(\frac{y}{D}\right)^{0.66}\right), \tag{5.2}$$

$$\frac{p}{\sigma'_v D} = 7\left(\frac{q_c}{\sigma'_v}\right)^{0.29} tanh\left(5.18\left(\frac{y}{D}\right)^{0.73}\right), \tag{5.3}$$

while the one proposed by Wang *et al.* (2022)

$$\frac{p}{\sigma'_v D} = \left[2.7 q_{c/}\sqrt{\sigma'_v p_\alpha}\right] tanh\left(4.2\left(\frac{y}{D}\right)^{0.55}\right), \tag{5.4}$$

which and the one suggested by API (2000)

$$P = A \times p_u \times tanh\left[\frac{k \times H}{A \times p_u} \times y\right], \tag{5.5}$$

are used to generate p-y curves for each link/element located at distinct depths, y, of the pile with respect to q_c (or ϕ and D_r for the API method), ψ'_v values of the soil at the corresponding depth. Each generated curve is then entered in the "Link/Support Directional Properties" tab, as shown in Figure 5.6. Displacement and force magnitudes are defined with a minus sign; that way, these structural elements mobilize only under compression.

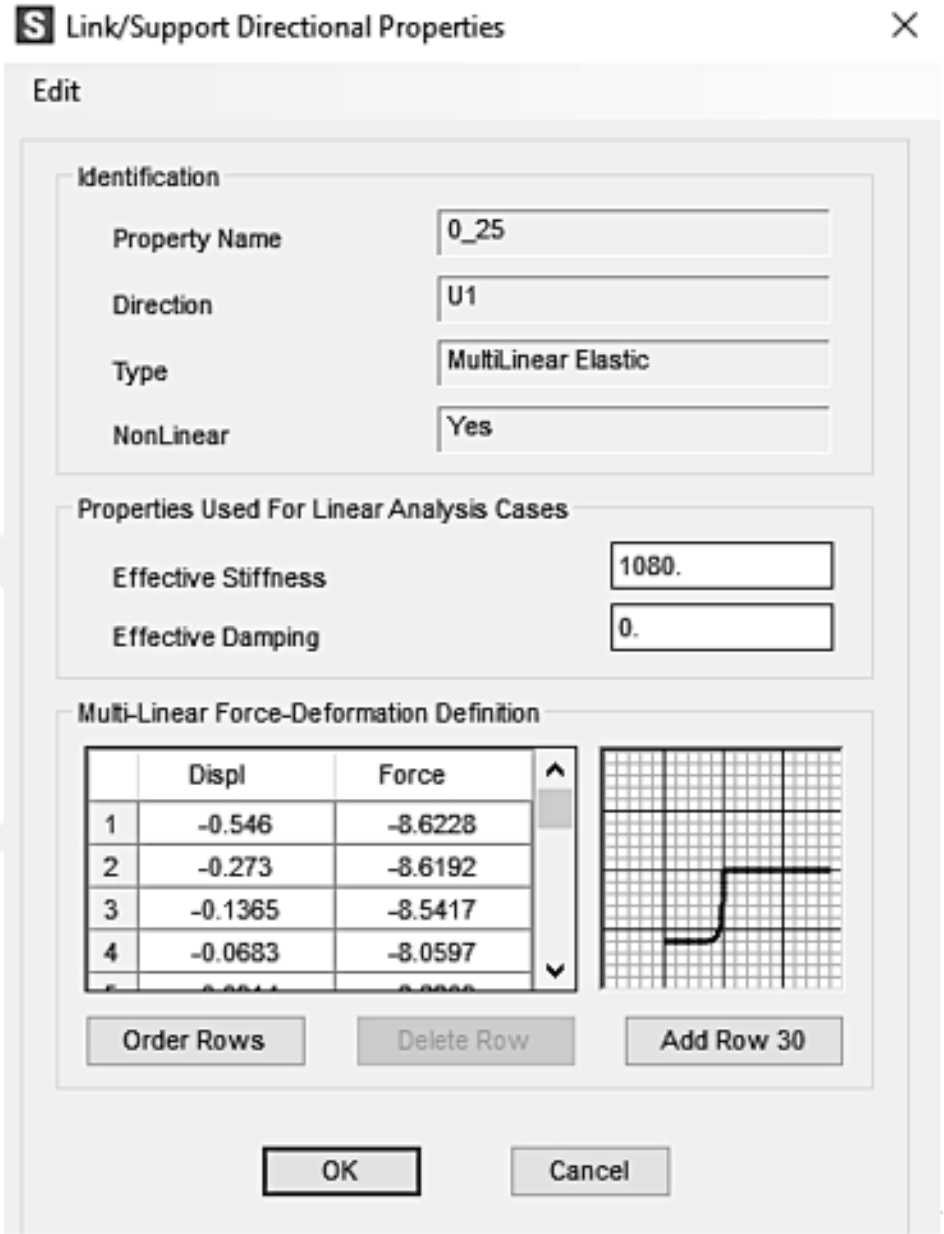

Figure 5.6. Link/support directional properties tab in SAP 2000.

Spring elements, another built-in feature provided by SAP 2000, are assigned to the same joints where one end of link/support elements joins the pile model. This is done to specify t-z and Q-z curves, following the procedure suggested by the API specifications. These curves characterize the pile model for axial load transfer capacity, accounting for skin friction and end bearing/tip load due to axial displacement. An analysis is executed using the created "Nonlinear Static" load case and results are saved for multiple states, typically at least ten. Lateral displacements and bending mo-

ments/rotations occurring at specified joints are measured for each state. Subsequently, the measured data is exported to another Excel spreadsheet for comparison with the analysis results from the FE models of the same field test, created with different p-y equations.

5.2.2. Numerical Modeling of Anchor Piles using Plaxis 3D

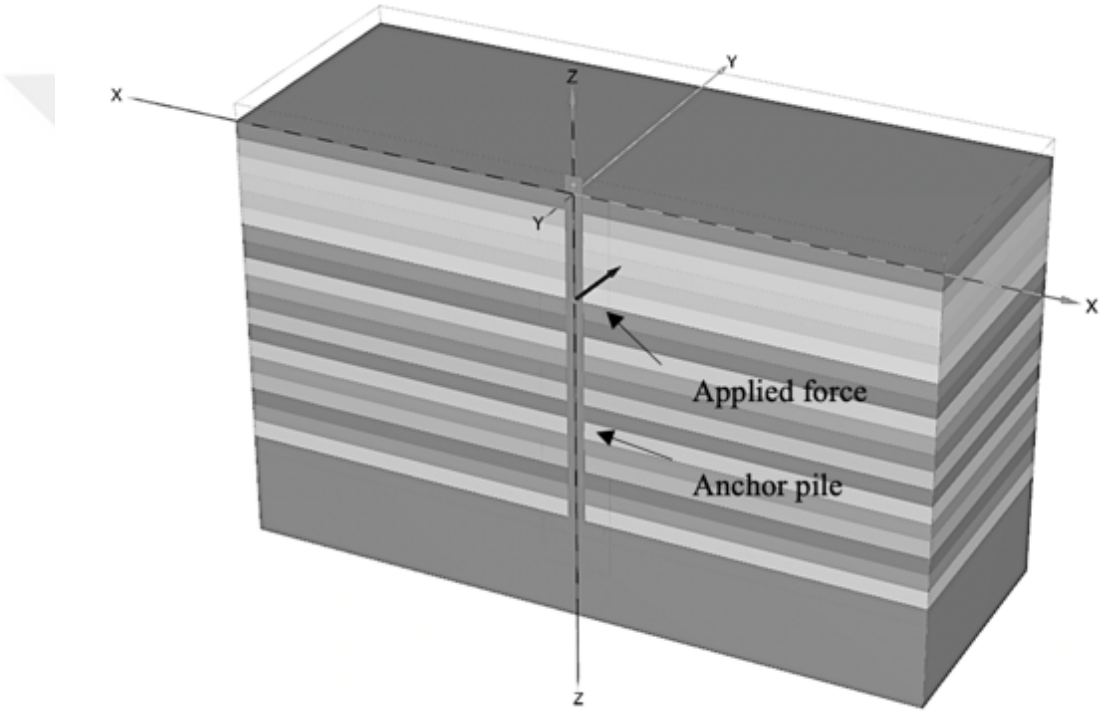

Figure 5.7. An anchor pile FE model in Plaxis 3D.

Three Finite Element (FE) models, incorporating variations in soil profile and pile diameter, were created and designated as AP_Model1, AP_Model2 and AP_Model3. As outlined in Table 5.3, all three FE models feature a non-porous volume pile modeled with a linear elastic material. The pile has a unit weight of 0.1 kN/m^3, a notably high stiffness, Young's modulus of 2.0E+08, a Poisson ratio of 0.3 and a length of 20m. The diameter of the pile is 0.65m for both AP_Model1 and AP_Model2 and 1.0m for AP_Model3.

Table 5.3. Pile properties for anchor pile FE models in Plaxis 3D.

Material type	**Linear elastic model**
Drainage type	Non-porous
Unit weight of the pile [kN/m^3], γ	0.1
Young's Modulus [kPa], E_{ref}	2.0E+08
Poisson's ratio, υ	0.3
Length [m]	20
Diameter [m]	0.65-1.0

In Figure 5.8, it is illustrated for all anchor pile FE models that a point load was applied at an angle of 43.5° to the horizontal at 6m depth, similar to those in geotechnical engineering practice (Jeanjean *et al.*, 2006).

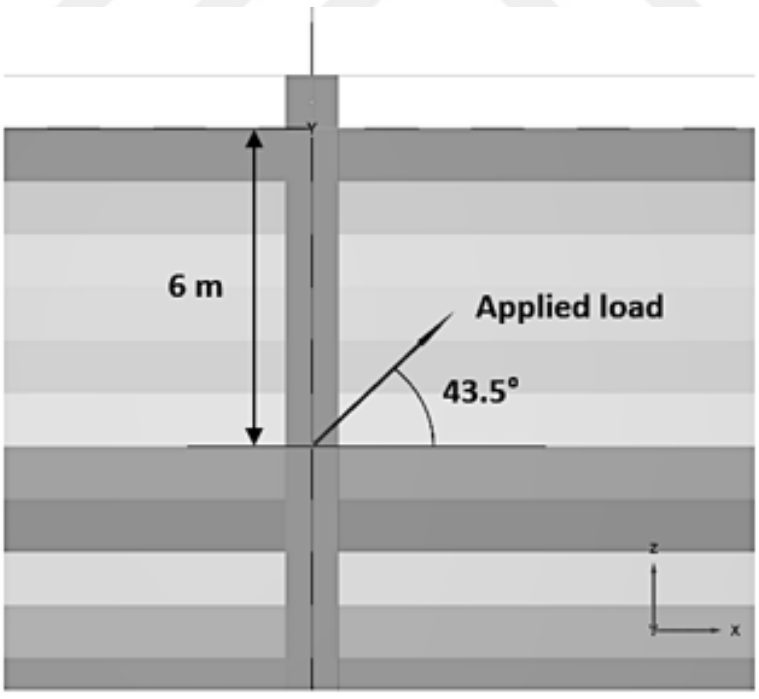

Figure 5.8. Location of the applied load in anchor pile FE models.

As listed in Table 5.3, the soil configuration surrounding the pile in AP_Model1 was simulated using the Hardening Soil (HS) model for dense Sile sand with a K_0 value of 0.3. For AP_Model2 and AP_Model3, the soil in the upper half-length of the pile,

extending from the ground surface to a depth of 10m, was modeled with loose Sile sand featuring a K_0 value of 0.5. In contrast, the portion of the soil below the 10m depth mark was represented using the HS model for dense Sile sand with a K_0 of 0.3.

Table 5.4. Properties of the FE anchor pile models.

Model ID	**Pile length** **m**	**Pile diameter** **m**	**Soil profile** **-**	K_0 **-**
AP_Model1	20	0.65	Dense Sile sand (at depths 0-25 m)	0.3
AP_Model2	20	0.65	Loose Sile sand (at depths 0-10 m) Dense Sile sand (at depths 10-25 m)	0.5 0.3
AP_Model3	20	1.0	Loose Sile sand (at depths 0-10 m) Dense Sile sand (at depths 10-25 m)	0.5 0.3

Throughout the Finite Element (FE) analysis, the load, administered as a prescribed displacement, incrementally increased during each calculation phase until reaching a resultant displacement of 0.1516m, inclined at an angle of 43.5^o to the horizontal in "Phase 15" (loading commenced in "Phase 2"). Subsequently, a load-deflection curve was generated by measuring lateral soil resistances at stress points within the corresponding soil layer at the specified depth, as determined through the FE analysis.

5.3. Results and Discussions

This chapter conducts a comprehensive comparison between measurements obtained from field tests and Plaxis 3D FE models with the results derived from corresponding SAP 2000 models. Throughout the chapter, figures are accompanied by a legend that includes labels such as "Field Test", "This study (Load)", "This study (Trans.)", "Wang *et al.* (2022)", "Suryasentana and Lehane (2014)", "Dyson and Randolph" and "API (2000)". The term "Field Test" denotes measurements from the field test, "This study (Load)" represents results from the SAP 2000 model utilizing curves

extracted by the equation developed for the "force at the pile head" loading mode, "This study (Trans.)" illustrates results from the SAP 2000 model employing curves derived for the "translation" loading mode, "Wang *et al.* (2022)" shows results from the SAP 2000 model using curves proposed by Wang et al. (2022), and "API (2000)" signifies results from the SAP 2000 model implementing curves suggested by the API (2000).

5.3.1. Results of the Shenton Park Test Site, Australia

A static pile load test was conducted at the Shenton Park test site on a pile with a length of 1.5 m and a diameter of 0.273 m. This test was examined and modeled in SAP 2000. The pile has a ratio of embedded length to diameter of 3.28, which makes the pile classified as short (rigid). Data provided by Wang *et al.* (2022) on applied lateral load – ground level displacement and bending moment – depth measurements have been utilized. In Figure 5.9a, lateral load–ground level displacement measurements from the field are compared with the results of six SAP 2000 models, each employing different p-y equations. These equations used in SAP 2000 models are proposed by Wang *et al.* (2022), Suryasentana and Lehane (2014), Dyson and Randolph (2001) and API (2000).

The other two are formulations derived in this study based on loading modes of "translation" and "loading (force) at the pile head". The model results, utilizing the API (2000), Dyson and Randolph (2001) and the 'translation' curves from this study, yield inconclusive outcomes. Furthermore, the model incorporating curves by Wang *et al.* (2022) demonstrates good agreement at small displacements in the range of 0 mm - 10 mm; however, it exhibits a stiffer response with increasing displacements. The model results using the 'loading' curves from this study exhibit a slightly smooth response at small displacements, followed by convergence with the field data for the remainder of the test. Results of the model created using Suryasentana and Lehane (2014) p-y curves exhibits good agreement with the field test results until lateral displacement of 20 mm, graphs are observed to be divergent later on. In Figure 5.9b, bending moments

obtained from the four SAP 2000 models, resulting from the same applied load of 12.84 kN, are compared with those extracted from the field test measurements. All models exhibit consistent results with the field test, except for a slightly higher variation, approximately around 10%, observed in the magnitude of the peak bending moment in the 'translation' p-y curve model developed in this study.

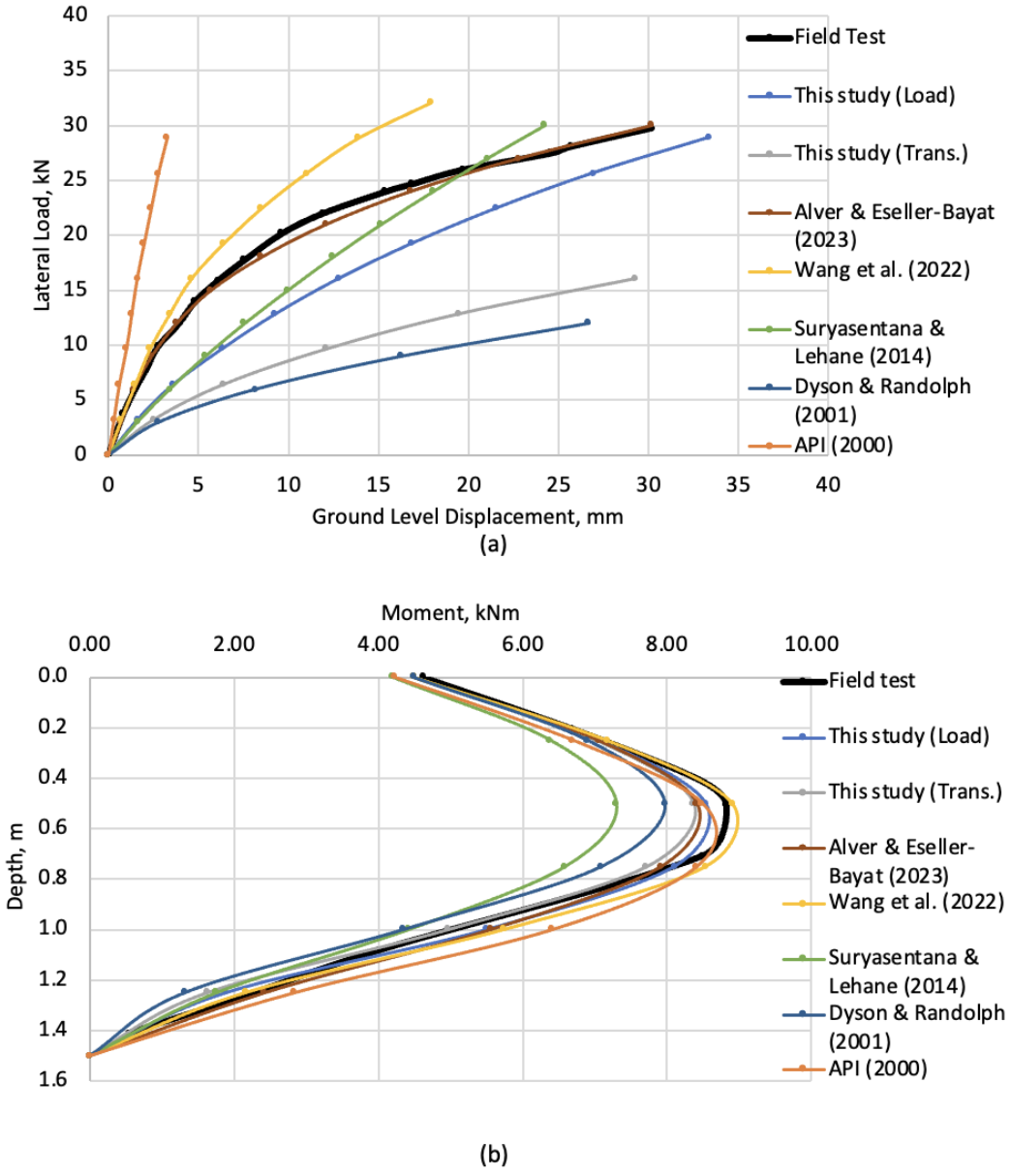

Figure 5.9. Field test measurements and results of the SAP 2000 models for the Shenton Park test.

5.3.2. Results of the Blessington Test Site, Ireland

A static pile load test was conducted at the Blessington test site on a pile with an embedded length of 7 m and a diameter of 0.34 m (Li *et al.*, 2014). This test was examined and modeled in SAP 2000 following the procedure explained in Chapter 5.2. The length-to-diameter ratio, L/D, is calculated as 20.6 for the test pile, which makes the pile classified as flexible (long). Experimental data regarding applied lateral load – ground level displacement and bending moment-rotation at the ground level measurements were provided by Li *et al.* (2014).

In Figure 5.10a, lateral load–ground level displacement measurements from the field are compared with the results of four distinct SAP 2000 models created using different p-y curves. These include curves proposed by Wang *et al.* (2022), Suryasentana and Lehane (2014), Dyson and Randolph (2001) and API (2000).

The other two are derived by this study based on loading modes of "translation" and "loading (force) at the pile head". The model results using the API (2000) and the Wang *et al.* (2022) curves present overly stiff responses compared to the field test results. The models generated with the curves by "This study (Load)" and "Suryasentana and Lehane (2014)" agree well with the field test results. However, the "This study (Trans.)" and "Dyson and Randolph (2001)" results, using the "translation" curves of this study, show a substantially smooth response, as expected.

In Figure 5.10b, bending moments-rotation at ground level results obtained from the specified SAP 2000 models are compared with those extracted from the field test measurements. Results from the "This study (Load)" exhibit the best fit among all SAP2000 models to the field test measurements.

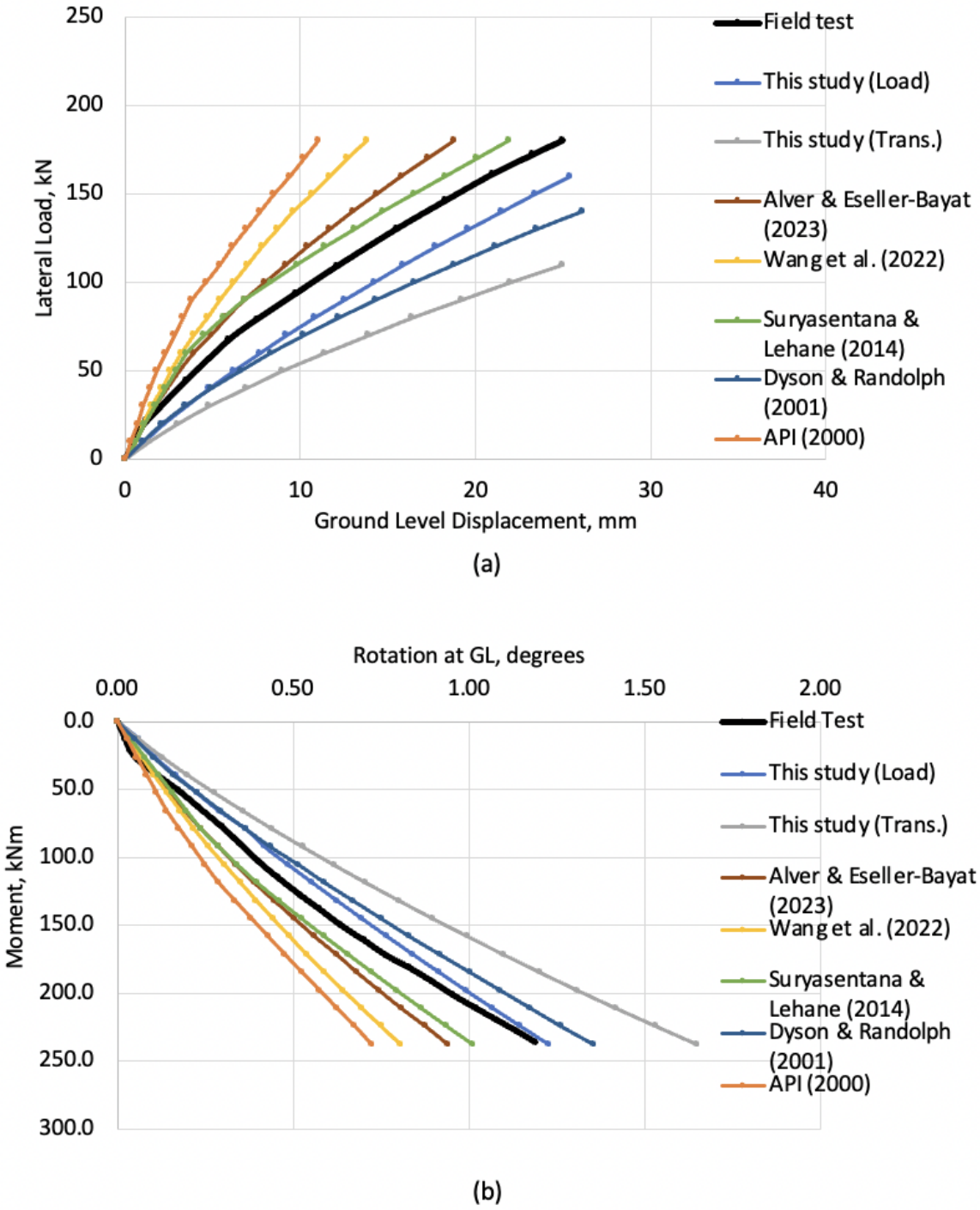

Figure 5.10. Field test measurements and results of the SAP 2000 models for the Blessington test.

5.3.3. Results of the Dunkirk Sand Deposit Test Site, France

Following the procedure explained in Chapter 5.2, a static pile load test at the Dunkirk test site was conducted on a pile with an embedded length of 6.02 m and a diameter of 0.762 m. This test was then examined and modeled in SAP 2000 using the information summarized in Chapter 5.1. The embedded length-to-diameter ratio, L/D, was determined as 8 for the test. McAdam *et al.* (2020) have provided data on applied lateral load – ground level displacement and bending moment – depth. Figure 5.11a compares lateral load–ground level displacement measurements from the field with the results of four distinct SAP 2000 models created using the p-y curves specified in this study. The model results using the Wang *et al.* (2022) curves exhibit a stiff response compared to the field test results. The model generated with the curves by "This study (Load)" shows a good agreement with the field test results with an average variation of approximately 18%. The model created with "Suryasentana and Lehane (2014)" curves shows best fit to the field test results up to a lateral displacement of 36mm, which corresponds to approximately 0.05 times the diameter, at the pile head. However, the response in the model deviates from the field test results as the displacement increases further. The "This study (Trans.)", "Dyson and Randolph (2001)" and the "API (2000)" results exhibit significantly smoother responses compared to field test results.

Bending moments distributed along the depths of the pile, caused by a lateral load of 440 kN, obtained from the specified SAP 2000 models are compared with those extracted from the field test measurements in Figure 5.11b. Peak values appear divergent for all models. Any small discrepancy may account for this difference considering the location of the force is at an elevation of 10m. Nevertheless, both models created with the curves from this study exhibit better fits than that of Wang *et al.* (2022), considering the depth below 2m.

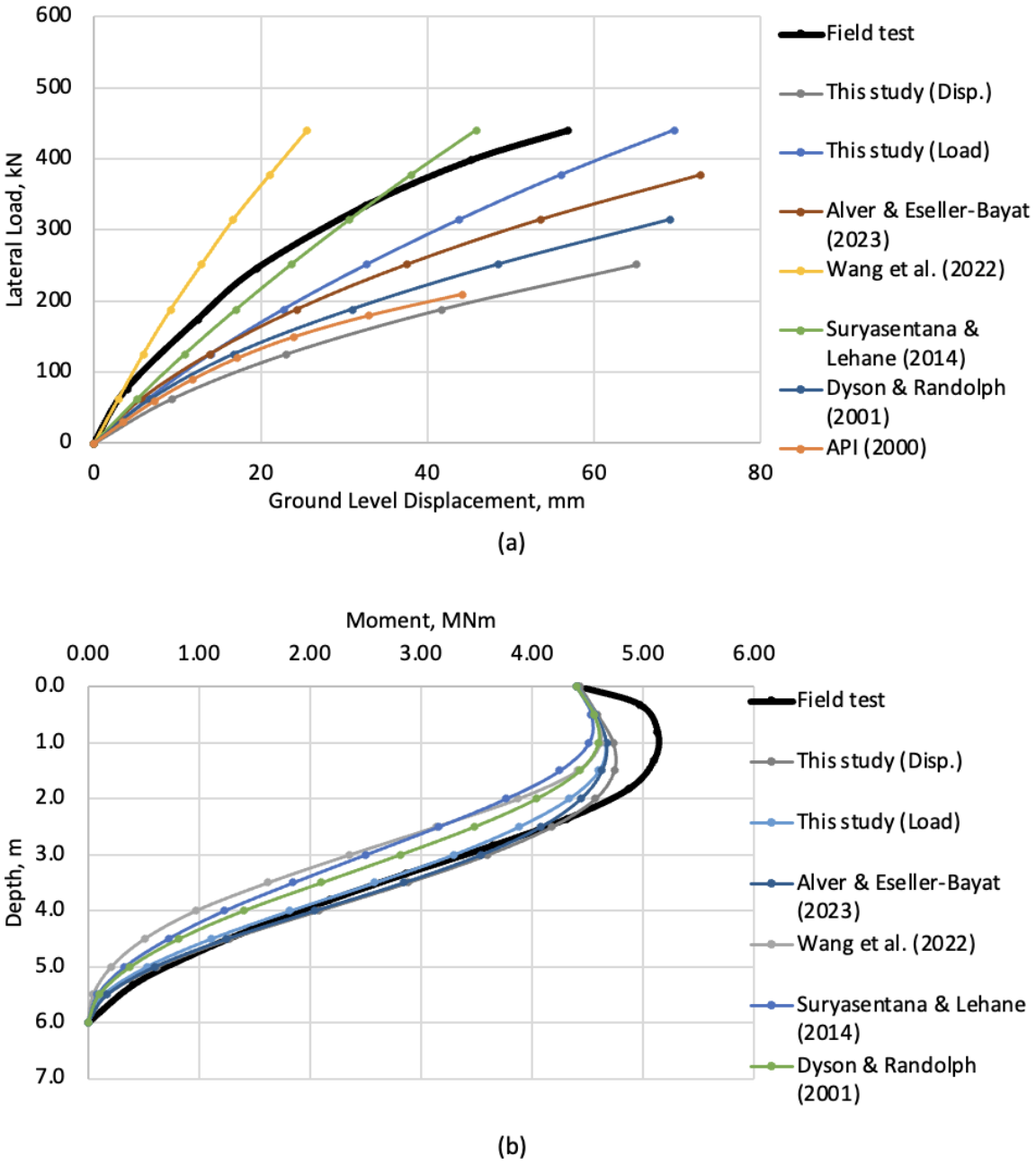

Figure 5.11. Field test measurements and results of the SAP 2000 models for the Dunkirk test.

5.3.4. Results of the AP_Model1

The AP_Model1, which represents an anchor pile structure generated in Plaxis 3D, consists of a pile with a length of 20m and a diameter of 0.65m and loaded at a depth of 6m. The pile is fully embedded in dense Sile sand, as described in Chapter 5.2.

Two SAP 2000 FE models using p-y curves based on the equations "Wang *et al.* (2022)" and "This study (Trans.)" are generated to simulate the AP_Model1 created in Plaxis 3D. Figure 5.12 demonstrates normal force due to displacement results for depths of 2.5m and 9.5m, which coincide approximately five times the diameter above and below the location of the loading point. The term "normal force" represents an absolute value of the force read from the link/support element at the corresponding depth in the SAP 2000 model. In contrast, "displacement" refers to the lateral displacement in the positive "x" direction read at the joint on the pile at the same depth. The value "normal force" obtained from the Plaxis 3D is the same as the soil resistance described in Chapter 4.1.2. Results from the SAP 2000 model generated with curves of the "This study (Trans.)" equation show good agreement for both depths. However, results from the model created using the equation "Wang *et al.* (2022)" are inconsistent with AP_Model1 results. These findings strongly support the significance of the loading mode in determining the p-y curves and the case being modeled.

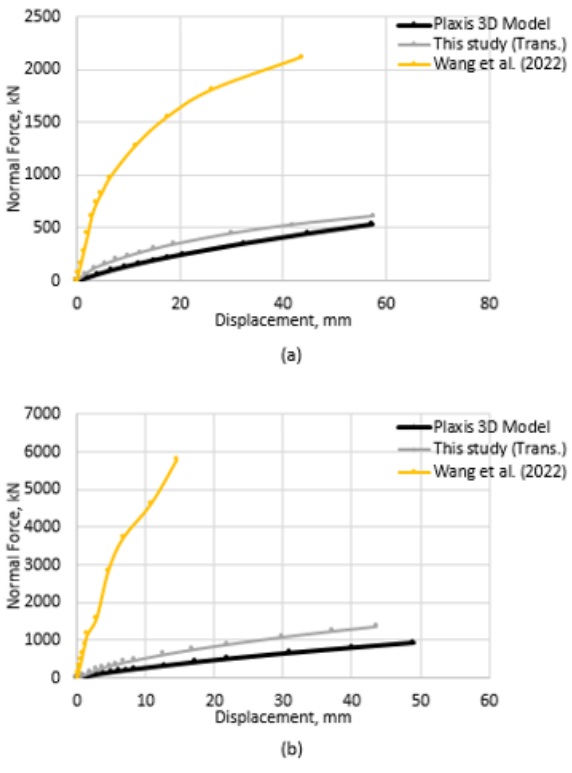

Figure 5.12. Results of Plaxis 3D and SAP 2000 analyses for the AP_Model1 model:(a) at 2.5m depth, (b) at 9.5m depth.

5.3.5. Results of the AP_Model2

The AP_Model2, created in Plaxis 3D, consists of a pile with a length of 20m and a diameter of 0.65m. The anchor pile model is loaded at a depth of 6m. The pile is fully embedded in a loose Sile sand layer that has a thickness of 10m, overlying dense Sile sand as described in Chapter 5.2. Two SAP 2000 FE models using "Wang *et al.* (2022)" and "This study (Trans.)" equations are generated to simulate the AP_Model2 and investigate the validity of the specified equations. The normal force-displacement results captured for the depths of 2.5m and 9.5m, which coincide approximately five times the diameter above and below the location of the loading point, are shown in Figure 5.13. Results from the SAP 2000 model generated with curves of the "This study (Trans.)" equation show a good agreement for the depth of 2.5m. However, the results of "This study (Trans.)" and the AP_Model2 diverge as displacement increases at a depth of 9.5m. The model based on "Wang *et al.* (2022)" equation yields significantly divergent results compared to the results of AP_Model2. These also support the hypothesis that the loading mode has a great deal of influence on the p-y curves.

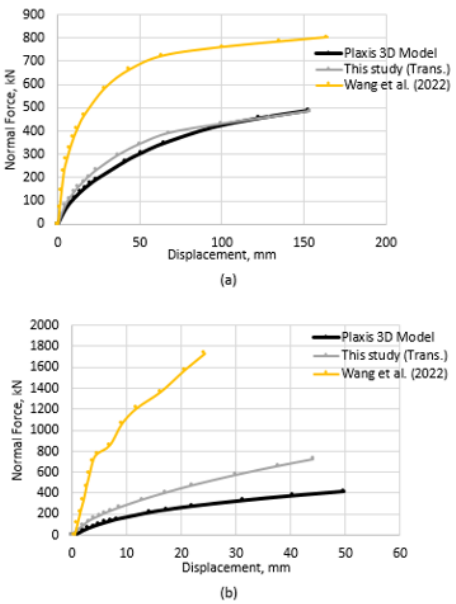

Figure 5.13. Results of Plaxis 3D and SAP 2000 analyses for the AP_Model2 model:(a) at 2.5m depth, (b) at 9.5m depth.

5.3.6. Results of the AP_Model3

The AP_Model3, an anchor pile model created in Plaxis 3D, consists of a pile with a length of 20m and a diameter of 1m. The model is loaded at a depth of 6m, similar to AP_Model1 and AP_Model2. The pile is fully embedded in a loose Sile sand layer with a thickness of 10m, overlying dense Sile sand, which constitutes the same soil profile as AP_Model2. Analyses with two SAP 2000 FE models in which the "Wang *et al.* (2022)" and "This study (Trans.)" p-y equations are employed are performed for another validation attempt. The normal force-displacement results examined for the depths of 2.5m and 9.5m, which coincide approximately 3.5 times the diameter above and below the location of the loading point, are shown in Figure 5.14. Results acquired for the depth of 2.5m exhibit that the model created with the "This study (Trans.)" converges with the AP_Model3 perfectly. However, for the depth of 9.5m, the results of "This study (Trans.)" and the AP_Model3 diverge slightly as displacement increases. Once again, within this comparison, the model with "Wang *et al.* (2022)" p-y equation yields significantly divergent results at both levels of depths.

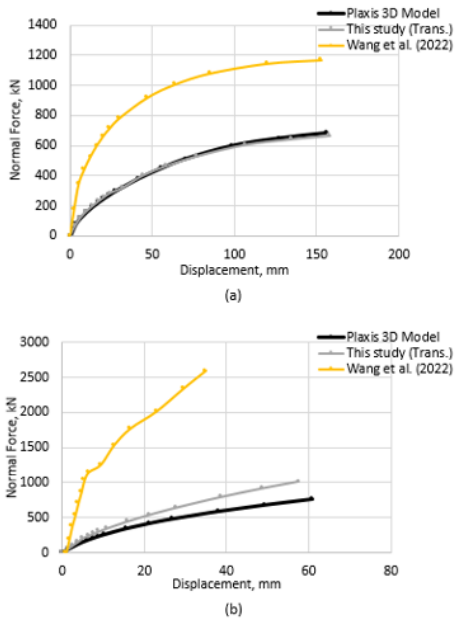

Figure 5.14. Results of Plaxis 3D and SAP 2000 analyses for the AP_Model3 model: (a) at 2.5m depth, (b) at 9.5m depth.

6. SUMMARY

This chapter summarizes the outcomes of the main sections included in this dissertation. Each part presents its outcomes and collectively, the three sections conclude coherent CPT-based p-y formulations for use in FE analysis of piled structures.

6.1. Prediction of Cone Tip Resistance Using a Numerical Method

In this chapter, the focus is on establishing formulations for obtaining lateral soil resistance using q_c, exploring numerical prediction methods applicable to cohesionless soils. Recent studies in this field have employed a method that yields reliable results by implementing the SCE theory within a FE model in Plaxis 2D. This approach is validated through a series of FE analyses using well-known Toyoura and Ticino sands. The plim values obtained from these analyses are then utilized in two distinct empirical equations to predict q_c values, which are subsequently compared to results from calibration chamber tests. The key findings and conclusions of this section are summarized

- The validity of the spherical cavity expansion method in Plaxis 2D, employing an axisymmetric model incorporating the MC soil model, is confirmed through a comparison of results with those obtained from an analytical closed-form solution.
- The parameters of the HS constitutive model for Toyoura and Ticino sands are determined using results from triaxial compression tests. p_{lim} values for these sands are obtained through SCE analyses conducted on samples with varying stress states and densities. Two transition equations are investigated by comparing numerical results and data from calibration chamber tests. Subsequently, the following equation by Cudmani and Osinov (2001) is identified as yielding accurate predictions

$$q_c = p_{lim} \times k_q = p_{lim} \times \left(1.5 + \frac{5.8(I'_D)^2}{(I'_D)^2 + 0.11}\right). \tag{6.1}$$

- The laboratory test results for the sand collected from the northern coast of Istanbul, namely Sile sand, are examined to determine HS model parameters. Then, q_c profiles for nine distinct configurations, involving variations in density and K_0 properties of Sile sand, are extracted. This is achieved by conducting ninety SCE analyses in Plaxis 2D for each 1-meter-thick sand layer, covering a depth of 20 meters. These soil profiles serve as a crucial component in the upcoming chapter, forming part of the parametric study.

6.2. CPT-Based Determination of p-y Curves for Rigid Piles in Sand According to Loading Modes

In this chapter, CPT-based p-y formulations for piles in sand are derived considering different loading modes through a parametric study held within the 3D FE program Plaxis 3D. Fifty-four 3D FE analyses on a single pile employ two loading modes. These modes are "acting a force at the pile head" and "lateral translation of whole pile body". Verification of the FE model is confirmed by modeling a benchmark full-scale field test conducted in Mustang Island by Reese *et al.* (1974), which involved a lateral loading test of a single pile. Using the similar geometry of the verified model and the generated soil profiles of Sile sand, 20-meter-long single piles with diameters of 0.65m, 0.8m and 1.0m are analyzed. A significantly high stiffness is defined for piles. Therefore, stress and deflection data are extracted along the entire length of the piles under conditions where no plastic hinge occurred. Genetic Algorithm (GA) code is utilized to interpret results and derive final forms of the formulations. Besides, ultimate soil resistance and effects of specific parameters are investigated. The conclusions of this chapter are listed

- Discrepancies are evident in the 3D FE analysis results when comparing the two selected sets of triplet analyses. Using a lateral displacement of 0.1D as a reference,

the ratio of soil resistance in the 'force at the pile head' mode to that in the 'translation' mode varies between 0.55 and 0.71.

- Findings from the 3D finite element model analyses conducted under the translation mode of loading indicate that the soil surrounding the pile does not reach ultimate resistance below a depth of 4 times the diameter of the pile. In light of this, the measured stress data necessitate an evaluation to determine whether the soil near the stress points attains the ultimate resistance level. For the translation mode of loading, stress data gathered along the entire pile interface were categorized into two separate data sets at a specific depth where ultimate resistance is no longer attainable.
- Investigation of results collated from 3D FE analyses using GA code shows that $\frac{z}{D}$ and K_0 have no significant effects in p – y formulation directly. However, the potential effects due to the nature of these parameters appear to be incorporated into the q_c value. CPT-based p-y formulations are derived for three conditions after a series of optimization processes. For the translation mode of loading and shallow depths case, the p-y equation was determined

$$\frac{p}{\sigma'_v D} = 5.8 \left(\frac{q_c}{\sigma'_v}\right)^{0.29} tanh\left(4.2 \left(\frac{y}{D}\right)^{0.66}\right). \tag{6.2}$$

For the translation mode of loading and the depths deeper than 4D, the p-y equation was determined

$$\frac{p}{\sigma'_v D} = 7 \left(\frac{q_c}{\sigma'_v}\right)^{0.29} tanh\left(2.4 \left(\frac{y}{D}\right)^{0.66}\right). \tag{6.3}$$

For the acting force at the pile head mode of loading, the p-y equation was determined

$$\frac{p}{\sigma'_v D} = 5.2 \left(\frac{q_c}{\sigma'_v}\right)^{0.29} tanh\left(5.18 \left(\frac{y}{D}\right)^{0.73}\right). \tag{6.4}$$

6.3. Validation of the Derived p-y Formulations

In this chapter, three field tests of laterally loaded piles are modeled using SAP 2000, which is a widely-used commercial structural FE analysis program, with the derived CPT-based p-y equations, the equation proposed by Wang *et al.* (2022) and the API method. The validity of the obtained equation due to the "force at the pile head" mode is confirmed and the performance of the other equations is presented. Additionally, three FE models representing anchor pile structure, where the governing loading mode is the "translation", are generated and analyzed within Plaxis 3D. Then their FE models in SAP 2000 by assigning p-y springs that employ the derived "translation" equation and the Wang *et al.* (2022) equation are analyzed. The conclusions of this chapter are listed

- All three field tests in this chapter show that the derived equation with the relevant loading mode performs considerably well. They also prove that the equation suggested by API, which is highly dependent on the friction angle of sand, is not suitable for modeling piled structures under lateral loading.
- The observed lateral soil resistance due to lateral displacement results, extracted from the FE analysis of anchor piles in Plaxis 3D, are compared with those extracted from the analyses in SAP 2000 models representing those created in Plaxis 3D. The SAP 2000 models using the derived CPT-based equation due to the loading mode of "translation" for assigning p-y springs exhibit good agreement with their counterpart model in Plaxis 3D as expected.

7. CONCLUSION

In conclusion, the robust formulation of p-y springs, crucial for modeling soil-pile interaction in finite element (FE) analysis of piled structures, remains an essential aspect of geotechnical engineering. Notably, formulations based on direct measurements of cone tip resistance (q_c) from cone penetration testing (CPT) offer significant advantages, eliminating inherent risks associated with equations dependent on friction angle (ϕ'). Numerous studies have derived p-y formulations through experimental or numerical methods, demonstrating good validation with field tests under identical loading modes. However, it is imperative to acknowledge that changes in loading modes can introduce variations in soil behavior surrounding the pile, particularly in terms of soil resistance due to lateral displacements. To address this, a parametric numerical analysis program was implemented, considering two distinct loading modes on a single pile within this dissertation. This led to the development of two nonlinear formulations for p-y springs based on direct q_c measurements of CPT in sands. The parametric study, utilizing a validated numerical method involving spherical cavity expansion (SCE), provided accurate q_c profiles. Additionally, an investigation of transition equations preceding the parametric study revealed the reliability of an empirical transition equation incorporating the pressure-dependent density index (I'_D). The CPT-based p-y formulations, derived using the Genetic Algorithm (GA) code, were then compared with two other formulations and validated through field tests and numerically generated anchor pile models. The results demonstrated a considerable agreement between each formulation and the reference results for relevant cases, emphasizing the efficacy of CPT-based p-y formulations. This research contributes to the advancement of geotechnical engineering practices and offers valuable insights into understanding soil-pile interaction under lateral loading conditions. The findings underscore the importance of considering different loading modes in the development of accurate and reliable p-y formulations for practical engineering applications.

REFERENCES

Alver, O., and E.E. Eseller-Bayat, 2023, "A Dynamic p–y Model for Piles Embedded in Cohesionless Soils", *Bulletin of Earthquake Engineering*, Vol. 21, No. 7, pp. 3297–3320.

Anusic, I., B.M. Lehane, G.R. Eiksund and M.A. Liingaard, 2019, "Influence of Installation Method on Static Lateral Response of Displacement Piles in Sand", *Géotechnique Letters*, Vol. 9, No. 3, pp. 193-197.

American Petroleum Institute (API), 2000, "Recommended Practice for Planning, Designing and Constructing Fixed Offshore Platforms - Working Stress Design", *American Petroleum Institute*, Vol. 21, No. 1, pp. 123-136.

Arda, C. and Ö. Çinicioğlu, 2021, "Influence of Grain Shape on Stress-Dilatancy Parameters", *Granular Matter*, Vol. 23, No. 2, pp. 1-19.

Ariannia, S.S., 2015, *Determination of p-y Curves by Direct Use of Cone Penetration Test (CPT) Data*, Ph.D. Thesis, University of California.

Bishop, R.F., R. Hill and N.F. Mott, 1945, "Theory of Indentation and Hardness Tests", *Proceedings of the Physical Society*, Vol. 57, No. 3, pp. 147-158.

Bolton, M.D., 1986, "The Strength and Dilatancy of Sands", *Géotechnique*, Vol. 36, No. 1, pp. 65-78.

Broms, B.B., 1964, "Lateral Resistance of Piles in Cohesionless Soils", *Journal of the Soil Mechanics and Foundations Division*, Vol. 90, No. 3, pp. 123-156.

Cao, L.F., C.I., Teh and M.F. Chang, 2001, "Undrained Cavity Expansion in Modified

Cam Clay I: Theoretical Analysis", *Géotechnique*, Vol. 51, No. 4, pp. 323-334.

Carter, J.P., J.R. Booker and S.K. Yeung, 1986, "Cavity Expansion in Cohesive Frictional Soils", *Géotechnique*, Vol. 36, No. 3, pp. 349-358.

Chen, S.L. and K. Liu, 2019, "Undrained Cylindrical Cavity Expansion in Anisotropic Critical State Soils", *Géotechnique*, Vol. 69, No. 3, pp. 189-202.

Choo, Y.W. and D. Kim, 2016, "Experimental Development of the p-y Relationship for Large-Diameter Offshore Monopiles in Sands: Centrifuge Tests", *Journal of Geotechnical and Geoenvironmental Engineering*, Vol. 142, No. 1, pp. 58-68.

Çinicioglu, Ö. and A. Abadkon, 2015, "Dilatancy and Friction Angles Based on In Situ Soil Conditions", *Journal of Geotechnical and Geoenvironmental Engineering*, Vol. 141, No. 4, pp. 19-27.

Cudmani, R. and V.A. Osinov, 2001, "The Cavity Expansion Problem for the Interpretation of Cone Penetration and Pressuremeter Tests", *Canadian Geotechnical Journal*, Vol. 38, No. 3, pp. 622-638.

Dodds, A.M. and G.R. Martin, 2007, "Modeling Pile Behavior in Large Pile Groups under Lateral Loading", *MCEER-Earthquake Engineering to Extreme Events*, Vol. 45, No. 3, pp. 456-468.

Dyson, G.J. and M.F. Randolph, 2001, "Monotonic Lateral Loading of Piles in Calcareous Sand", *Journal of Geotechnical and Geoenvironmental Engineering*, Vol. 127, No. 4, pp. 346-352.

El Naggar, H. and M.H. El Naggar, 2012, "Expansion of Cavities Embedded in Cohesionless Elastoplastic Half-Space and Subjected to Anisotropic Stress Field", *Geotechnical and Geological Engineering*, Vol. 30, No. 5, pp. 1183-1195.

EN 1997-1: Eurocode 7: Geotechnical Design-Part 1, General Rules, 2004.

Fioravante, V. and D. Giretti, 2015, "Unidirectional Cyclic Resistance of Ticino and Toyoura Sands From Centrifuge Cone Penetration Tests", *Acta Geotechnica*, Vol. 11, No. 4, pp. 953-968.

Fukushima, S. and F. Tatsuoka, 1984, "Strength and Deformation Characteristics of Saturated Sand at Extremely Low Pressures", *Soils and Foundations*, Vol. 24, No. 4, pp. 30-48.

Gavin, K.G. and B.C., O'Kelly, 2007, "Effect of Friction Fatigue on Pile Capacity in Dense Sand", *Journal of Geotechnical and Geoenvironmental Engineering*, Vol. 133, No. 1, pp. 63-71.

Gavin, K. and J. Xue, 2009, "Use of a Genetic Algorithm to Perform Reliability Analysis of Unsaturated Soil Slopes", *Geotechnique*, Vol. 59, No. 6, pp. 545-549.

Hetenyi, M., 1946, *Beams on Elastic Foundation: Theory with Applications in the Fields of Civil and Mechanical Engineering*, M.S. Thesis, University of Oxford.

Houlsby, G.T. and R. Hitchman, 1988, "Calibration Chamber Tests of a Cone Penetrometer in Sand", *Géotechnique*, Vol. 38, No. 10, pp. 39-44.

HS Yu, J.C., 2002, "Rigorous Similarity Solutions for Cavity Expansion in Cohesive-Frictional Soils", *International Journal of Geomechanics*, Vol. 2, No. 2, pp. 233-258.

Hu, Q., F. Han, M. Prezzi, R. Salgado, and M. Zhao, 2022, "Finite-Element Analysis of the Lateral Load Response of Monopiles in Layered Sand", *Journal of Geotechnical and Geoenvironmental Engineering*, Vol. 148, No. 4, pp. 04022001-04022025.

Huang, M., S. Tong and Z. Shi, 2021, "Solution for Spherical Cavity Expansion in

State-Dependent Soils", *Acta Geotechnica*, Vol. 16, No. 6, pp. 1773-1788.

Igoe, D.J.P., K.G.Gavin and B.C. O'Kelly, 2011, "Shaft Capacity of Open-Ended Piles in Sand", *Journal of Geotechnical and Geoenvironmental Engineering*, Vol. 137, No. 10, pp. 903-913.

Jeanjean, P., D. Znidarcic, R. Phillips, H.Y. Ko, S. Pfister, Ö. Çinicioğlu and K. Schroeder, 2006, "Centrifuge Testing on Suction Anchors: Double-Wall, Over-Consolidated Clay and Layered Soil Profile", *Offshore Technology Conference*, Vol. 2, pp. 18007-18017.

Kirk, T., W. Kristian, L. Rasmussen, M. Hansen, H. Ravn, R. Lars and B. Ibsen, 2013, "Assessment of p-y Curves from Numerical Methods for a Non-Slender Monopile in Cohesionless Soil", *Council of Europe DCE Technical Memorandum*, Vol. 4, pp. 24-35.

Ladanyi, B. and A. Foriero, 1998, "A Numerical Solution of Cavity Expansion Problem in Sand Based Directly on Experimental Stress-Strain Curves", *Canadian Geotechnical Journal*, Vol. 35, No. 4, pp. 541-559.

Lehane, B.M., M.A. Ismail and M. Fahey, 2004, "Seasonal Dependence of in Situ Test Parameters in Sand Above the Water Table", *Géotechnique*, Vol. 54, No. 3, pp. 215-218.

Li, A.Z. and B.M. Lehane, 2010, "Embedded Cantilever Retaining Walls in Sand", *Géotechnique*, Vol. 60, No. 11, pp. 813-823.

Li, W., D. Igoe and K. Gavin, 2014, "Evaluation of CPT-Based p-y Models for Laterally Loaded Piles in Siliceous Sand", *Géotechnique Letters*, Vol. 4, No. 2, pp. 110-117.

Li, X.S. and Y.F. Dafalias, 2000, "Dilatancy for cohesionless soils", *Géotechnique*, Vol.

50, No. 4, pp. 449-460.

Lim, J.K. and B.M. Lehane, 2014, "Characterisation of the Effects of Time on the Shaft Friction of Displacement Piles in Sand", *Géotechnique*, Vol. 64, No. 6, pp. 476-485.

Lunne, T., J.J.M. Powell and P.K. Robertson, 2002, *Cone Penetration Testing in Geotechnical Practice*, In Cone Penetration Testing in Geotechnical Practice, Chemical Rubber Company CRC Press, New York.

Matlock, H., 1970, "Correlation for Design of Laterally Loaded Piles in Soft Clay", *Open Journal of Civil Engineering*, Vol. 1, No. 1, pp. 23-34.

McAdam, R.A., B.W. Byrne, G.T. Houlsby, W.J.A.P. Beuckelaers, H.J. Burd, K.G. Gavin, D.J.P. Igoe, R.J. Jardine, C.M. Martin, A. Muir Wood, D.M. Potts, J. Skov Gretlund, D.M.G. Taborda and L. Zdravković, 2020, "Monotonic Laterally Loaded Pile Testing in a Dense Marine Sand at Dunkirk", *Géotechnique*, Vol. 70, No. 11, pp. 986-998.

McClelland, B. and J.A. Focht, 1958, "Soil Modulus for Laterally Loaded Piles", *Transactions of the American Society of Civil Engineers*, Vol. 123, No. 1, pp. 1049-1063.

Mezazigh, S. and D. Levacher, 1998, "Laterally Loaded Piles in Sand: Slope Effect on p-y Reaction Curves", *Canadian Geotechnical Journal*, Vol. 35, No. 3, pp. 433-441.

Mo, P.Q. and H.S. Yu 2017, "Undrained Cavity Expansion Analysis with a Unified State Parameter Model for Clay and Sand", *Géotechnique*, Vol. 67, No. 6, pp. 503-515.

Murchison, J.M. and M.W. O'Neill, 1983, *An Evaluation of P-y Relationships in Sands*, PhD Thesis. University of Houston-University Park.

Osinov, V.A. and R. Cudmani, 2001, "Theoretical Investigation of the Cavity Expansion Problem Based on a Hypoplasticity Model", *International Journal for Numerical and Analytical Methods in Geomechanics*, Vol. 25, No. 5, pp. 473-495.

Porcino, D.D. and V. Marcianò, 2017, "Bonding Degradation and Stress-Dilatancy Response of Weakly Cemented Sands", *Geomechanics and Geoengineering*, Vol. 12, No. 4, pp. 221-233.

Poulos, H.G. and E.H. Davis, 1980, *Pile Foundation Analysis and Design*, John Wiley and Sons Inc, New Jersey.

Qi, W.G., F.P. Gao, M.F. Randolph and B.M. Lehane, 2016, "Scour Effects on p-y Curves for Shallowly Embedded Piles in Sand", *Géotechnique*, Vol. 66, No. 8, pp. 648-660.

Randolph, M.F., R. Dolwin and R. Beck, 1994, "Design of Driven Piles in Sand", *Géotechnique*, Vol. 44, No. 3, pp. 427-448.

Reese, L.C., 1986, "Behavior of Piles and Pile Groups under Lateral Load, United States, Department of Transportation", *Federal Highway Administration*, Vol. 5, pp. 85-106.

Reese, L.C., W.R. Cox and F.D. Koop, 1974, "Analysis of Laterally Loaded Piles in Sand", *Proceedings of the Annual Offshore Technology*, Vol. 13, pp. 465-480.

Reese, L.C. and H. Matlock, 1956, "Non-Dimensional Solutions for Lateral Loaded Piles with Soil Modulus Assumed Proportional to Depth", *Proceedings of the 8th Texas Conference on Soil Mechanics and Foundation Engineering*, Vol. 1, pp. 1-41.

Rodrigo Salgado Rodrigues, 1993, *Analysis of Penetration Resistance in Sands*, Ph.D. Thesis, University of California.

Salgado, R., J.K. Mitchell and M. Jamiolkowski, 1997, "Cavity Expansion and Penetration Resistance in Sand", *Journal of Geotechnical and Geoenvironmental Engineering*, Vol. 123, No. 4, pp. 344-354.

Salgado, R. and M. Prezzi, 2007, "Computation of Cavity Expansion Pressure and Penetration Resistance in Sands", *International Journal of Geomechanics*, Vol. 7, No. 4, pp. 251-265.

Salgado, R. and M.F. Randolph, 2001, "Analysis of Cavity Expansion in Sand", *International Journal of Geomechanics*, Vol. 1, No. 2, pp. 175-192.

Schanz, T., P.A. Vermeer and P.G. Bonnier, 1999, "The Hardening Soil Model: Formulation and Verification, Beyond 2000 in Computational Geotechnics", *Ten Years of PLAXIS International, Proceedings of the International Symposium*, Vol. 14, pp.345-468, Amsterdam, Holland.

Schnaid, F. and G.T. Houlsby, 1991, "An Assessment of Chamber Size Effects in the Calibration of in Situ Tests in Sand", *Géotechnique*, Vol. 41, No. 3, pp. 437-445.

Scott, R.F., 1981, "Foundation Analysis", *New Jersey: Prentice-Hall*, Vol. 5, No. 4; pp. 578-560.

Suryasentana, S.K. and B.M. Lehane, 2014, "Numerical Derivation of CPT-Based p-y Curves for Piles in Sand", *Geotechnique*, Vol. 64, No. 3, pp. 186-194.

Suryasentana, S.K. and B.M., Lehane, 2016, "Updated CPT-Based p-y Formulation for Laterally Loaded Piles in Cohesionless Soil Under Static Loading", *Géotechnique*, Vol. 14, pp. 156-165.

Suzuki, Y. and B.M. Lehane, 2015, "Analysis of CPT end Resistance at Variable Penetration Rates Using the Spherical Cavity Expansion Method in Normally Con-

solidated Soils", *Computers and Geotechnics*, Vol. 69, pp. 141-152.

Taborda, D.M.G., L. Zdravkovic, D.M. Potts, H.J. Burd, B.W. Byrne, K.G. Gavin, G.T. Houlsby, R.J. Jardine, T. Liu, C.M. Martin and R.A. McAdam, 2020, "Finite-Element Modelling of Laterally Loaded Piles in a Dense Marine Sand at Dunkirk", *Geotechnique*, Vol. 70, No. 11, pp. 1014-1029.

Terzaghi, K., 1955, "Evalution of Conefficients of Subgrade Reaction", *Géotechnique*, Vol. 5, No. 4, pp. 297-326.

Tolooiyan, A. and K. Gavin, 2011, "Modelling the Cone Penetration Test in sand using Cavity Expansion and Arbitrary Lagrangian Eulerian Finite Element Methods", *Computers and Geotechnics*, Vol. 38, No. 4, pp. 482-490.

Wang, C., H. Zhou, H. Liu and X. Ding, 2022, "Analysis of Undrained Spherical Cavity Expansion in Modified Cam Clay of Finite Radial Extent", *European Journal of Environmental and Civil Engineering*, Vol. 26, No. 3, pp. 952-963.

Wang, H., B.M. Lehane, M.F. Bransby, L.Z. Wang and Y. Hong, 2022, "Field and Numerical Study of the Lateral Response of Rigid Piles in Sand", *Acta Geotechnica*, Vol. 17, No. 12, pp. 5573-5584.

Wang, H., B.M. Lehane, M.F. Bransby, L.Z. Wang, Y. Hong and A. Askarinejad, 2023, "Lateral Behavior of Monopiles in Sand Under Monotonic Loading: Insights and a New Simple Design Model", *Ocean Engineering*, Vol. 4, pp. 277-287.

White, D.J., 2022, "CPT Equipment: Recent Advances and Future Perspectives, Cone Penetration Testing 2022-Proceedings of the 5th International Symposium on Cone Penetration Testing", *CPT 2022*, Vol. 4, pp. 66-80.

Winkler, E., 1867, *Die Lehre von Elasticitaet und Festigkeit*, Bauakademien, Ingenieure,

Maschinenbauer, Architecten, Dominicus.

Xu, X., 2007, *Investigation of the end Bearing Performance of Displacement Piles in Sand*, Ph.D. Thesis, The University of Western Australia.

Xu, X. and B.M. Lehane, 2008, "Pile and Penetrometer end Bearing Resistance in Two-Layered Soil Profiles", *Géotechnique*, Vol. 58, No. 3, pp. 187-197.

Yasufuku, N., H. Ochiai and S. Ohno, 2001, "Pile End-Bearing Capacity of Sand Related to Soil Compressibility", *Soils and Foundations*, Vol. 41, No. 4, pp. 59-71.

Yu, H.S. and G.T. Houlsby, 1991, "Finite Cavity Expansion in Dilatant Soils: Loading Analysis", *Géotechnique*, Vol. 41, No. 2, pp. 173-183.

Yu, H.S., 2000, "Cavity Expansion Methods in Geomechanics", *Springer Netherlands*, Vol. 4, pp. 9-31.

Zdravković, L., R.J., Jardine, D.M.G., Taborda, D. Abadias, H.J. Burd, B.W. Byrne, K.G. Gavin, G.T. Houlsby, D.J.P. Igoe, T. Liu, C.M. Martin, R.A. McAdam, A. Muir Wood, D.M. Potts, J. Skov Gretlund and E. Ushev, 2020, "Ground Characterisation for PISA Pile Testing and Analysis", *Géotechnique*, Vol. 70, No. 11, pp. 945-960.

Zhang, Y., K.H. Andersen and G. Tedesco, 2016, "Ultimate Bearing Capacity of Laterally Loaded Piles in Clay-Some Practical Considerations", *Marine Structures*, Vol. 50, pp. 260-275.

APPENDIX A: THE TRIAXIAL TEST RESULTS USED FOR NUMERICAL HS MODELLING OF SILE SAND

Triaxial test results for reconstituted Sile sand samples are provided.

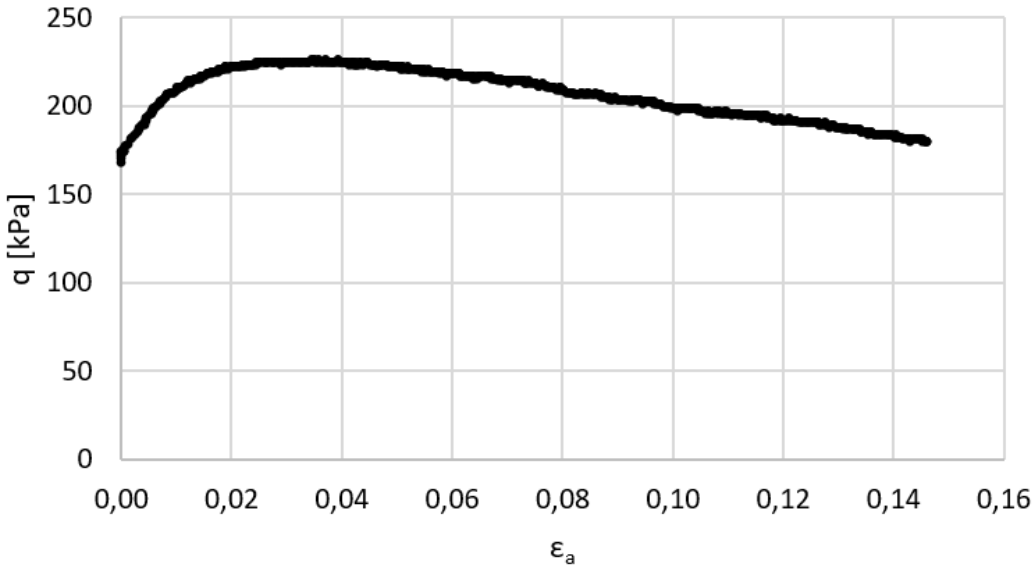

Figure A.1. S2.

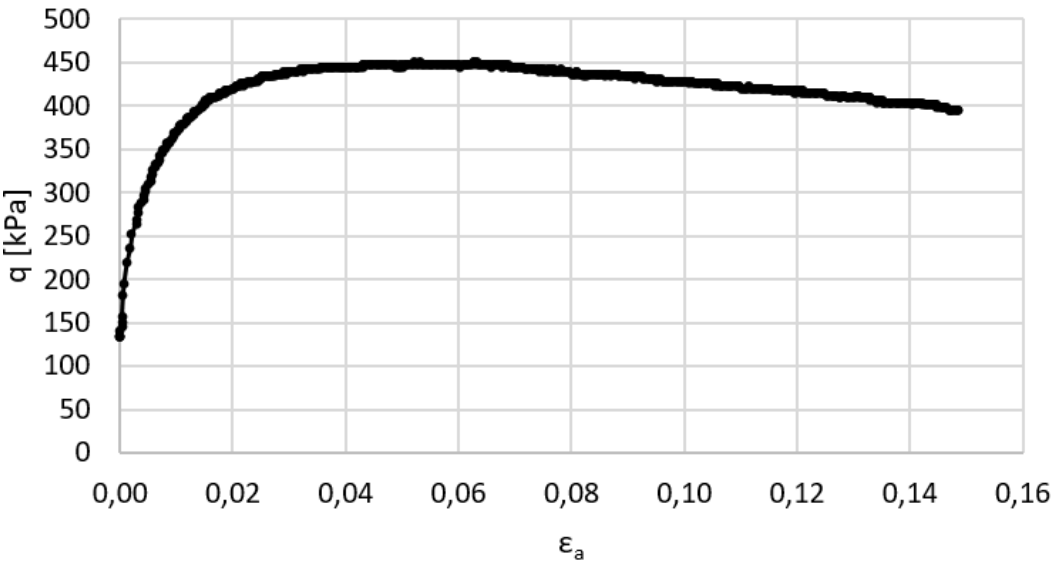

Figure A.2. S3.

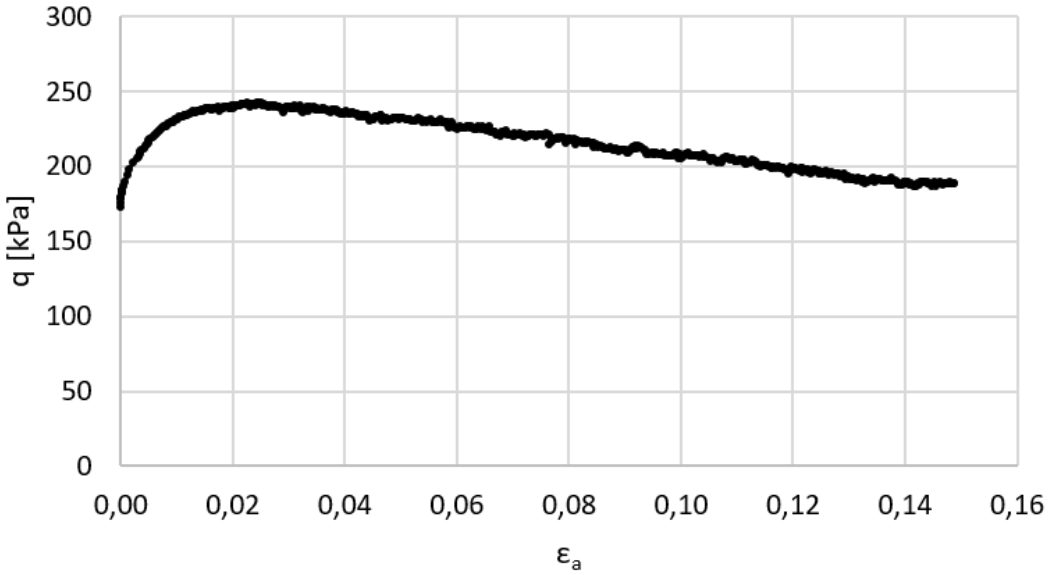

Figure A.3. S4.

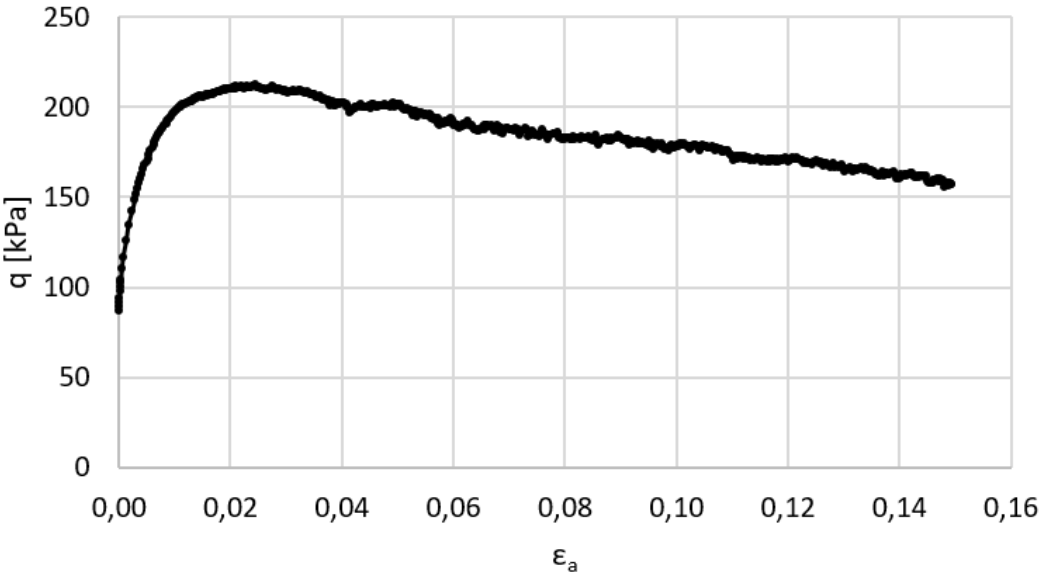

Figure A.4. S5.

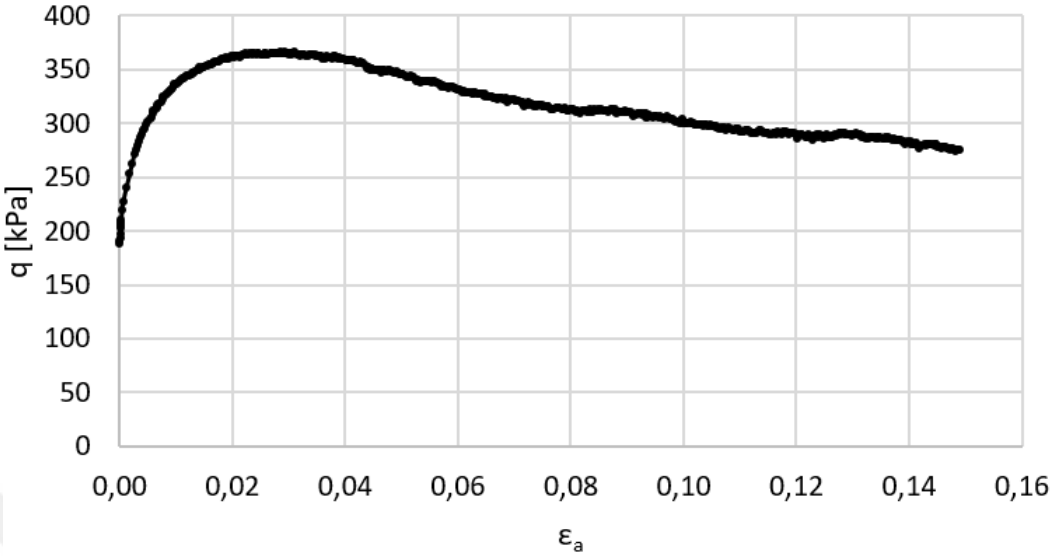

Figure A.5. S6.

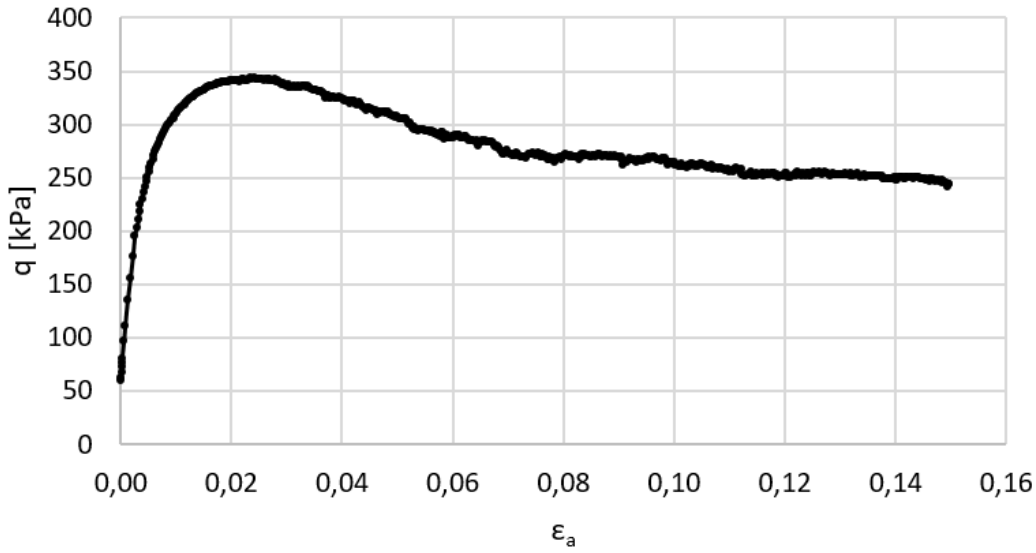

Figure A.6. S7.

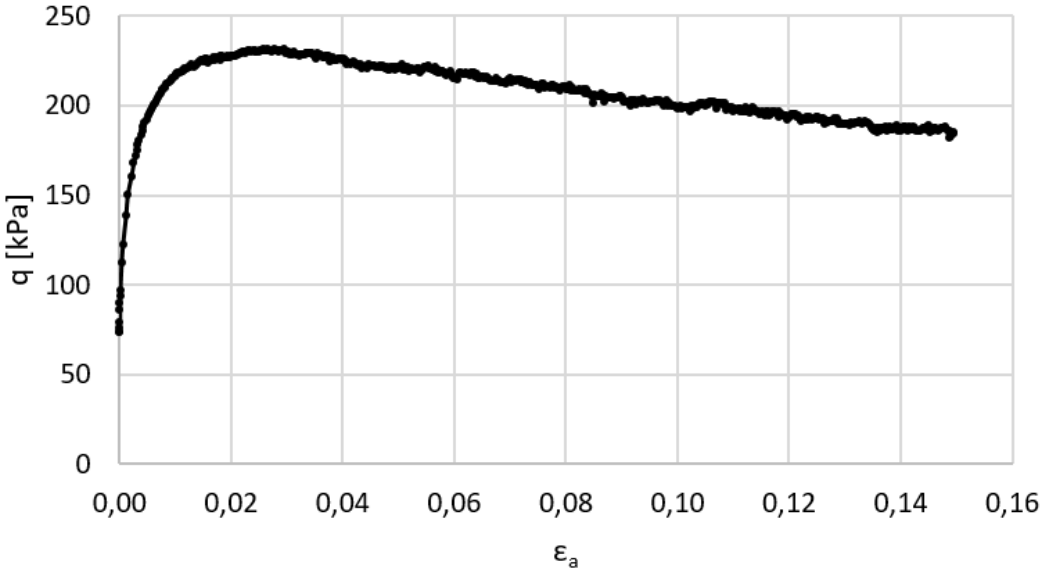

Figure A.7. S8.

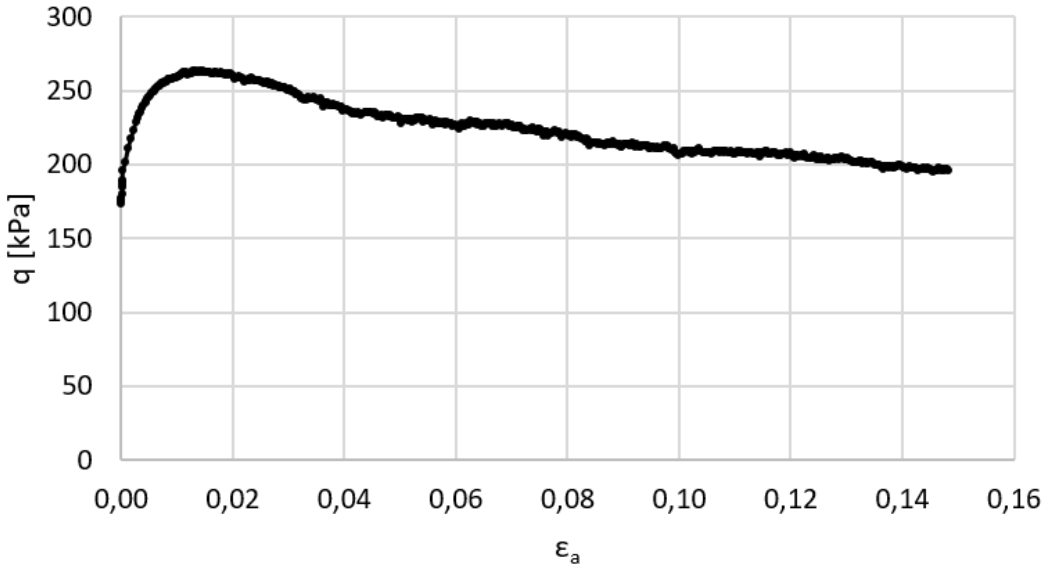

Figure A.8. S9.

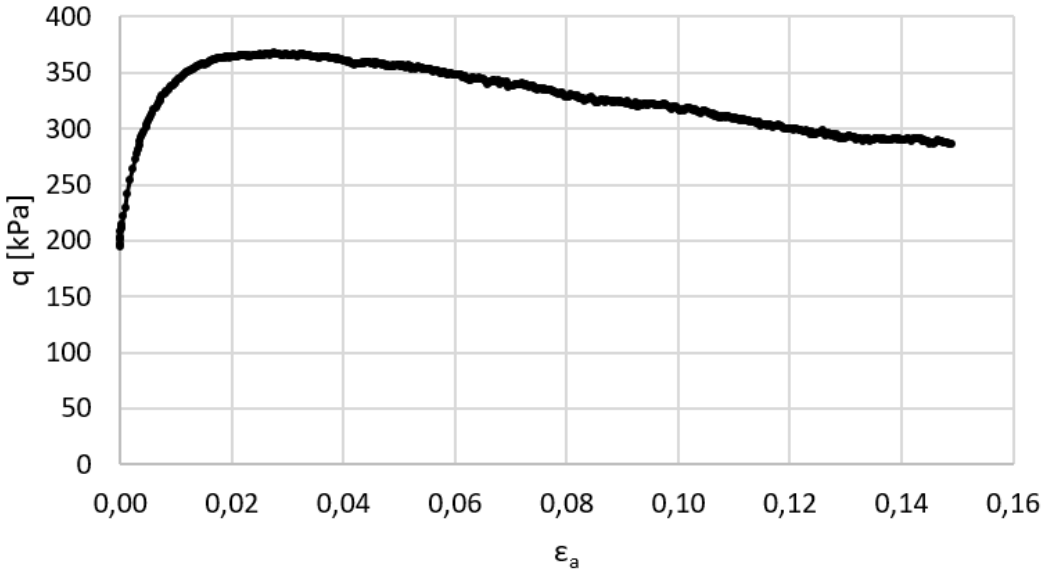

Figure A.9. S10.

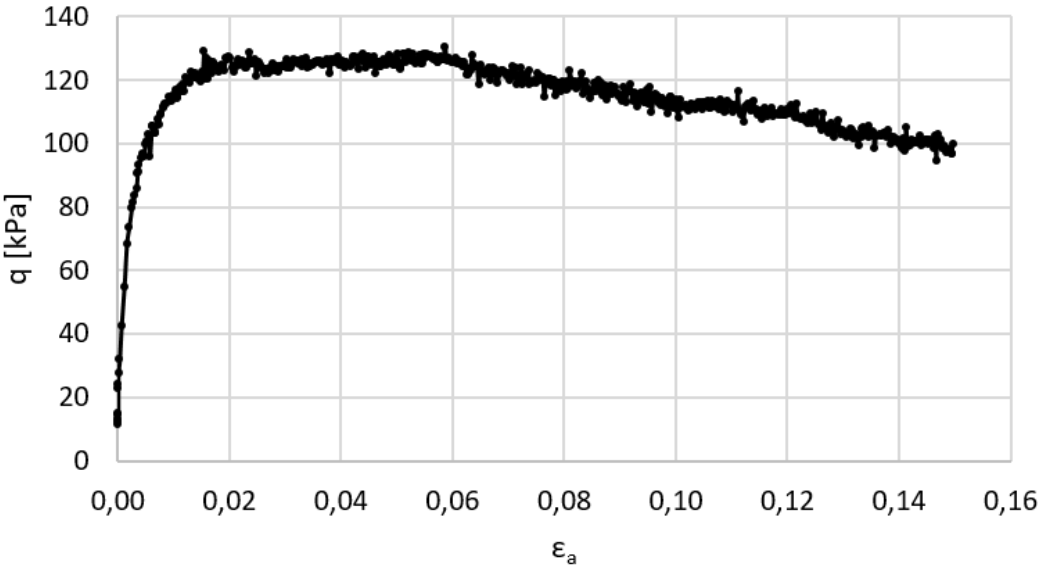

Figure A.10. S11.

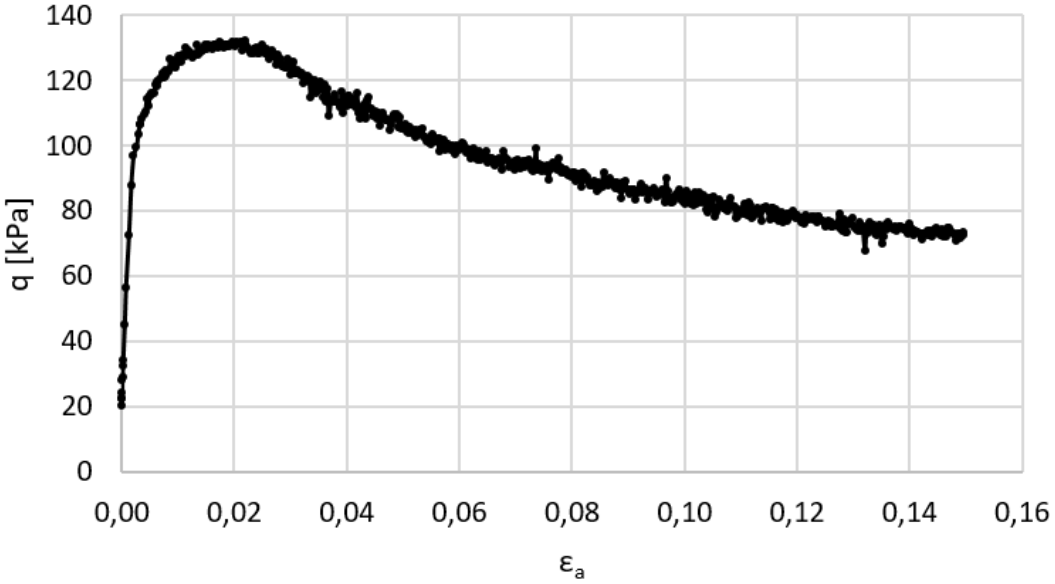

Figure A.11. S12.

APPENDIX B: THE NUMERICALLY OBTAINED CONE TIP RESISTANCE PROFILES FOR SOIL MODELS OF SILE SAND

Nine q_c profiles of Sile sand are presented in this section.

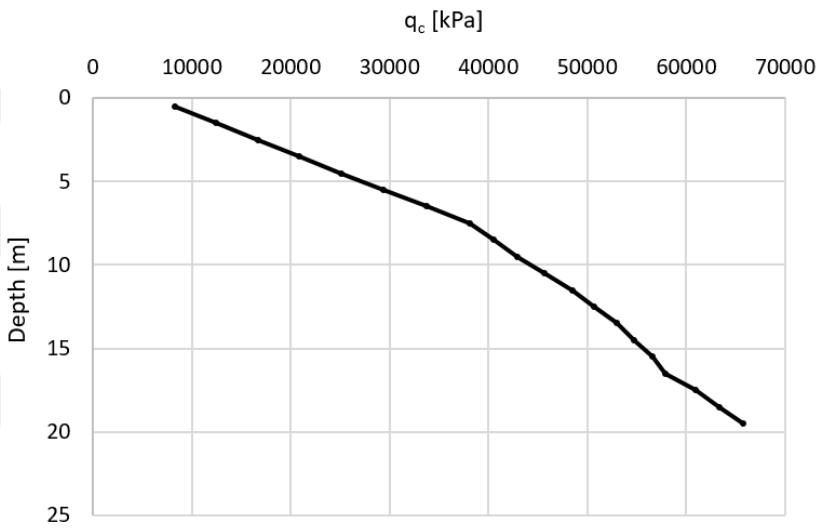

Figure B.1. Sile-K03-D.

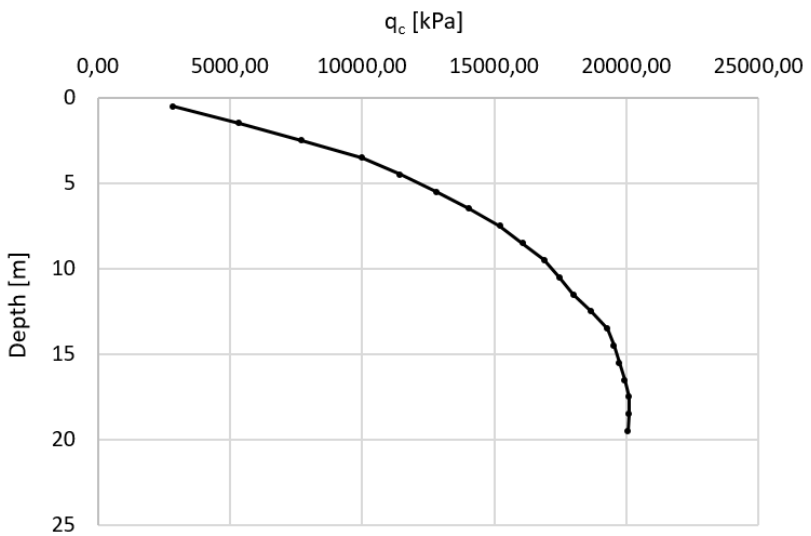

Figure B.2. Sile-K03-M.

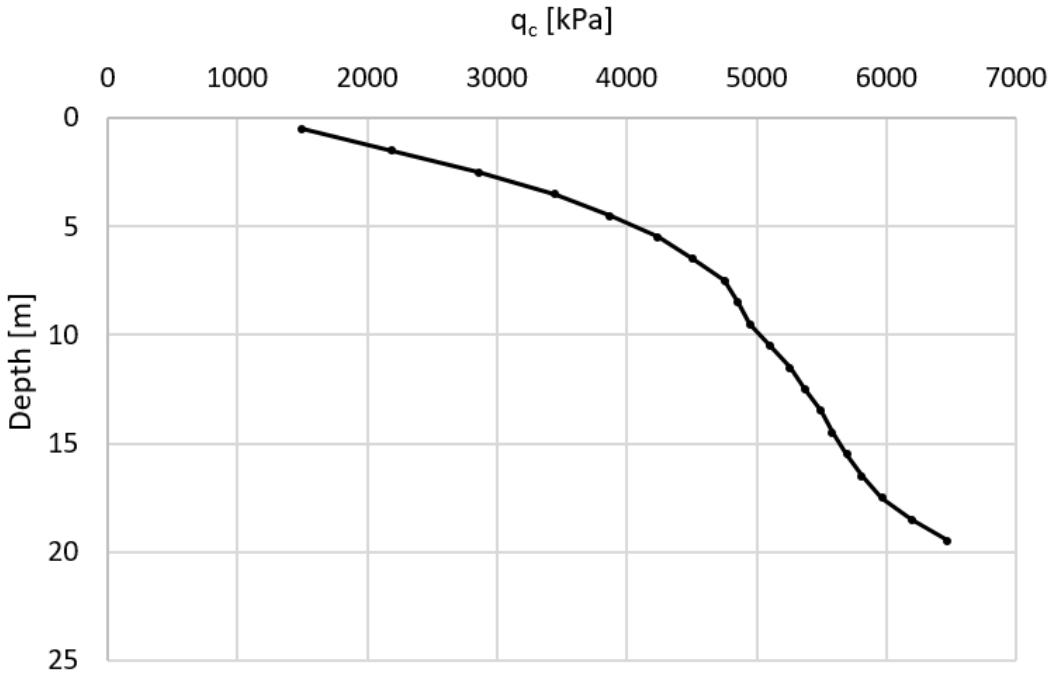

Figure B.3. Sile-K03-L.

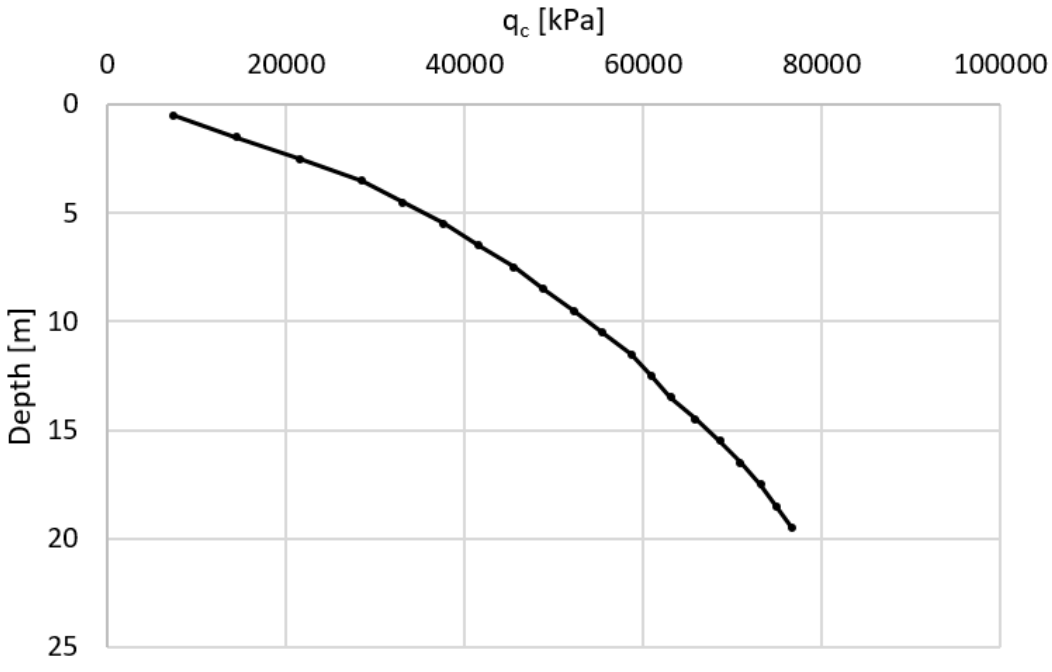

Figure B.4. Sile-K05-D.

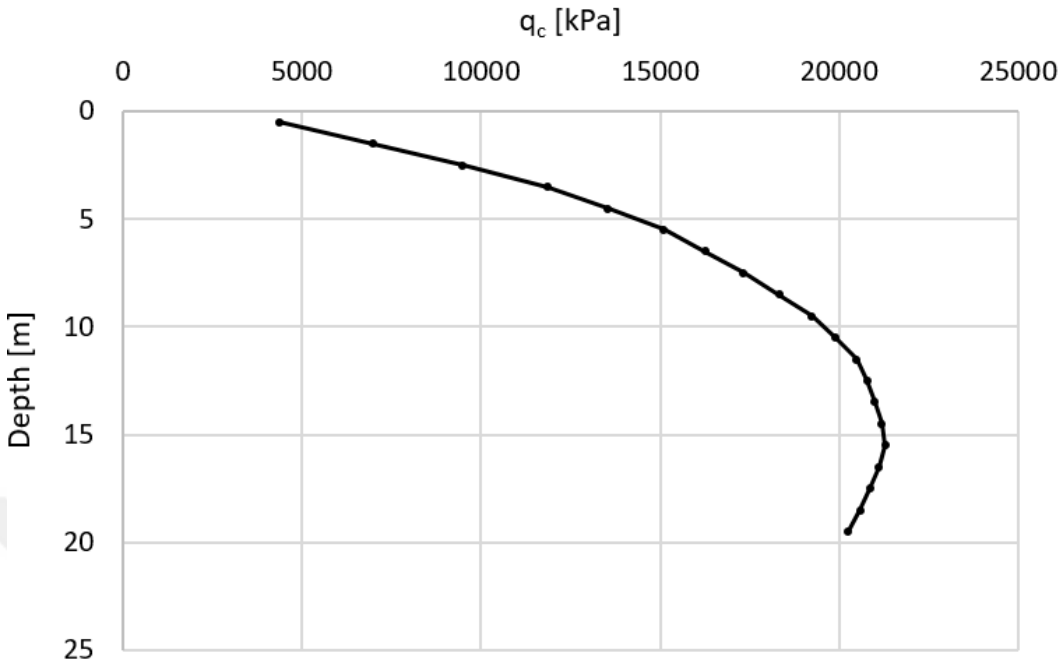

Figure B.5. Sile-K05-M.

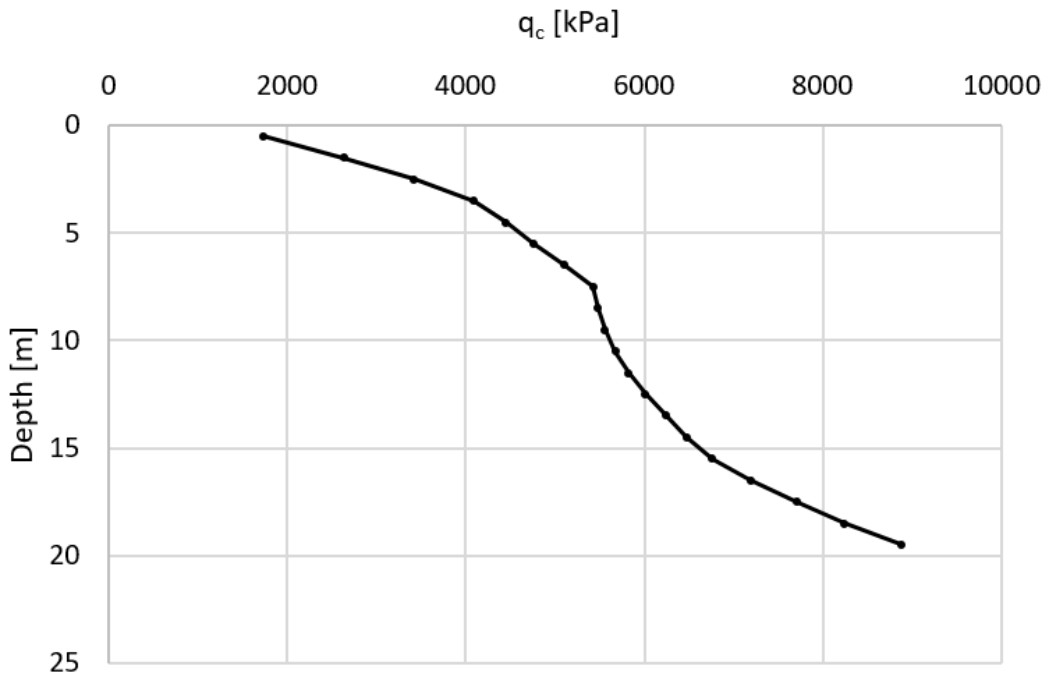

Figure B.6. Sile-K05-L.

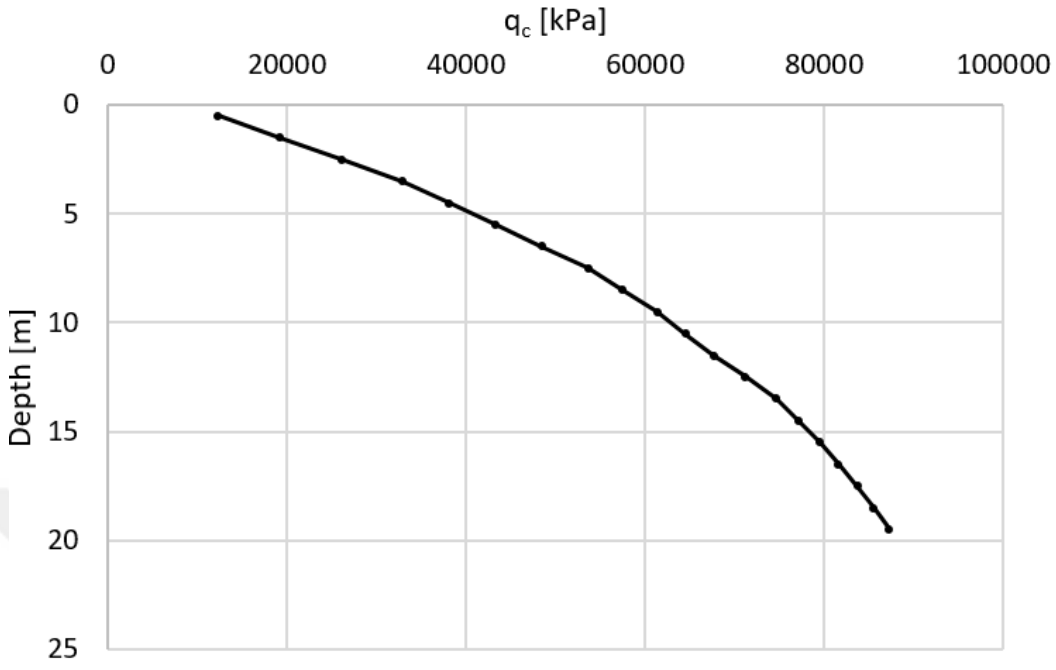

Figure B.7. Sile-K07-D.

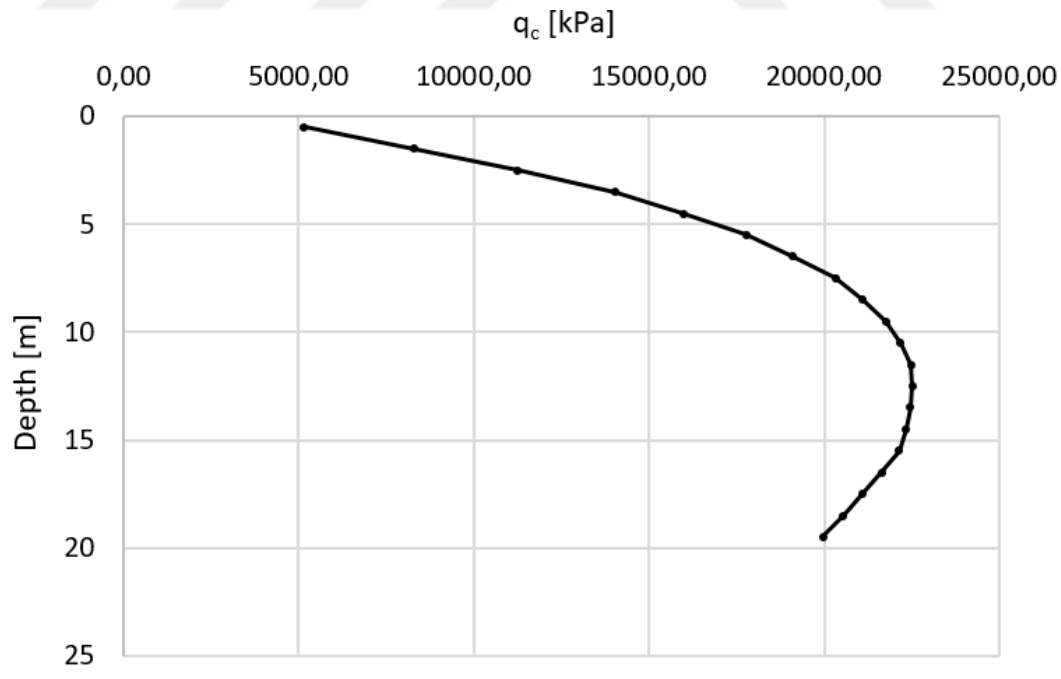

Figure B.8. Sile-K07-M.

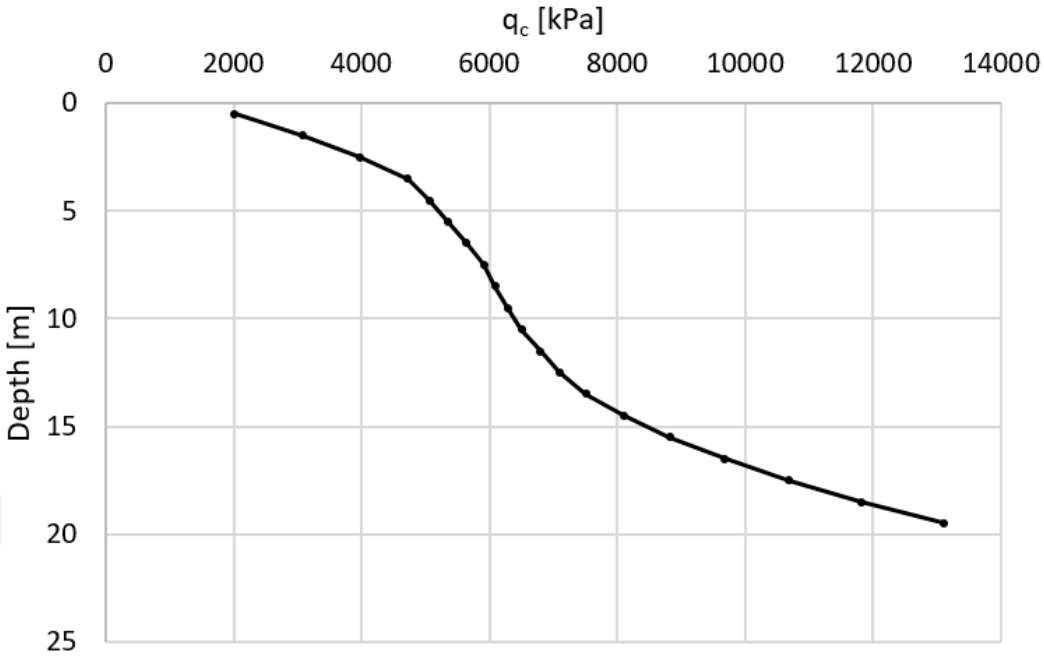

Figure B.9. Sile-K07-L.